Alma Mater Studiorum – Università di Bologna

DOTTORATO DI RICERCA IN

MECCANICA E SCIENZE AVANZATE DELL'INGEGNERIA (DIMSAI)

Ciclo XXX

Settore concorsuale: 09/C2 Fisica tecnica e Ingegneria nucleare
Settore scientifico disciplinare: ING-IND/19 Impianti nucleari

Thermal-hydraulic analysis of the LORELEI test device for the Jules Horowitz Reactor

Presentata da: Battistoni Paolo

Coordinatore Dottorato:
Prof. Marco Carricato

Supervisore:
Prof. Sandro Manservisi

Co-Supervisore:
Prof. Marco Sumini

Esame finale anno 2018

Abstract

LORELEI (Light Water One-Rod Equipment for LOCA Experimental Investigation) test device is currently under design in the framework of the planned experimental facilities of the Jules Horowitz Reactor. The main objective of this device is to analyze the thermal-mechanical behavior of the fuel rod and its consequences during a Loss of Coolant Accident (LOCA). The objective of this Thesis is to produce a comprehensive thermal analysis of the LORELEI apparatus by means of CATHARE2 code in order to verify the behavior of the device and to determine the best thermal-hydraulic conditions for the experimental performing. The preliminary part of this thesis aims to illustrate the system and mathematical architecture of the code with a general explanation of the thermal mechanical laws implemented for the FUEL module. An overview of the experimental apparatus, devised so far, is briefly presented to show the characteristics of LORELEI apparatus that can be considered the State of the Art of the LOCA-type facilities. According to the last updated LORELEI geometry, an exhaustive description of apparatus is finalized for a better understanding the CATHARE modeling proposed. This work is aimed to simulate the experimental phase called Re-irradiation phase. This is not a part of the LOCA accidental sequence but it is modeled to provide a study concerning the nominal conditions and to find out the device thermal-hydraulic limits. In this first phase, needed to create a realistic fission product inventory, the device is filled with water and the fuel rod is cooled by using convection flow. The work of this Thesis starts with the simulation of the first part of a LOCA accidental scenario. The fuel cladding temperature is increased and a small amount of water is set in the bottom of the device to produce steam needed for exothermic reactions of the fuel cladding. The final objective is to determine the best thermal conditions to reach an acceptable fuel cladding temperature profile. The distribution of all the gases present inside the device (steam and non condensable gases) is investigated and a thermal-mechanical analysis for the fuel rod is performed. An analysis of the velocity of the device toward the core is analyzed in order to limit the heat-up rate of the fuel cladding. The final part of this work is dedicated to a preliminary thermal-hydraulic analysis of the last experimental phase during which the device is completely re-flooded. We show the results of the fuel quenching behavior and the evolution of the system pressure. This phase is performed with a certain value of liquid mass flow injected, in accordance with different operational conditions.

Contents

Introduction

Since the 1970s, the behavior of the nuclear reactor during the lost of coolant accident (LOCA), has been the accident of reference in the framework of the electric power industry. The occurrence of this type of accident causes possible knock-on phenomena which compromise the safety of the entire nuclear power plant. The increase of the fission gases pressure inside the fuel cladding, following the loss of the liquid cooling inventory, leads to the deformation and the burst of the cladding itself. The failure of the fuel cladding also means the loss of the first primary barrier for the generated fission products which start spreading inside the primary circuit. The zirconium over-heating reacts with the steam and the hydrogen produced could be source of dangerous explosions such as those occurred in 2011 for the containment buildings in the units 1,2 and 3 in the Fukushima-Daichi Nuclear Power Plant (Song and Kim, 2014). All these chain events must be prevented by the Emergency Core Cooling System (ECCS) whose triggering should lead to a gradual safety of the site. Obviously, the time-line of the events previously described changes in accordance with the thermal-hydraulic conditions, fuel and cladding materials in agreement with different types of nuclear reactors. The interest to study these important issues has inspired the world of the Nuclear Research to design new type of experimental facilities in order to expand the State of Art of the fuel behavior during a LOCA condition. By the way, a large number of separate-effects test facilities, tests-with-moderate-integration or fully-integrated-tests has been design to investigate particular issues which may occur in this kind of Design Basic Accident (DBA). The objective of several experimental campaigns has been to analyze the mechanical aspects of the fuel cladding rather then the thermal-hydraulic phenomena or both of them. In these last 50 years, the French Nuclear Industry has concentrated its efforts on this topic. In order to understand the evolution of the technology in this field, one must think back to the test devices with moderate integration as EDGAR and EDGAR-2 (Forgeron et al., 2000) where the creep test in steam atmosphere have been conducted, or the LOCA test series program performed in the PHEBUS experimental reactor at the CEA Nuclear Center of Cadarache (Adroguer et al., 1983). During this test, both the mechanical and thermal-hydraulic phenomena have been studied in a 5x5 fuel bundle reactor. In the scientific literature it is also worth remembering some integral test campaigns such as those ones performed inside the FR2 research reactor and inside the Power Burst Facility at the Idaho National Laboratory (McCardell and MacDonald, 1983; Clément

et al., 2003; Wiesenack, 2013) etc. A step forward on this topic is the LORELEI test facility.

LORELEI (Light Water One-Rod Equipment for LOCA Experimental Investigation) apparatus is currently under design in the framework of the planned experimental facilities of the Jules Horowitz Reactor (Bignan, 2016). The objectives of this experimental device is to analyze the thermal-mechanical behavior of the fuel rod and the radiological consequences during a Loss of Coolant Accident. This LOCA-type device is based on single rod experimental strategy and it will be installed in the water channel inside the Jules Horowitz reflector together with other experimental devices. In order to investigate the real conditions of the LOCA scenario, this apparatus passes through three different phases which are briefly described below and in more detail in the Chapter 3 of this Thesis. The first experimental phase is called Re-irradiation phase during which the pressure inside the device is of the order of 70 *bar* and the fluid is water below the saturation temperature in a natural circulation loop. This phase is correctly designed to create a short life fission products inventory in the fuel. The Dry-out phase is the second experimental phase during which all the water is discharged out of the device, the internal pressure inside the apparatus device is reduced and the displacement device moves toward the core in order to increase the fuel power. During this phase the cladding temperature increases up to 800-1100 $^{\circ}C$ (according to the initial condition of the fuel sample) leading to the cladding ballooning and burst. Once the plateau phase around 1200 $^{\circ}C$ is reached, the high temperature oxidation steam-zirconium is studied. During the last phase of the experimental sequences, some cold water is injected inside the device and the fuel sample quenching is studied.

In the case of the LORELEI apparatus the IAEC (Israel Atomic Energy Commission), who is in charge of the design of the device, has conducted several studies. In particular the IAEC has started some important studies on the Re-irradiation phase and Dry phase by means of software such as as COMSOL Multiphysics® and FLUENT® (Gitelman et al., 2014; Korotkin et al., 2014; Ferry et al., 2014). However, the results obtained by these simulations refer only to single-phase case and neglect some two-phase phenomena that may occur inside the device. For this reason it has been considered necessary to conduct further examinations to verify the previous calculations with a two-phase system code such as CATHARE (Code for Analysis of THermal hydraulics during an Accident of Reactor and safety Evaluation). In general, in the framework of the Jules Horowitz project, the CATHARE code is an important calculation tool for the licensing process of the JHR itself and in the analysis of the consequences of possible abnormal conditions that could arise in the conduct of all the experimental programs. The CATHARE code (Geffraye et al., 2011) is the result of a collaboration among the major leaders of the French nuclear industry such as AREVA-NP, CEA, EDF and IRSN. As widely described in the first introductory chapter of this Thesis, the CATHARE code has a modular structure where every module represents the elements composing the circuit. In order to create the entire layout, the modules must be connected with others through junctions. The energy, momentum and mass balance equations are solved numerically at the junctions and grid points.

Chapter 1

CATHARE code

The CATHARE (Code for Analysis of THermal hydraulics during an Accident of Reactor and safety Evaluation) is a system code for the thermal-hydraulic analysis of nuclear power plants. The code is used to evaluate the safety of complex systems during accidental conditions and to define criteria for licensing procedure. This code is the result of a long collaboration among the major leaders of the French nuclear industry such as the reactor vendor AREVA-NP, the France Alternative Energies and Atomic Energy commission CEA, the French utility EDF and the Nuclear Safety Institute IRSN. At the beginning of the development, the code was employed to simulate mainly the design basis accidents (DBAs) in the framework of water nuclear plants such as, for example, Loss Of Coolant Accidents (LOCAs) and Main Stream Line Break accident (MSLB). Recently new modules has been introduced to the study of new reactors types such as Sodium-cooled Fast-Breeder Reactors (SFR), Gas Cooled Reactors (GCR) and Supercritical Water-Cooled Reactors (SCWR). The CATHARE code may evaluate important thermal-hydraulic phenomena such as forced-natural convection, mono-two phase turbulent flow, changing phase due to boiling or condensation in different flow regimes, etc. All the thermal-hydraulic quantities are obtained by resolving the one-dimensional equations for the two-phase-two-field model for the mass, momentum and energy balance together with some closure laws. The code might include up to 4 type of non-condensable gases and 12 type of radio-chemical components. Successive versions of the code have been developed in order to improve the structure and its framework. The objective of this continuous improvement is to include new modules, sub-modules and to implement update corrections of errors contained in previous versions. The aim of this chapter is to describe the general structure of the code and illustrate the main equations implemented. Clearly for a far more comprehensive explanation, one can recommend the consultation of manuals and tutorials such as the manual (Lavialle, February, 2006)

1.1 The modular structure of the code

The CATHARE code has a modular structure. This means that the entire circuit layout is created by connecting some specific operators called modules. Volume and surface modules properties can be modified with the use of sub-modules and gadgets. The energy, momentum and the mass balance equations are solved numerically at the junctions and grid points.

1.1.1 Code modules

The main used modules are: axial 1-D, volume 0-D and boundary condition modules. Below the main module features are summarized.

Axial 1-D module. This module describes the components within which the fluid motion is fundamentally one-dimensional as for example pipes, steam generators, down-comer etc. The mesh nodalization is specified by the user in accordance with the physical phenomena considered.

Volume 0-D module. This module is used, for example, to model pressurizer, accumulator and plenum of steam generator. Also by using this module it is possible to study the water-level variation and its partial stratification by considering two sub-volumes divided by a water free surface. Inside these sub-volume all the physical properties are constant along the horizontal plane and all the inertial forces are neglected compare to the gravitational force. On the surface of the two sub-modules an equation describes the mass exchange which may take into account the formation and separation of droplets. If the heat exchange may occur, then the condensation or liquid evaporation are modeled.

Volume 3-D module. The 3-D module is based on the porous two-fluid six equations model. For each phase, the mass, momentum and energy equations are defined. For this module is also implemented the $(k-\epsilon)$ model to describe the turbulence diffusion of one or both the phases. The main utilization of this module is made to describe the PWR vessel or for a three-dimensional modeling of an empty of solid structures element.

Boundary condition module. These modules are connected through junctions which allow to set one or more hydraulic conditions such as, for example, pressure, velocities, liquid mass flow and void fraction. The figure 1.1 shows an example of `BC3B` type boundary condition. In this specific case the liquid and gas temperatures `TL` and `TG`, the void fraction `ALFA`, the mass fraction of one non-condensable gas `X1` and the liquid and gas velocities, `VL` and `VV` are assigned. The command `ABSTIME` defines the time intervals where the variables assigned change linearly.

```
 bc_inlet = BCONDIT j_ent DSTREAM ;
MODEL bc_inlet BC3B
TL (REALLIST 100.0 100.0 100.0 100.0 )
TG (REALLIST -1.  -1.  -1.  -1.  )
ALFA (REALLIST 1.0E-5 1.0E-5 1.E-5 1.E-5 )
X1 (REALLIST 1.0E-5 1.0E-5 1.E-5 1.E-5 )
VL (REALLIST 0.1 0.1 1.E-5 1.E-5 )
VV (REALLIST 0.1 0.1 1.E-5 1.E-5 )
ABSTIME (REALLIST 0.0 1000.  1001.  1000000.  );
```

Figure 1.1: Example of boundary conditions.

1.1.2 Code sub-modules

Sub-modules are elements which allow to modify the module attributes. Usually one sub-module modifies the thermal hydraulic behavior of the modules to which it is connected. Below are listed the most used sub-modules.

Thermal structure. There are three types of thermal structures: sub-modules for multilayer walls (`WALL`), heat exchangers (`EXCHANGER`) and fuel rod (`FUEL`). A more detailed description of the sub-module `FUEL` is presented in the last part of this chapter. Inside the multilayer walls and the heat exchanger, the 1-D equation of heat conduction is solved by finite element scheme. The conditions imposed could be of Newman type (heat flux imposed) or can be assigned the values of external temperature together with the heat transfer coefficient. With the sub-module `EXCHANGER` it is possible to couple thermally two modules belonging to the same or different circuit. To define a wall and a heat exchange is necessary to assign the type of material they are made of, the heating perimeter, the thickness and, if present, a power source.

Reflooding. This sub-module is used to calculate the quenching along the hot wall or along the fuel rods. The quenching can be distinguished into two types based on the liquid-front direction respect to the surface to quench: from the bottom towards the top *bottom-up re-flooding* and from the top towards the bottom *top-down re-flooding*.

1.1.3 Gadgets

In order to complete the circuit layout, further elements called *Gadget* can be connected to a specific module. The main gadget are listed below:

- `SOURCE/SINK`: they are utilized to inject or to extract inside the system a certain volume of a scalar quantity such as the mass of the liquid/gas or a certain amount of power;
- `TEE` junction: this gadget is utilized to simulate a tee branch;
- `CCFL`: this gadget allows to model the *Counter Current Flow Limitation* for complex geometries;
- `BREAK`: this gadget makes possible the modeling of a rupture along the modules to which is connected.

1.2 Equations for two-phase flow

In order to describe the behavior of two-phase flow inside a 1-D module the set of equations which describe the energy, momentum and the mass balance equation are solved. Together with the steam-liquid phases, a number of non condensable gases may be considered. Since all the equations are integrated over the cross section area A, they depend on the axial coordinate along the length of the pipe. The main simplifications used to define these equations are listed below (Lavialle, February, 2006):

- The axial component of the viscous stress tensor and its work are neglected;
- The axial heat conduction is neglected;
- The axial mass diffusion is neglected (in case of non condensable gas transport);
- The liquid and gas proprieties which are valid for local instantaneous variables are assumed also valid for averaged variables and they are calculated with the value of the mean pressure and not with the phase pressure ($P = \alpha P_v + (1 - \alpha)P_l$);
- The work of inter-facial forces and pressure distribution forces are neglected in the energy balance equation.

The equation of the mass, momentum and energy balance at the interfaces of the different phases are written by considering the following hypothesis:

- The interface has not thickness and mass;
- In the momentum equation, the superficial tension is neglected;
- In the energy balance, the contribution of the superficial tension is neglected;
- Both phases have the same velocity at the interface which is supposed uniform.

Mass conservation. For the liquid phase we write (Scardovelli and Manservisi, 2012):

$$\frac{\partial}{\partial t}((1-\alpha)\rho_l A) + \frac{\partial}{\partial z}((1-\alpha)\rho_l u_l A) = -A\Gamma + S_l\,, \tag{1.1}$$

and for the gas phase

$$\frac{\partial}{\partial t}(\alpha\rho_g A) + \frac{\partial}{\partial z}(\alpha\rho_g u_g A) = A\Gamma + S_v + \sum_{j=1}^{n_I} S_j \tag{1.2}$$

where n_I is the number of non-condensable gases which are described with the following mass balance equation:

$$\frac{\partial}{\partial t}(\alpha\rho_g X_j A) + \frac{\partial}{\partial z}(\alpha\rho_g u_g X_j A) = S_j \;\text{ with }\; j = 1, ...n_I\,. \tag{1.3}$$

The terms S_l, S_v, S_j represent the source of mass for unit volume for each phase. Γ is the mass flux on the interface due to the changing phase

$$\Gamma = \frac{-q'''_{in\to l} - q'''_{in\to v} + \chi_h q''_{w\to in}/A}{h_v - h_l} + \Gamma_r\,, \tag{1.4}$$

where

- $q'''_{in\to l}$: interface to liquid heat flux $[W/cm^3]$;
- $q'''_{in\to v}$: interface to vapor heat flux $[W/cm^3]$;
- $q''_{w\to in}$: wall to interface heat flux $[W/m^2]$;
- χ_h: wet perimeter $[m]$.

The parameter Γ_r is a parameter given by

$$\Gamma_r = \begin{cases} -\rho_g\Big(\dfrac{\alpha-\alpha_{min}}{\theta_v}\Big) & \text{when } \alpha < \alpha_{min} \quad \text{vaporization} \\ 0 & \text{when } \alpha_{min} < \alpha < \alpha_{max} \\ -\rho_l\Big(\dfrac{\alpha-\alpha_{max}}{\theta_l}\Big) & \text{when } \alpha_{max} < \alpha \quad \text{condensation} \end{cases} \tag{1.5}$$

with $\alpha_{min} = 10^{-5}$, $\alpha_{max} = 1 - 10^{-6}$ and $\theta_v = \theta_l = 10^{-5}$.

The momentum equation. For the liquid phase we write

$$\begin{aligned} &(1-\alpha)\rho_l A\Big(\frac{\partial}{\partial t} + u_l\frac{\partial}{\partial z}\Big)u_l + (1-\alpha)A\frac{\partial P}{\partial z} + P_{in}A\frac{\partial(1-\alpha)}{\partial z} - \\ &\beta\alpha(1-\alpha)\rho_{mix}A\Big(\Big(\frac{\partial}{\partial t} + u_g\frac{\partial}{\partial z}\Big)u_g - \Big(\frac{\partial}{\partial t} + u_l\frac{\partial}{\partial z}\Big)u_l\Big) = \\ &-A\Gamma(u_{in} - u_l) + A\tau_{in} - \chi_f C_l\frac{\rho_l}{2}u_l|u_l| + (1-\alpha)\rho_l A g_x + R\frac{\alpha}{4}P_{in}\frac{\partial A}{\partial z} + m_l \end{aligned} \tag{1.6}$$

and for the gas phase we have

$$\begin{aligned}\alpha\rho_g A\Big(\frac{\partial}{\partial t}+u_g\frac{\partial}{\partial z}\Big)u_g+\alpha A\frac{\partial P}{\partial z}+P_{in}A\frac{\partial\alpha}{\partial z}+\\ \beta\alpha(1-\alpha)\rho_{mix}A\bigg(\Big(\frac{\partial}{\partial t}+u_g\frac{\partial}{\partial z}\Big)u_g-\Big(\frac{\partial}{\partial t}+u_l\frac{\partial}{\partial z}\Big)u_l\bigg)=\\ A\Gamma(u_{in}-u_g)-A\tau_{in}-\chi_f C_g\frac{\rho_g}{2}u_g|u_g|+\alpha\rho_g Ag_x+R\frac{(1-\alpha)}{4}P_{in}\frac{\partial A}{\partial z}+m_g\ .\end{aligned}\tag{1.7}$$

In order to simplify the model, the stress τ_{xx} and the surface tension σ are neglected. Table 1.1 provides a detailed explanation of all the terms appeared in the [1.7].

Conservation of energy. For the liquid phase we write

$$\begin{aligned}A\frac{\partial}{\partial t}\bigg((1-\alpha)\rho_l\big(h_l+\frac{u_l^2}{2}\big)\bigg)+\frac{\partial}{\partial z}\bigg((1-\alpha)\rho_l Au_l\big(h_l+\frac{u_l^2}{2}\big)\bigg)-(1-\alpha)A\frac{\partial P}{\partial t}=\\ Aq'''_{in\to l}+\chi_c q''_{w\to l}-A\Gamma\big(h_l+\frac{u_{in}^2}{2}\big)+(1-\alpha)\rho_l Au_l g_x+SE_l\ .\end{aligned}\tag{1.8}$$

and for the gas phase we have

$$\begin{aligned}A\frac{\partial}{\partial t}\bigg(\alpha\rho_g\big(h_g+\frac{u_g^2}{2}\big)\bigg)+\frac{\partial}{\partial z}\bigg(\alpha\rho_g Au_g\big(h_g+\frac{u_g^2}{2}\big)\bigg)-\alpha A\frac{\partial P}{\partial t}=\\ Aq'''_{in\to v}+\chi_c q''_{w\to v}+A\Gamma\big(h_v+\frac{u_{in}^2}{2}\big)+\alpha\rho_g Au_g g_x+SE_g\ .\end{aligned}\tag{1.9}$$

The first and the second term are respectively the variation of the density of energy over the time and its gradient, the third term is the variation of the pressure over the time. In the second member, the first two terms are the power exchanged per unit of volume between the interface and the liquid/steam ($q'''_{in\to l}/q'''_{in\to v}$) and the power per unit area between the wall of the pipe and the fluid/steam ($q''_{w\to l}/q_{w\to v}$), see figure 1.2. The last three terms represent the change of the phase on the surface, the work done by the weight force and any external power source.

If in the system are present n_I number of non-condensable gases, the total density ρ_j, the pressure P and the gas enthalpy h_g are written as

$$\rho_j=X_j\rho_g\ ,\tag{1.10}$$

with

$$\rho_g=\sum_{j=1}^{n_I}\rho_j+\rho_v(T_g,h_v)\ ;\tag{1.11}$$

$$P_j=\rho_j R_j T_g\tag{1.12}$$

with

$$P=\sum_{j=1}^{n_I}P_j+P_v\ ,\tag{1.13}$$

Table 1.1: List of the terms constituting the momentum equation [1.7].

Term	Description
$\alpha\rho_g A\Big(\frac{\partial}{\partial t}+u_g\frac{\partial}{\partial z}\Big)u_g$	Inertial term
$\alpha A\frac{\partial P}{\partial z}$	Pressure gradient
$P_{in}A\frac{\partial\alpha}{\partial z}$	Pressure difference P_{in} on the interface and the variation of the level of the stratified flow due to the changing of the void fraction along the z-axis
$\beta\alpha(1-\alpha)\rho_{mix}A\Big(\Big(\frac{\partial}{\partial t}+u_g\frac{\partial}{\partial z}\Big)u_g-\Big(\frac{\partial}{\partial t}+u_l\frac{\partial}{\partial z}\Big)u_l\Big)$	β is the *added mass coefficient*. This term represents the inertia added to the single phase: the fluid during the acceleration/deceleration must move a volume of the other fluid adjacent
$A\Gamma(u_{in}-u_l)$	Phase changing on the interface, u_{in} is the velocity of the interface between the two phases. $u_{in}=\alpha u_l+(1-\alpha)u_g$
$A\tau_{in}$	τ_{in} is the *interfacial friction* $[N/m^3]$. This term represents the pressure drop on the interface (opposite sign in the [1.6])
$\chi_f C_g\frac{\rho_g}{2}u_g\lvert u_g\rvert$	C_g gas wall friction coefficient. The term represents the pressure drop on the wall (same sign in the [1.6])
$\alpha\rho_g A g_x$	Gravitational term, g_x is the projection of the gravity vector onto the axis of the pipe
$R\frac{(1-\alpha)}{4}P_i n\frac{\partial A}{\partial z}$	Level changing in the stratified flow due to the variation of the cross section along the pipe. R_s is the rate of stratification
m_g	Source of momentum

$$h_g=\big(1-\sum_{j=1}^{n_I}X_j\big)h_v+\sum_{j=1}^{n_I}X_j\big(h_0+Cp_j(T_g-T_0)\big)\,, \tag{1.14}$$

where the gas perfect hypothesis as assumed, $h_v=h_v(P_v,T_g)$ is the steam enthalpy and h_0 and T_0 are two referent values.

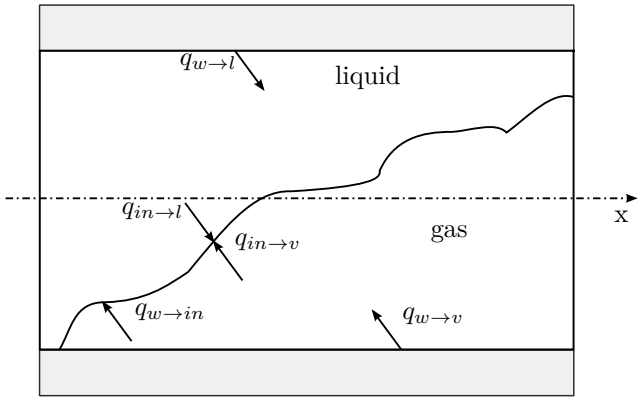

Figure 1.2: Heat flux to the wall and to the interface in 1-D element.

1.3 Closure equations

In total CATHARE contains 13 closure laws for: $q''_{w\to l}$, $q''_{w\to v}$, $q''_{w\to in}$, $q'''_{in\to l}$, $q'''_{in\to v}$, E, P_{in}, R_s, τ_{in}, β, u_{in}, C_g and C_l. These closure laws are derived from physical considerations and/or empirical data from appropriate experiments (Ghione, 2015).

1.3.1 Flow patterns

Some variables, such as pressure drop, void fraction and velocity vary according to flow pattern or regime. In CATHARE, the flows patterns are characterized by several values of the stratification ratio R_s and the entrainment rate E.

For every type of pipe (Annulus, Rod bundle, Pipe), the typical representation of the flow patterns is showed in figure 1.3. The solid lines are the transitions explicitly modeled: the transition between stratified and not stratified flows and the transition between annular and annular-mist flow. The dashed line marks the transition between the annular and bubbly/churn flow. In this last case, the transition is derived from the void fraction criteria and it is taken into account only for inter-facial friction and heat transfer.

1.3.2 Convective heat exchange: forced or natural convection in liquid

In case of natural or forced convection in liquid, the heat transfer $q_{con}|_l$ from the heated surface to the liquid can be expressed with the Newton's cooling law:

$$q_{con}|_l = h_{con}|_l \Delta T\,. \tag{1.15}$$

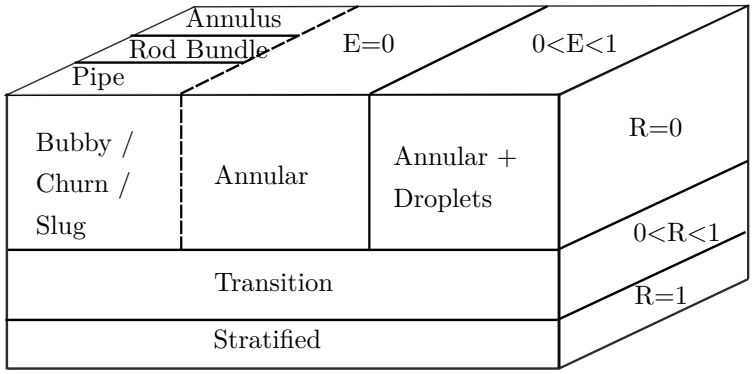

Figure 1.3: Flow patterns described in CATHARE code.

$h_{conv}|_l$ is the heat transfer coefficient and ΔT is termed as *excess temperature*. In CATHARE this last term can be expressed according to the values of $T_{sat}(P)$, T_l and T_w, in particular:

$$\Delta T = \begin{cases} (T_w - T_l) & \text{if } T_l < T_w < T_{sat}(P) \quad \text{single phase flow} \\ (T_{sat}(P) - T_l) & \text{if } T_l < T_{sat}(P) < T_w \quad \text{sub saturated boiling} \\ 0 & \text{if } T_{sat}(P) < T_l < T_w \quad \text{saturated boiling} \ . \end{cases} \tag{1.16}$$

$h_{con}|_l$ is expressed as:

$$h_{con}|_l = \max(h_{lam,NC}|_l, h_{tur,NC}|_l, h_{lam,FC}|_l, h_{tur,FC}|_l) \ , \tag{1.17}$$

where the subscript *lam* and *tur* indicates the flow regime which can be respectively laminar or turbulent, *NC* and *FC* if the mechanism of the heat transport is by natural (free) or by forced convection. The expression [1.17] does not consider the case when both the natural and forced convection are present. Normally $Nu_l = f(Re_l, Gr_l, Pr_l)$ and the combined effects of free and forced convection should be considered when $Gr_l/Re_l^2 \approx 1$, where Gr_l, Re_l and Pr_l are respectively the Grashof, Reynold and Prandtl numbers for liquid flow defined as:

$$Gr_l = \frac{\text{buoyancy forced}}{\text{viscous forces}} = \frac{g\beta_l \rho_l^2 D_{h,l}'^3}{\mu_l^2}(T_w - T_l) \tag{1.18}$$

$$Re_l = \frac{\text{inertia}}{\text{viscous forces}} = \frac{\rho_l u_l D_{h,l}'}{\mu_l} \ , \tag{1.19}$$

$$Pr_l = \frac{\text{momentum}}{\text{thermal diffusivity}} = \frac{c_{p,l}\mu_l}{k_l} \ , \tag{1.20}$$

with $\beta = -\frac{1}{\rho_l}\left(\frac{\partial \rho_l}{\partial T_l}\right)_p$.

The Nusselt number for liquid flow is defined as

$$Nu_l = \frac{\text{convection heat transfer}}{\text{conduction heat transfer}} = \frac{hD_{h,l}'}{k_l} \ . \tag{1.21}$$

$D'_{h,l}$ is a modified hydraulic diameter defined by

$$D'_{h,l} = D_{h,l}(1 - \sqrt{\alpha F_{num}}) \ , \tag{1.22}$$

where F_{num} is a numerical correction that limits the minimum liquid film thickness to the value $10^{-3}D_{h,l}$; in single-phase flow $D'_{h,l} = D_{h,l}$.

Natural convection in liquid. In the natural convection flow ($Gr_l/Re_l^2 >> 1$), the forced convection effects may be neglected and $Nu_l = f(Gr_l, Pr_l)$. Two cases can be distinguished:

- for laminar flow
$$Nu_{lam,NC}|_l = 0.55(Ra_l)^{1/4} \ ; \tag{1.23}$$
- for turbulent flow
$$Nu_{tur,NC}|_l = 0.13(Ra_l)^{1/3} \ , \tag{1.24}$$

where $Ra_l = Gr_l Pr_l$ is the Rayleigh number.

Forced convection in liquid. In the forced convection flow ($Gr_l/Re_l^2 << 1$), the free convection effects may be neglected and $Nu_l = f(Re_l, Pr_l)$. Two cases can be distinguished:

- for laminar flow
$$Nu_{lam,FC}|_l = 3.66 \ , \tag{1.25}$$
- for turbulent flow the heat transfer coefficient is computed with the the Dittus-Boelter equation (Dittus and Boelter, 1985)
$$Nu_{tur,FC}|_l = 0.023 Re_l^{0.8} Pr_l^{0.4} \ . \tag{1.26}$$

1.3.3 Nucleate boiling and critic flux regions

In order to take into account heat transfer in boiling phenomena in the code are implemented many correlations.

Nucleate boiling. In CATHARE code the Thom correlation (Thom et al., 1967) is used to describe the heat exchanged between the wall and the liquid for pressure P between 5-14 MPa. In particular the code sets

$$(T_w - T_{sat}(P)) = 22.5(q'')^{0.5} e^{\frac{-P}{8.7}} \ , \tag{1.27}$$

where P, q'' and T are expressed respectively in MPa, MW/m^2 and K. The heat flux q'' is therefore computed as :

$$q'' = 1.97\,10^3 (T_w - T_{sat}(P))^2 e^{0.23P} \ . \tag{1.28}$$

Point of Net Vapor Generation (NVG). The NVG or Onset of Significant Void (OSV) is the point at which the amount of bubble becomes significant in the sub-cooled region. To determine this point is very important to study the transient response in a reactor. In CATHARE the analysis of this point depends on the Peclet number Pe defined as

$$Pe = RePr = \frac{Nu}{St} \ , \tag{1.29}$$

where St is the Stanton number:

$$St = \frac{q''}{GCp_l(T_{sat} - T_l)} \ , \tag{1.30}$$

with G is the mass velocity $[kg/m^2s^{-1}]$. In particular the sub-cooled liquid reaches the NVG point if $\Delta h_c = \max(\Delta h_c*; 10^4)$, where the value 10^4 has been introduce for numerical reasons. The value Δh_c* depends on the Peclet number (Saha and Zuber, 1974). In particular one sets

$$\Delta h_c* = \begin{cases} \frac{5q''Cp_lD_{h,l}}{k_lPe_065\,10^{-4}} & \text{if } \ Pe < 0.52Pe_0 \\ \frac{2q''Cp_lD_{h,l}}{k_lPe_065\,10^{-4}(Pe/Pe_0)^{1.4}} & \text{if } \ Pe > 0.52Pe_0 \ , \end{cases} \tag{1.31}$$

for $Pe_0 = 70000$ and below this value the local Nusselt number is a constant ($Nu \approx 455$), for values greater than Pe_0 the Stanton number is a constant ($St \approx 0.0065$). The criteria expressed in the [1.31] is a modified version of the Saha correlation validated at the CEA-Grenoble using KIT experiments (Sabotinov, 1974). The NGV point is reached if $h_{l,sat} - h_l \leq \Delta h_c$.

Pre-CHF region. In the Pre-CHF region the total heat flux q'' imposed on the wall can be expressed as:

$$q'' = q''_{w\to l} + q''_{w\to in} \ . \tag{1.32}$$

The values of $q''_{w\to l}$ and $q_{w\to in}$ depend on the values of T_l, T_w, $T_{sat}(P)$ and Υ. This last parameter, varies between 0 and 1 and it determines the rate of vaporization in sub-cooled boiling regime. Υ is based on the NVG criteria, in particular:

$$\Upsilon = \begin{cases} 1 & \text{if } \ h_l - h_{l,sat} > 10000 \\ 1 - (\Delta h_{aux} - 1)^6(1 + 6\Delta h_{aux}); & \text{if } \ -\Delta h_c < h_l - h_{l,sat} < 10000 \\ 0 & \text{if } \ h_l - h_{l,sat} < -\Delta h_c \ , \end{cases} \tag{1.33}$$

with

$$\Delta h_{aux} = \max\Big(0; \frac{\Delta h_c + (h_l - h_{l,sat})}{\Delta h_c + 10000}\Big) \ . \tag{1.34}$$

Three different cases can be distinguished:

- Single-phase flow: $T_w < T_{sat}(P)$:

$$q''_{w\to l} = q''_{conv}, \quad q''_{w\to in} = 0, \quad T_w = T_l + \frac{q''}{h_{conv}} \ . \tag{1.35}$$

- Sub-cooled boiling: $T_l < T_{sat} < T_w$:

$$q''_{w\to l} = q''_{conv} + (1-\Upsilon)q''_{nb}, \quad q''_{w\to i} = \Upsilon q''_{nb} \, . \tag{1.36}$$

- Saturated boiling: $T_l > T_{sat}$:

$$q''_{w\to l} = 0, \quad q''_{w\to in} = q''_{nb} \, . \tag{1.37}$$

Critical heat Flux (CHF). Once the mass flux $\hat{G}$, the pressure P and steam quality $\hat{x}$ are known, the CHF is calculated by interpolating with the cubic splines the values obtained by the look-up table of Groeneveld (Groeneveld et al., 1986). The mass flux is given by the following expression:

$$\hat{G} = |G_g| + |G_l| = |\alpha\rho_g u_g| + |(1-\alpha)\rho_l u_l| \, . \tag{1.38}$$

The steam quality $\hat{x}$ is defined as:

$$\hat{x} = \frac{\alpha\rho_g + (1-\alpha)\rho_l x}{\alpha\rho_g + (1-\alpha)\rho_l} \text{ with } x = \frac{h_l - h_{l,sat}}{h_{l\to g}} \, . \tag{1.39}$$

The critical heat flux (CHF) is expresses as:

$$q''_{CHF} = F_1 F_2 F_3 q''_{CHF}(I)(\hat{G}, P, \hat{x}) \, , \tag{1.40}$$

where $q''_{CHF}(I)$ is the value obtained by the interpolation. F_1, F_2 and F_3 represent the correction factors expressed as:

$$F_1 = \max\Big(\frac{8\,10^{-3}}{D_h}, 0.79\Big)^{1/3} \, , \tag{1.41}$$

$$F_2 = \begin{cases} 1 & \text{standard value} \\ 0.6 & \text{bundle geometry} \, , \end{cases} \tag{1.42}$$

$$F_3 = \begin{cases} 1 & \text{if } \hat{x} < 0.9 \\ 10(1-\hat{x}) & \text{if } \hat{x} \geq 0.9 \, . \end{cases} \tag{1.43}$$

Dry-out mechanism. In the dry-out condition the main heat exchange mechanism is by natural or forced convection in gas. In particular in CATHARE code the dry out criteria is reached if one of the three following conditions are satisfied:

- The flow is in pure gas $\alpha > 0.99999$.
- The wall temperature is such that $T_w > T_{mfs}$.

- The heat flux wall-to-liquid q_{wl} and the heat flux wall-to-interface $q''_{w\to in}$ are such that: $q''_{w\to l} + q''_{w\to in} > q''_{CHF}$.

The same criteria utilized for the liquid in the [1.15]-[1.17] can be replaced in a gas environmental. For *natural convection* two cases can be distinguished:

- for laminar flow
$$Nu_{lam,NC}|_g = 0.401(Ra_g)^{1/4} \,, \tag{1.44}$$
- for turbulent flow
$$Nu_{turb,NC}|_g = 0.12(Ra_g)^{1/3} \,. \tag{1.45}$$

The Grashof number Gr and $D_{h,g}$ are defined as :

$$Gr_g = \frac{g\beta_g\rho_g^2 D_{h,g}^3|T_w - T_g|}{\mu_g^2} \,, \tag{1.46}$$

$$D'_{h,g} = D_{h,g}(1 - \sqrt{\max(0; 0.9999 - \alpha)}) \,. \tag{1.47}$$

For the *forced convection* two cases can be distinguished:

- for laminar flow
$$Nu_{lam,FC}|_g = 3.66 \,, \tag{1.48}$$
- for turbulent flow
$$Nu_{tur,FC}|_g = 0.023 Re_g^{0.8} Pr_g^{0.4} \,. \tag{1.49}$$

For the gas convection $Pr_g = 1$ and Re_g is computed as:

$$Re_g = \frac{\rho_g u_g D_{h,g}}{\mu_g} \,. \tag{1.50}$$

The heat transfer coefficient in boiling. Boiling heat transfer occurs when the heat transfer involves the change of phase. The literature identifies two main types of boiling, see (Tong and Tang, 1997): *pool boiling* and *flow boiling*. In the first case the heating surface is submerged in a pool of initially quiescent liquid, in the *flow boiling* the heating surface may be the channel wall confining the flow. In both cases there are several boiling regimes, in particular the buoyancy effects are significant in a *pool boiling* system while the forced-convection effects are significant in the *flow boiling* inside the channel.

The structure of CATHARE code is based on the typical regimes of pool boiling, see figure 1.4. All these regimes are previously observed by Leidenfrost (1756), Lang (1888), Nukiyama (1934), McAdams et al. (1941) and Farber and Scorah (1948). In the CATHARE code, the boiling heat transfer shall be divided in three cases: A, B and C. The zone A in turn is classified in 5 sub-zones depending on whether the liquid is heated or cooled by convection, with or without

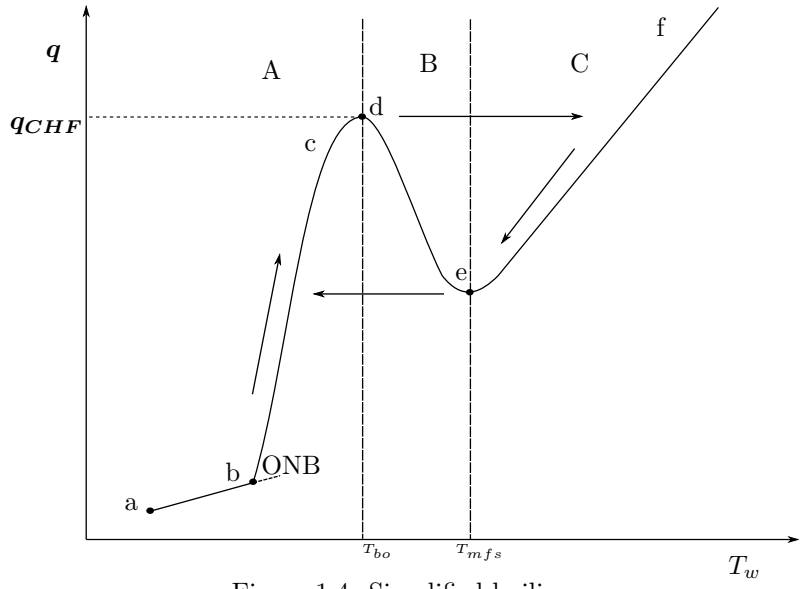

Figure 1.4: Simplified boiling curve.

nucleated boiling or only nucleated boiling. The zone B includes only one heat flux, the zone C is subdivided in three sub-zones which depend on the way to reach this point. All the heat flux are selected on the basis of a table which contains all the numerical index which values depends on the heat flux considered.

Zone A *Convection in liquid (zone a-b).* In this range the water is heated by single phase natural convection. The heat transfer coefficient is calculated by applying the criteria expressed in the [1.17].

Sub-cooled and nucleated boiling (zone b-c). This zone starts with a point called *Onset of Nucleated Boiling* ONB, starting from this point, local bubble near to the wall tend to condense. In this region the contribution to the nucleated boiling is calculated with the [1.28].

Zone B *Transition boiling (zone d-e).* By increasing the heat flux, the average temperature of the liquid rises above the saturation temperature, in this case the bubbles do not collapse, some of these start to merge into jets that feed into large over head bubble or "slugs" of vapor. Near to the point (d) the bubbles may obstruct the path of incoming liquid, the vapor forms an insulating blanket which covers the heating surface by deteriorating dramatically the heat exchange. The maximum heat flux just before the thermal crisis is called *Critical Heat Flux* q_{CHF} which value is computed with the expression [1.40]. The temperature calculated in this point is called T_{bo} (burnout temperature).

Zone C *Heat flux to dry wall (zone e-f).* In this region the film condensation in contact with a sub-cooled wall may occur. In case of convection, the expression [1.17] for the gas is utilized. The Berenson correlation is used to take into account the heat flux for film evaporation. By increasing the wall temperature the heat flux is mainly dissipated by radiation.

1.4 Space and time discretization

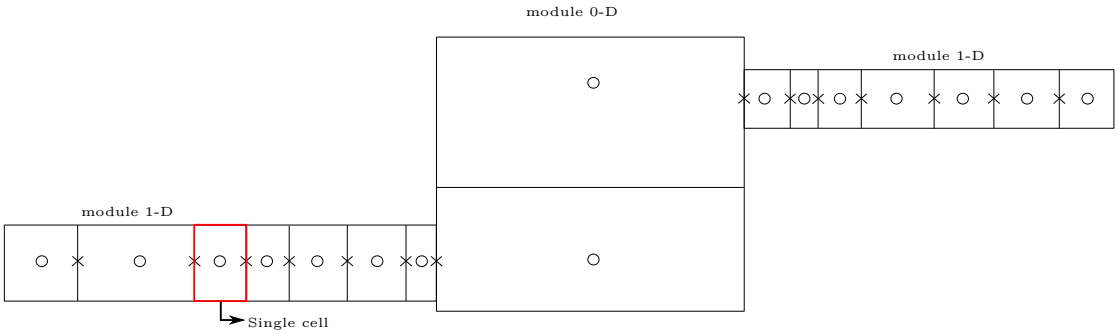

Figure 1.5: Example of a hydraulic circuit composed by the assembling of two axials and one volume element.

Figure 1.5 shows an example of a 1-D (axial) and 0-D (volume) elements connected each others. All the scalar variable (eg. void fraction, the enthalpy etc.) are computed in the center of the cell (0), while the velocities are computed on the cell faces (X). The scalar variables and the velocities can be staggered along the length of the axial element. To define the flux it is necessary to interpolate the values of the velocities in the points where are defined the scalar variables and vice-versa. The interpolation is based on a first order upwind scheme and the time integration is fully implicit. The system of non-linear equations is solved by Newton-Raphson method and the time step can be changed to optimize the number of the iterations.

1.5 Fuel rods in CATHARE code

In this section are described a general description of the main physic laws implemented in the Fuel sub-module. The Fuel rod in CATHARE is constituted by four different materials: the fuel pellet, the gap, the internal oxide layer, the cladding and the external oxide layer, see figure 1.6. Below are listed some ad hoc assumptions necessary for the mathematically modeling of this object.

- The fuel rod has a perfect symmetry of revolution;
- Along the fuel rod only the radial conduction is taken into account;
- The convection exchange inside the fuel gap is negligible;
- The fragility of the retained-alpha layer is not considered;
- There is no contact pellet-cladding (the thermal expansion of the fuel pellet never influences the cladding deformation).

Table 1.2 lists all fuel alloy types that the User can use. In the following a brief mathematically description of the physic models implemented inside this sub-module are presented, see figure1.7.

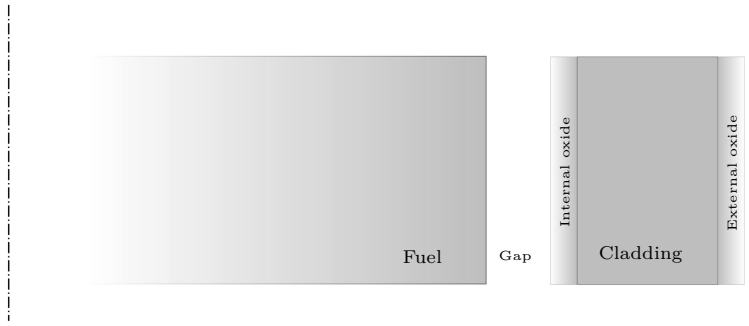

Figure 1.6: Graphical representation of the fuel sample in CATHARE code.

1.5.1 The thermal expansion

In the fuel pellet and in the cladding zone, the thermal expansion is taken into account. In particular for cylinder of radius r, it is possible to write the following thermal expansion equation

$$\frac{1}{R}\frac{\partial R}{\partial t} = \alpha_{exp}\frac{\partial T}{\partial t} \ , \tag{1.51}$$

where α_{exp} is the coefficient of the thermal expansion. Obviously, in parallel with the resolution of the [1.51], for each fuel and cladding mesh, the mass balance (continuity equation) must be satisfied.

Table 1.2: Fuel cladding type in CATHARE code.

Keyword	Description
ZRPHEBUS	PHEBUS type cladding (stress relieved Zircaloy)
ZRCEA	CEA type cladding (recrystallised Zircaloy)
ZRFRA	Framatome-ANP Zircalloy-4 type 1 cladding
ZRFRA2	Framatome-ANP Zircalloy-4 type 2 cladding
ZRM5	Framatome-ANP alloy-M5^{TM} type cladding
ZR4	Framatome-ANP Zircalloy-4 AFA-2G type cladding
ZR4H600	Framatome-ANP Zircalloy-4 AFA-2G hydrided to 600 ppm type cladding

Figure 1.7: Summary of the physic phenomena implemented inside the Fuel rod sub-module.

1.5.2 The creep strain

In the fuel cladding the creep strain is expressed as

$$\dot{\epsilon} = \frac{1}{R'_m}\frac{\partial R_m}{\partial t} = A_c \sigma_{es}^{n_c} \exp\Big(-\frac{Q_c}{\mathrm{R}T}\Big) \, . \tag{1.52}$$

R'_m is the initial value of the cladding mean radius, σ_{es} is the elastic stress expressed as

$$\sigma_{es} = \Delta P \frac{R_m}{\zeta_{clad}} \, , \tag{1.53}$$

where ΔP is the pressure difference between the fuel gap and the exterior, ζ_{clad} is the cladding thickness and R_m is the average value of the cladding radius defined as

$$R_m = \frac{R_{clad,e} + R_{fuel} + \zeta_{gap}}{2} \, . \tag{1.54}$$

ζ_{gap} is the fuel-cladding gap thickness. In the [1.50], A_c is an experimental constant which depends on the material and the particular creep mechanism, n_c is the stress exponent, Q_c is the activation energy. The [1.52] can be expressed also as

$$\ln\dot{\epsilon} = \ln A_c + n_c \sigma_{es} - \frac{Q_c}{\mathrm{R}T} \, . \tag{1.55}$$

By using the [1.55] is possible to derive experimentally:

(i) Q_c by plotting the natural logarithm of the creep strain against the reciprocal of temperature.

(ii) n_c by plotting the natural logarithm of the creep strain as a function of the natural logarithm of the elastic stress.

In the LORELEI test device design, a re-crystallized CEA type cladding is used. For this specific cladding, the Code implements the some specific correlations to calculate the the creep strain Holta (1970).

1.5.3 The elastic strain

To take into account the elastic strain, the following equation is implemented

$$\frac{1}{R_m}\frac{\partial R_m}{\partial t} = \frac{1}{\mathrm{E}}\frac{\partial \sigma_{es}}{\partial t} \, , \tag{1.56}$$

where E is the Young modulus.

1.5.4 Criterion for the Rupture of fuel cladding

Three different criteria are implemented inside the Code to take into account the fuel cladding failure:

- the Burst Criterion;
- the Strain Criterion;
- the Fragile Rupture criteria.

The fuel sample placed inside the LORELEI apparatus, satisfies always the first criteria, in particular the cladding failure is due mainly to a burst produced by a pressure difference between the fuel gap and external pressure. In the following the Burst Criterion is described.

Burst Criterion

To calculate the pressure gap P_{gap} inside the fuel sample, the code divides the fuel sample in m volumes v, see figure 1.8. Inside the $i-th$ volume the temperature can be considered uniform. Once the temperature in all the volumes has known, the perfect gas law is used

$$P_{gap} = \frac{n\mathrm{R}}{\sum_{i=1}^{m} \frac{v_i}{T_i}} \ . \tag{1.57}$$

The criteria of the rupture of the fuel cladding is derived from the EDGAR test analysis. In particular, the rupture occurs if the total cladding stress σ_{es} satisfies the following condition

$$\sigma_{es} = \Delta P \frac{R_m}{\zeta_{clad}} > \sigma_{es,b} \ . \tag{1.58}$$

The burst stress $\sigma_{es,b}$ depends on many factors as the average temperature of the cladding and the $\alpha \rightarrow \beta$ transition in the molecular structure of the zirconium alloy.

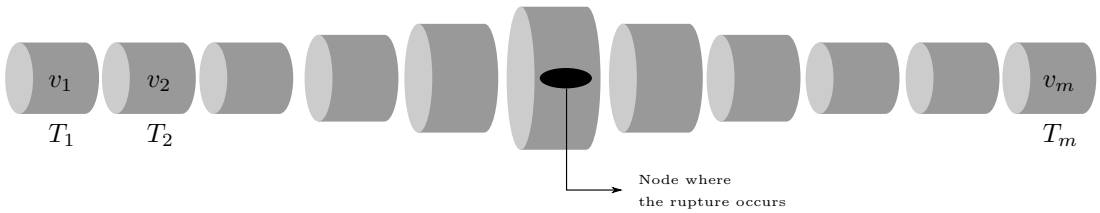

Figure 1.8: Graphical representation of the axial nodalization of the fuel sample in CATHARE code.

1.5.5 The radiative heat transfer inside the fuel gap

The radiation between the fuel pellet and the cladding is taken into account by considering an equivalent thermal resistance R_{rad} (Delhaye, 2012). In particular, the global thermal resistance

R_{tot} inside the fuel gap is expressed as

$$\frac{1}{\Omega_{tot}} = \frac{1}{\Omega_{cond}} + \frac{1}{\Omega_{rad}} \ . \tag{1.59}$$

Ω_{con} is the conduction resistance expressed as

$$\frac{1}{\Omega_{cond}} = \frac{k_{gap}}{\zeta_{gap}} \ , \tag{1.60}$$

where k_{gap} is the coefficient of conduction inside the gas gap. The resistance due to the radiation Ω_{rad} is obtained as

$$\frac{1}{\Omega_{rad}} = \frac{\sigma_{sb}}{\frac{1}{\epsilon_{fuel}} + \frac{1}{\epsilon_{clad}} - 1} \Big(\frac{T^4_{fuel} - T^4_{clad,i}}{T_{fuel} - T_{clad,i}} \Big) \ , \tag{1.61}$$

where σ_{sb} is the Stefan-Boltzman constant, ϵ_{fuel} and ϵ_{clad} are respectively the fuel and cladding emissivity.

1.5.6 The oxidation process

The reaction between the zirconium and steam is also taken into account in the Fuel rod sub-module. The exothermic reaction occurs for high value of temperature ($T > 1000\ ^\circ C$) and the chemical reaction is expresses in the form

$$Zr + 2H_2O \rightarrow ZrO_2 + 2H_2 + 586\, kJ \ .$$

If ω is the mass of Zircaloy reached per unit area $[kg/m^2]$, this can be expressed as

$$\omega^2 = K_p t \ . \tag{1.62}$$

In the [1.62] t is the Reaction Time and K_p is the Parabolic Reaction Rate constant which is expressed by using the Arrhenius equation

$$K_p = A e^{\frac{-E}{RT}} \ . \tag{1.63}$$

In the [1.63] A is the Pre-exponential factor expressed in $[kg^2/m^4 s^{-1}]$, E is the reaction activity energy $[J/mole]$, R is the gas constant $[J/K\, mole^{-1}]$ and T $[K]$ is the temperature. Several studies have carried out to investigate the value of K_p, in particular in the table 1.3 are listed the values of K_p for some common correlations found in the literature (Urbanic and Heidrick, 1978; Baker and Just, 1962; Cathcart et al., 1977; Leistikow and Schanz, 1987). By using the Fuel rod sub-module, only the Cathcart and the Baker and Just correlations may be chosen by the Code's User. By substituting $\omega = \rho_{Zr}\zeta_{oxy}$ in the [1.62] and by differentiating with respect to the time t, we obtain

$$\frac{d\zeta_{oxy}}{dt} = \frac{K_p}{2\rho^2_{Zr}\zeta_{oxy}} \ , \tag{1.64}$$

Table 1.3: Parabolic Reaction Rate according to some common correlations.

Reference	K_p $[kg^2/m^4 s^{-1}]$
Urbanic and Heidrick	$29.6\exp(-16820/T)$
Baker and Just	$3330\exp(-22896/T)$
Cathcart	$294.2\exp(-20100/T)$
Leistikow and Schanz	$425.8\exp(-20962/T)$

where ζ_{oxy} is the thickness of the zirconium oxidized and ρ_{Zr} is the zirconium density. We assume that the total energy released by 1 kg of zirconium oxidized is nearly $6.45\,10^6\,J$. Therefore it is easy to find the value of the heat flux q'' $[W/m^2]$ released on the Zircaloy surface as

$$q'' = (6.45\,10^6)(\rho_{Zr})\frac{d\zeta_{oxy}}{dt} = 2.13\,10^{10}\frac{K_p}{\rho_{Zr}^2\zeta_{oxy}} \quad . \tag{1.65}$$

If $\Delta\zeta_{oxy}$ is the thickness of zirconium reached in a period of time Δt then the total number of moles of hydrogen released per unit area is

$$\Phi_{H_2} = \frac{2\rho_{Zr}}{M_{Zr}}\Delta\zeta_{oxy} = 1.44\,10^5\Delta\zeta_{oxy} \; . \tag{1.66}$$

The Reaction Rate (R.R.) defines the speed of the chemical reaction, it may be defined as the variation of the concentration of substance along the time

$$\text{R.R} = -\frac{dN_{Zr}}{dt} = -\frac{1}{2}\frac{dN_{H_2O}}{dt} = \frac{dN_{ZrO_2}}{dt} = \frac{1}{2}\frac{dN_{H_2}}{dt} \quad . \tag{1.67}$$

The hydrogen mass flow produced $\dot{m}_{H_2}$ is then determined as

$$\frac{1}{2M_{H_2}}\dot{m}_{H_2} = \frac{1}{M_{ZrO_2}}\dot{m}_{ZrO_2} \quad . \tag{1.68}$$

If H is the height of the fuel cladding, the zirconium dioxide mass flow can be expressed as

$$\dot{m}_{ZrO_2} = 2\pi H R_{clad,e}\rho_{ZrO_2}\frac{d\zeta_{oxy}}{dt} \; . \tag{1.69}$$

By substituting the [1.69] in the [1.68], we obtain the mass flow of hydrogen released

$$\dot{m}_{H_2} = 4\frac{M_{H_2}}{M_{ZrO_2}}(\pi H R_{clad,e}\rho_{ZrO_2})\frac{d\zeta_{oxy}}{dt} \; . \tag{1.70}$$

By substituting the [1.63]-[1.64] in the [1.70], we obtain

$$\dot{m}_{H_2} = 2\frac{M_{H_2}}{M_{ZrO_2}}\frac{\rho_{ZrO_2}}{\rho_{Zr}^2}\frac{\pi H R_{clad,e}}{\zeta_{oxy}}Ae^{\frac{-E}{RT}} \; . \tag{1.71}$$

As said previously, numerically the Fuel sub-model is divided into m different meshes to which the height h_j is associated. Considering that the densities depends on the temperature computed

in each single mesh, the total hydrogen mass flow produced may be expresses as

$$m_{H_2} = 2\pi \frac{M_{H_2}}{M_{ZrO_2}} \sum_{j=1}^{m} \left(\frac{\rho_{ZrO_2}}{\rho_{Zr}^2} \frac{HR_{clad,e}}{\zeta_{oxy}} A e^{\frac{-E}{RT_{clad}}} \right)_j . \tag{1.72}$$

If $R_{oxy,e}$ is the radius of the cladding included the thickness of the external oxide then the variation in volume of the thickness oxide can be expressed as

$$\frac{\partial V_{oxy}}{\partial t} = \frac{[R_{oxy,e}^2(t+\Delta t) - R_{clad,e}^2(t+\Delta t) + R_{clad,e}^2(t) - R_{oxy,e}^2(t)]\pi H}{\Delta t} , \tag{1.73}$$

or if we consider the $n-th$ numerical time step as

$$\left.\frac{\Delta V_{oxy}}{\Delta t}\right|^n = \frac{[R_{oxy,e}^2|^{n+1} - R_{clad,e}^2|^{n+1} + R_{clad,e}^2|^n - R_{oxy,e}^2|^n]\pi H}{t^{n+1} - t^n} . \tag{1.74}$$

Finally the instantaneous power generated by the zirconium oxidation may be expressed as

$$P_{oxy}|^n = (586\,10^6) \sum_{j=1}^{m} \left(\frac{\Delta V_{oxy}}{\Delta t} \frac{\rho_{ZrO_2}}{M_{ZrO_2}} \right)\Bigg|^n . \tag{1.75}$$

Chapter 2

Overview of the LOCA accident and description of some integral LOCA-test devices

The study of the LOCA testing methodology involves a large number of different science-based approaches, this because this field of engineering differs in accordance with the specif purpose of study. In general, in the LOCA literature, a series of facilities go from a complete fuel bundle to a non-irradiated fuel assembly, are needed to investigate the thermal and mechanical stress of the fuel alloy elements, such as the alpha-beta transformation, the zirconium-steam oxidation or, physical problems involving the thermal-hydraulic of the system. Sometimes, the entire technical apparatus are quite expensive and complicated, in fact they require sophisticated instrumentation and post-test evaluation. This chapter describes a typical LOCA accident and its definition in a common Nuclear Regulatory, furthermore it provides to a general view of the main experimental facilities used to support this field of research in the previous years. At the end, a classification of LORELEI test device and an analysis of its technological similarities with other experimental devices is described.

2.1 Definition of Loss of coolant accident

The definition of Loss of coolant accident (LOCA) given by the United States Nuclear Regulatory Commission (U.S.NRC) can be summarized by the following definition. *Loss of coolant accident means those postulated accidents that result from the loss of reactor coolant at the rate in excess of the capability of the reactor coolant makeup system from breaks in the reactor coolant pressure boundary, up to and including a break equivalent in size to the double-ended rupture of the largest*

pipe of the reactor coolant system.

In the nuclear industry the accidental scenario are divided into three main categories, the Anticipated Operational Occurences (AOO's), the Design Basic Accident (DBA's) and Severe Accident. The AOO's are expected to occur one or more times during the operation life of the nuclear reactor. The DBA's are more serious events which are not expected to occur during the life in a nuclear power plant. The Severe Accidents are a very low frequency events during which the reactor core configuration might modify and a significant radionuclide released from the damage core is expected. For all the typologies of accident, numerous acceptance criteria must be fulfilled in such a way as to minimize the radiological consequences to the public. In the field of the DBA's inspection measures, every nuclear power plant before their licensing must follow some important norms introduced in a state-of-art report (Parson et al., 1986) and reported in the U.S.NRC regulation (Utited States Nuclear Regulatory Commission, b) or in others Nuclear Regulatory Commissions stabilized for various countries engaged in the nuclear industry. In this chapter we refer only to the rules applied by the U.S. Nuclear Regulatory Commission.

2.2 Emergency Core Cooling System (ECCS)

If we are talking about of the DBA, it is necessary to define the concept of Emergency Core Cooling System (ECCS) which is the primary security system for this type of accident scenario. An Emergency Core Cooling system is a *system needed to provide abundant emergency core cooling. The system safety function shall be to transfer heat from the reactor core following any loss of reactor coolant at a rate such that (1) fuel and clad damage that could interfere with continued effective core cooling is prevented and (2) clad metal-water reaction is limited to negligible amounts...."*

Generally, inside a standard PWR the ECCS shall be divided into different parts: high, intermediate and low Pressure Injection System. For details one can refer to figure 2.1.

HPIS When the internal reactor pressure decreases under a certain limit, a signal triggers the High Pressure Injection System (HPIS) that provides water from the Refueling Water Storage Tank (RWST) through the use of a high pressure pump. The water is injected in the cold leg.

IPIS The Intermediate Pressure Injection System (IPIS) shall be activated when the internal pressure is still high (small and intermediate size of the break). The water is pumped from the RWST and injected inside the cold leg.

Cold leg Accumulator This is a passive system formed by a tank that contains a large amount of borated water with a pressurized nitrogen gas bubble in the top. When the pressure inside the primary system drops below a certain limit, the nitrogen forces the borated water out the tank into the reactor cooling system.

LPIS The Low Pressure Injection System (LPIS) is designed to be operational when the reactor pressure reaches very low values following a large break. This system allows to pump the water spilled from the break and collected in the containment sump. Before being injected inside the cold leg, the water passes trough an exchanger called Residual Heat Removal (RHR).

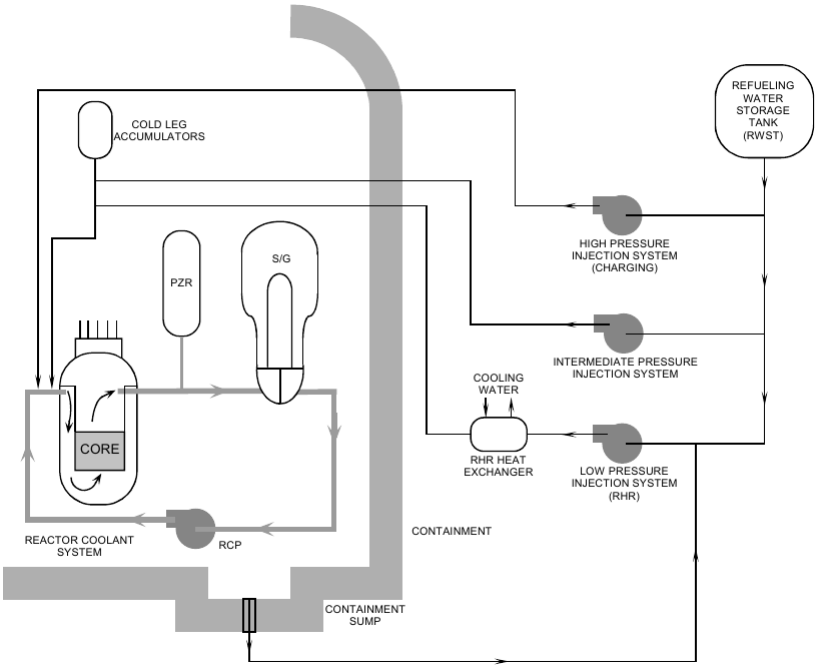

Figure 2.1: Emergency Core Cooling Reactor (ECCS) in a PWR, from (Utited States Nuclear Regulatory Commission, a, pp.25).

Acceptance criteria for the ECCS in the LWR

According to the United States Nuclear Regulatory Commission (U.S.NRC) the current legislation in the field of the *Acceptance criteria for emergency core cooling system for light-water nuclear power reactors* is readily available by visiting the web site of the U.S.NRC. The Appendix K sets forth the documentation requirements for each ECCS evaluation model. For example, the reader can found all the documentation of the Appendix K by consulting the U.S.NRC web site (Utited States Nuclear Regulatory Commission, c) or in other regulation written for different countries. The acceptance criteria for emergency core cooling system for light-water nuclear power reactors can be summarized in five classes: criteria for the Peak cladding temperature (a), Maximum cladding oxidation (b), Maximum hydrogen generation (c), Coolable geometry

(d) and Long-term cooling point (e). In details we have:

(a) Each boiling or pressurised light-water nuclear power reactor fueled with uranium oxide pellets within cylindrical Zircaloy or ZIRLO1 cladding must be provided with an emergency core cooling system (ECCS) that must be designed so that its calculated cooling performance following postulated loss-of-coolant accidents conforms to the criteria set forth in paragraph (b) of this section. ECCS cooling performance must be calculated in accordance with an acceptable evaluation model and must be calculated for a number of postulated loss-of-coolant accidents of different sizes, locations, and other properties sufficient to provide assurance that the most severe postulated loss-of-coolant accidents are calculated.

(b) The maximum fuel element cladding temperature shall not exceed $2200°F$.

(c) The calculated total oxidation of the cladding shall nowhere exceed 0.17 times the total cladding thickness before oxidation. As used in this subparagraph total oxidation means the total thickness of cladding metal that would be locally converted to oxide if all the oxygen absorbed by and reacted with the cladding locally were converted to stoichiometric zirconium dioxide. If cladding rupture is calculated to occur, the inside surfaces of the cladding shall be included in the oxidation, beginning at the calculated time of rupture. Cladding thickness before oxidation means the radial distance from inside to outside the cladding, after any calculated rupture or swelling has occurred but before significant oxidation. Where the calculated conditions of transient pressure and temperature lead to a prediction of cladding swelling, with or without cladding rupture, the unoxidized cladding thickness shall be defined as the cladding cross-sectional area, taken at a horizontal plane at the elevation of the rupture, if it occurs, or at the elevation of the highest cladding temperature if no rupture is calculated to occur, divided by the average circumference at that elevation. For ruptured cladding the circumference does not include the rupture opening.

(d) The calculated total amount of hydrogen generated from the chemical reaction of the cladding with water or steam shall not exceed 0.01 times the hypothetical amount that would be generated if all of the metal in the cladding cylinders surrounding the fuel, excluding the cladding surrounding the plenum volume, were to react.

(e) Calculated changes in core geometry shall be such that the core remains amenable to cooling.

(f) After any calculated successful initial operation of the ECCS, the calculated core temperature shall be maintained at an acceptably low value and decay heat shall be be removed for the extended period of time required by the long-lived radioactivity remaining in the core.

2.3 PWR large break LOCA

The Loss of Coolant Accident is one of the DBA's might occur in a LWR. In this type of accident, the initiating event is the double-ended guillotine break of the large coolant pipe that connect the reactor vessel with the main circulation pump, see figure 2.2(a)-(b). In accordance with the break size the LOCA are subdivided in small, medium and large break LOCA accident. Figure 2.3 shows a typical large breach LOCA transient:

1. *Blow down period [0-30 s]* During this first step, all the primary coolant is lost and the core voids within a few seconds after the break; the cladding temperature increases and departure from nuclear boiling is reached (first peak in the figure 2.3). The negative void reactivity and the SCRAM procedure immediately shut down the core. This leads to a fuel pellet central temperature drop and a flattening of the radial temperature profile. With the cooling decreasing and redistribution of fuel stored energy the cladding temperature increases. The dynamic interaction between the pump and the break might cause intermittent flow reversal. When the break occurs, the pressure inside the system decreases, the HPIS is triggered in order to pump water inside the reactor, see figure 2.2(c). When most of the water injected is lost by the break the injection from the Cold Leg Accumulator begins. However much of the injected water is swept around the downcomer into the cold leg and out of the break. Thanks to the RHR some water begins to cover the lower plenum vessel, see figure 2.2(d).

2. *Refill period [30-40 s]* The water accumulated begins to fill the lower plenum. However the fuel temperature increases due the decay heat and the pressure decrease leads to ballooning and burst when the cladding temperature (depending on the initial conditions) is around 700-1000 $°C$. This cladding ballooning could lead to a blockage of some of the flow channels.

3. *Reflood period [40-200 s]* After the lower plenum has filled, the water starts to refill the core. The quenching progress generates a two-phase mixture which cools slightly the upper part of the core. However the fuel cladding temperature continues to increase up to 1000-1200 $°C$ by leading to its oxidation. In this phase some additional fuel rods may burst. The hydrogen produced by the oxidation can interact with the metal (hydriding). When the quench front reaches the higher temperature fuel, the abrupt change of heat exchange and hence the thermal shock can lead to brittle fracture. Once the liquid enters into this fracture other fission products are released.

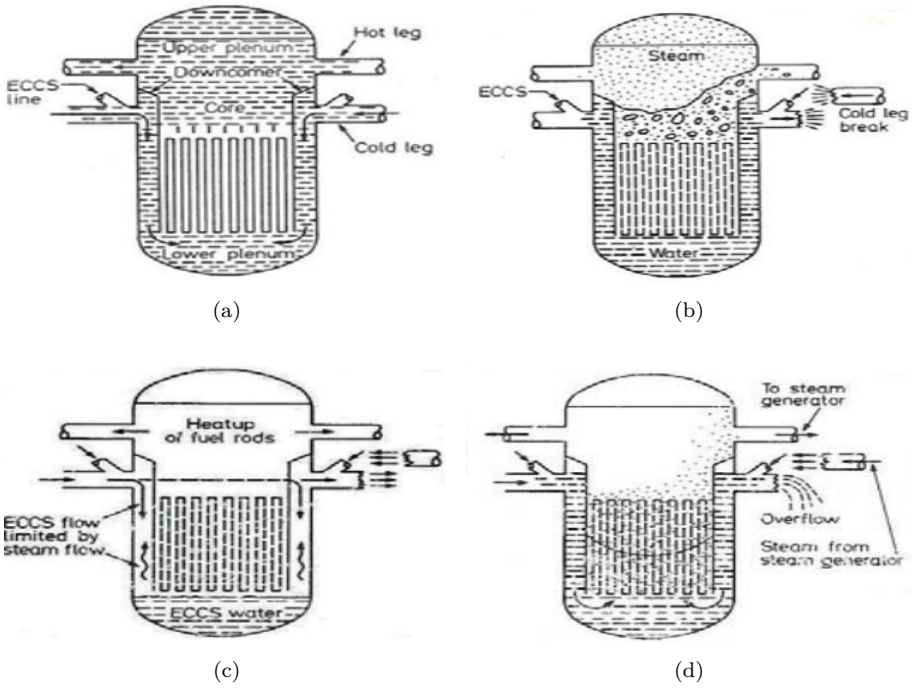

Figure 2.2: Nuclear reactor vessel: during the nominal condition (a), when the break in the cold break occurs (b), when ECCS is triggered and the water starts to be injected inside the reactor vessel (c), when the water overflow goes out from the break before being injected again in the reactor core by means of the LPIS (d), from (Hewitt, G F)

2.4 Overview of LOCA testing methodology

2.4.1 Introduction

The entire methodology to understand the main effects occurring following a LOCA required a large number of different techniques which differ according to the effects one want to investigate. The experimental experiences might consider the use of a complete fuel bundle irradiated or not, furthermore to set up the entire apparatus is quite complicated and requires specific instrumentation. A general classification of the different tests typology with regard to the study of the LOCA experimental apparatus is summarized in the figure 2.4. In the next paragraph a brief description of some fully integrated test (In-reactor test and Out-of-reactor-test) is presented. The reader can find a more detailed description of all the different type of test by consulting the Nuclear Energy Agency report (Pettersson et al., 2009).

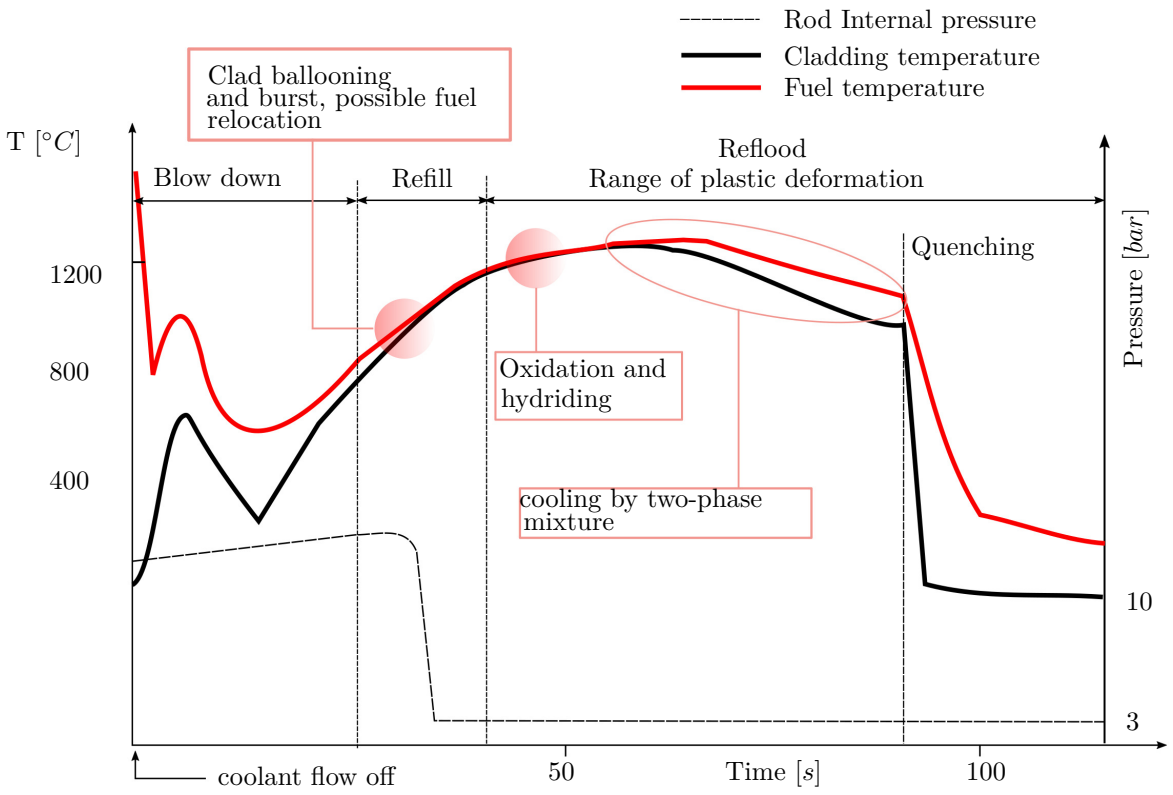

Figure 2.3: Typical large breach LOCA transient.

2.4.2 Fully integrated test

In-reactor test

The FR2 facility. The FR2 is a research reactor whose construction began in 1957 in Eggenstein-Leopoldshafen in Germany. The organization charged to build this heavy water cooled reactor was the Kernforschungszentrum Karsruhe evolved today in the Karlsruhe Institute of Technology (KIT). The main objective of this test campaign was to provide information about the effect on the fuel rod under a LOCA condition. Figure 2.5 shows a vertical section of the "in-pile" test. During the steady state, the pressure inside the system was maintained at 60 bar, the steam temperature at 300 $°C$ and the coolant mass flow along the sample was of 120 kg/s. The fuel rod had the same dimension of those located in a typical PWR German 1300 MW reactor with an active length of 50 cm. The tests were conducted with unirradiated and pre-irradiated fuel rod. The main parameters modified for each test were the burn-up, which varied between 2500 and 35000 $MWd/$t, the internal pressure gap P_{gap} between 25 and 125 bar and the heat-up rate between 6÷20 K/s. A certain number of reference tests by using an electrical heater were

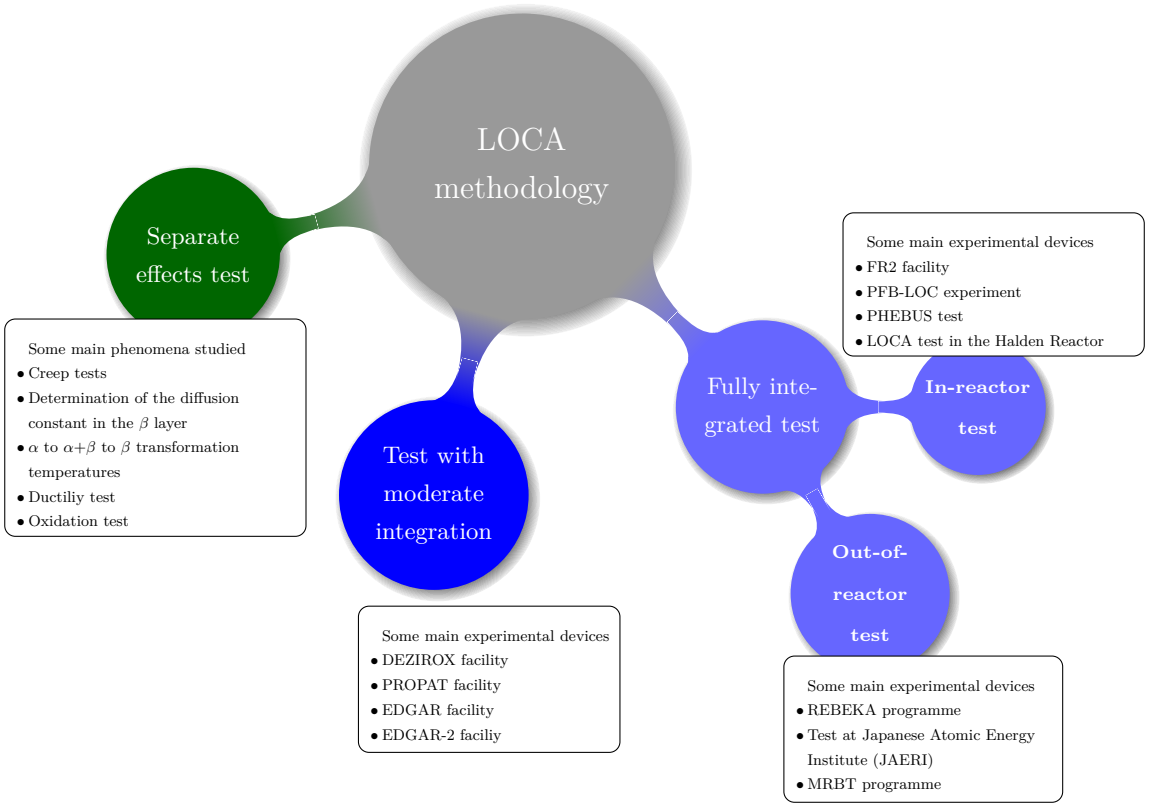

Figure 2.4: LOCA testing methodology.

conducted. During the pre-irradiation phase, the fuel rod was pressurized with helium at 0.3 *bar* and the coolant temperature was fixed at 60 $°C$ at 2.5 *bar*. The pre-irradiation phase started with the fuel rod pressurization by injecting helium into the fuel gap. During this phase, the rod was exposed to standard conditions associated to a typical PWR LB-LOCA transient with a Linear heat generation rate which varied from 250 to 425 W/cm. The accidental scenario started with the interruption of the coolant liquid flow by closing the *Shutoff valve*. The depressurization occurred by opening the *Relief valve* (up to 0.1 *bar* within 8 to 10 *s*), see figure 2.6. Once the fuel cladding reached the target value of temperature, the Reactor is triggered. When the fuel cladding stabilized, the *Shutoff* valve was opened again and the cooling mass flow was reactivated in order to study the quenching phase. Table 2.1 shows the results obtained from this test campaign (Karb et al., 1982).

PBF-LOC experiment in the Power Burst Facility. The Power Burst Facility (PBF) was a water cooled and moderated tank research reactor at the Idaho National Lab (INL). The "in-pile" device PFB-LOC located inside the reactor was utilized to simulate a large break LOCA. The test was performed with unirradiated and irradiated fuel rods, the entire apparatus

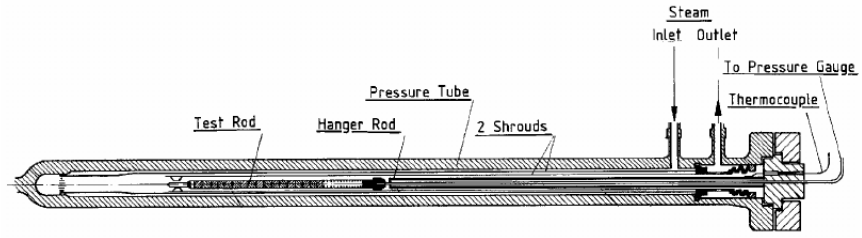

Figure 2.5: Cross section view of the FR2 "in-pile" device, from (Pettersson et al., 2009, pp.115).

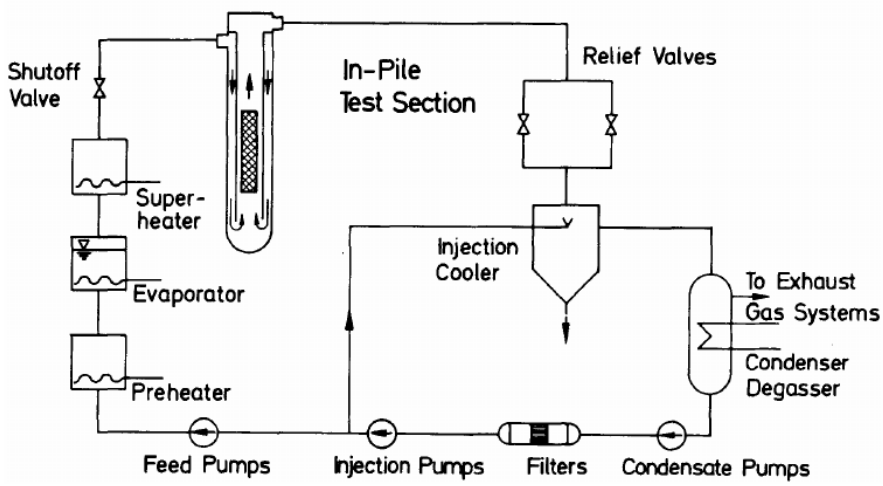

Figure 2.6: Simplified layout of the FR2 loop in the FR2 reactor, from (Pettersson et al., 2009, pp.115).

was design to investigate the major parameters determining the cladding circumferential strain during the ballooning, the corresponding cladding temperature and the differential pressure. The cross section view in the figure 2.7, depicts the four fuel rods installed inside the "in-pile" device. The active length of a single rod was of 0.91 m. The test sequence started with the steady-state transient during which the fuel rods were cooled with a certain liquid mass flow and the power maintained at 45 kW/cm. The accidental simulation started with the opening of the control valves and consequent water discharging. The maximum fuel cladding temperature was controlled in order to remain in a target range. Table 2.2 summarizes the main results of this test campaign (Pettersson et al., 2009, pp.246).

PHEBUS LOCA program. Placed at the CEA Nuclear Research Center of Cadarache, the PHEBUS facility was an experimental reactor that has been operational since 1978. The first part of this vast test campaign was to study the thermal-hydraulic and the mechanical behavior of the fuel cladding during a Large Break LOCA. This first part of the entire experience, performed

Table 2.1: Summary of the results conducted in the FR2 facility.

Test	Burnup $[GWd/t]$	Λ $[K/s]$	t_b $[s]$	$T_{clad,b}$ $[K]$	Max. T_{clad} $[K]$	$P_{gap,b}$ $[bar]$	Max P_{sys} $[bar]$	Maximum circumferential strain [%]
A1.0	0	7.0	79	1083	1275	50	54	64
A1.2	0	11.5	a	-	1281	-	-	-
A2.1	0	19.0	20	1093	1323	88	100	36
A2.2	0	12.1	38	1133	1301	58	75	56
A2.3	0	13.0	55	1288	1288	25	27	35
B1.1	0	17.5	40	1173	1304	52	59	30
B1.2	0	8.7	72	1118	1283	45	55	25
B1.3	0	12.5	37	1118	1258	61	71	34
B1.4	0	9.3	b	-	1291	-	-	-
B1.5	0	9.3	72	1183	1282	45	58	60
B1.6	0	8.2	56	1098	1288	80	90	38
B1.7	0	11.5	41	1113	1163	61	71	34
B3.1	0	10.0	46	1098	1289	79	91	37
B3.2	0	12.1	55	1188	1284	50	61	50
C1	2.5	14.0	47	1173	1290	46	56	51
C2	2.5	12.6	58	1218	1223	30	34	39
C3	2.5	13.2	32	1022	1046	98	112	37
C4	2.5	12.1	41	1088	1284	65	81	44
C5	2.5	9.3	78	1189	1276	22	25	62
E1	8	12.5	59	1183	1282	23	26	e
E2	8	11.7	29	981	1272	113	129	-
E3	8	11.2	47	1133	1273	49	56	-
E4	8	11.6	35	1054	1278	72	86	-
E5	8	11.5	63	1129	1206	19	26	67
F1	20	10.6	43	1163	1289	19	26	67
F2	20	8.7	57	1166	1280	53	62	38
F3	20	10.1	57	1205	1290	42	46	27
F4	20	11.1	37	1108	1322	72	84	34
F5	20	10.1	49	1153	1279	60	72	41
G1.1	35	10.1	a	-	1283	-	-	2
G1.2	35	c	55	1003	1282	68	75	30
G1.3	35	9.0	70	1163	1250	41	51	62
G1.4	35	6.1	58	1058	1244	83	91	33
G1.5	35	12.0	60	1053	1200	52	60	41
G2.1	35	13.6	38	1142	1225	37	d	32
G2.2	35	13.0	31	1119	1213	66	75	28
G3.1	35	12.3	55	1173	1203	33	d	46
G3.2	35	15.4	33	1111	1213	57	74	41
G3.3	35	9.8	29	1023	1220	111	128	32

[a] Rod leaked; no burst.
[b] No internal overpressure, no burst.
[c] Abnormal heat-up; burst during temperature plateau.
[d] Rod leaked; no max. pressure.

in a 5x5 fuel bundle reactor with pressurized rods, was called Phebus LOCA program and was divided in two different parts.

I) Eight tests were conducted between the years 1980-1982. The aim of these tests was to reach a prototypical tests series to reach the thermal-hydraulic conditions in order to evaluate the power history of the system, the size and the location of the break and the proper working of the ECCS.

II) Six more test were conducted between the years 1982-1984. During these tests, the study of the thermal-mechanical behavior involves the fuel rod during the LOCA accident was performed.

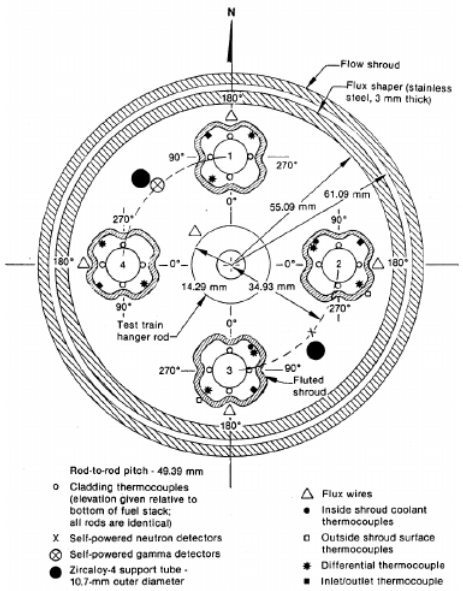

Figure 2.7: Cross section of the PBF-LOC, from (Pettersson et al., 2009, pp.117).

Table 2.2: Summary of the results conducted in the PFC-LOC facility.

Test	P_{gap} $[bar]$	Burnup $[MWd/t]$	Λ $[K/s]$	Maximum circumferential elongation [%]	t_{fail} $[s]$	$T_{clad,b}$ $[K]$
LOC-3	24.5	0	4.3	29	15.0	1190
	32.8	15960	20.0	40	7.9	1300
	49.2	0	15	20	10.1	1110
	47.5	16620	15	41.6	13.1	1120
LOC-5	24.1	17660	0	35	10.5	1350
	48.3	0	100	19	2.75	1160
	48.3	0	70	48	7.8	1350
LOC-6	24.1	0	-	<1	-	-
	24.1	10800	-	13.6	-	-
	47.4	0	100	31	5.2	1098
	48.3	10800	0	74	18.2	1066

Basically, the loop of the of the entire apparatus was composed by a pool type reactor inside which the nuclear power was supplied (LHGR_{hp} up to 57 W/cm) and a hydraulic loop to obtain the same hydraulic conditions inside a typical french PWR. During the LOCA phase, the power of the core was controlled to simulate the residual power in the experimental fuel rods. The test train was changed in accordance with the test performed. In the first Steady State phase (see figure 2.8), the fuel rods were cooled by a forced-convection liquid flow. To calibrate the inlet water temperature, the water, before being pumped in the bottom part of the core, passed inside in a heater to be heated up to 320 $°C$. At the end of this phase, the blowdown phase started,

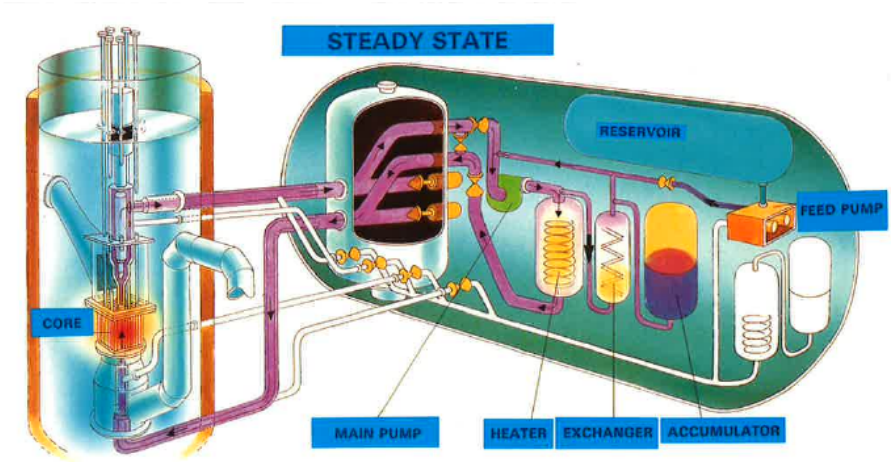

Figure 2.8: PHEBUS's schematic layout during the steady state phase, courtesy of CEA.

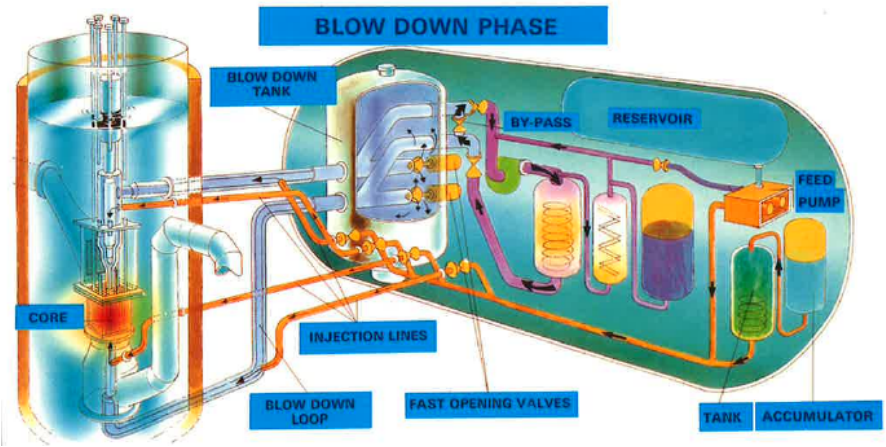

Figure 2.9: PHEBUS's schematic layout during the Blowdown phase, courtesy of CEA.

see figure 2.9. The blowdown started by opening the by-pass valves which allowed to deviate the feed water flow. The opening of some valves allowed to discharge out all the water remained inside the primary circuit in a blowdown tank by depressurizing the entire system. In the follow re-flooding phase, the water extracted from an accumulator was flowed inside an injection line connected with the reactor core. Tables 2.3-2.4 summarize the values obtained during the Part I and II of the Phebus LOCA program (Adroguer et al., 1983; CEN).

LOCA test at the Halden Reactor. The Halden nuclear Reactor is an experimental reactor became operative in the 1958 at the Institute of Energy Technology (IFE). Inside the reactor, the experimental experiences IFA-511X, IFA-54X and IFA-650X were conducted in order to investigate the behavior of the fuel rod during a LOCA accident.

Table 2.3: Results obtained from the Part I of the PHEBUS LOCA program.

Test	Break Location	LHGR$_{hp}$ $[W/cm]$	P_{gap} $[bar]$	Max. T_{clad} $[K]$
206	Hot leg	0	10	-
207	Hot leg	270	10	-
208	Cold leg	0	10	-
20	Cold leg	270	10	-
210	CL+HL X=1.3	0	10	-
21	CL+HL X=1.3	320	10	933
212	CL+HL X=1.3	460	10	1040
213A	CL+HL X=1.3	490	10	1380

X Ratio between the break size along the cold Leg (CL) and along the hot leg (HL).

Table 2.4: Results obtained from the Part II of the PHEBUS LOCA program.

	Test	215P	215R	216	217 ter	218	219
Steady state	LHGR$_{hp}$ $[W/cm]$	488	500	470	500	460	480
	P_{sys} $[bar]$	154	155	152	154	156	157
	Mass flow rate $[kg/s]$	10.1	10.2	10.1	10.2	9.9	10.3
	P_{gap} $[bar]$ at 20 $^{\circ}C$	40	40	30	30	30.5	30
Blow-down	t_{fail} $[s]$	50-60	23-26	146-171	23-33	115-127	215-234
	$P_{gap,fail}$ $[bar]$	60-75	60-75	33-37	40	55	40
	$T_{clad,b}$ $[^{\circ}C]$	800-860	800-860	900	900	850	880
	Max. T_{clad} $[^{\circ}C]$	900	1250	1400	1200	1400	1250
	Max. ϖ_e $[\mu m]$	30	41	77	50	80	120
	Deformation [%]	20-50	20-50	15-32	-	15-50	27-46

IFA-511 and IFA-54 apparatus. The IFA-511X and IFA-54X were pure thermal-hydraulic experimental tests. The cross section of the IFA-511 was composed by 7 fuel rods (6 peripheral rods and one central reference rod) in a circular configuration, see figure 2.10. Four triangular tubes were used as downcomers for the liquid coolant.

Figure 2.11 shows the cross section of the IFA-54 experimental device. In particular 5 instrumented fuel rods were located in a cruciform disposition. The IFA-511X test series were devised to compare possible thermal-hydraulic differences between the utilization of a real fuel rods and an electrical rod simulators during the quenching phase. The IFA-54X test series were performed to examine the thermal efficiency of the fuel cooling, once a significant reduction of the coolant flow area (as a result of the clad ballooning), has verify. Tables 2.5-2.6 summarize the type of the tests performed and the rod types utilized. Each IFA-511.2 test series were performed with a reflood liquid velocity of nearly 10 cm/s with a average LHGR equal to 10 W/cm (series A), 20 W/cm (series B) and 30 W/cm (series C). The other test series (D, E, F, G, and H) were conducted at an intermediate power of 20 W/cm with a low and intermediate flow rate ($2 \div 7$ cm/s). Some test with or without the blowdown phase, were performed by means of a semiscale

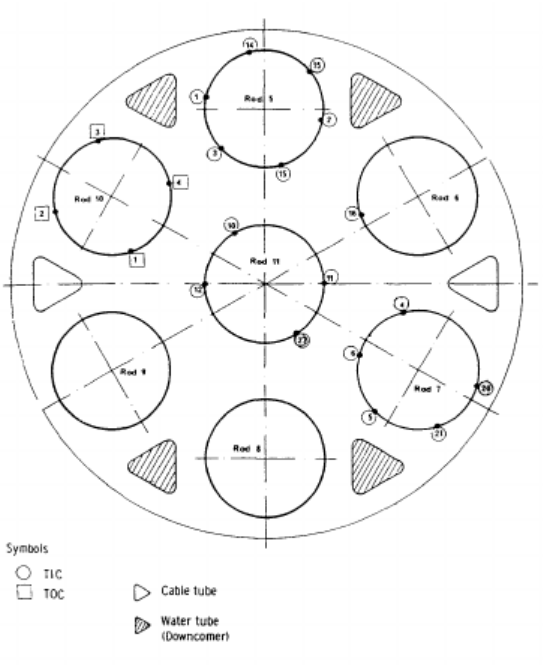

Figure 2.10: Cross section of the IFA-511 assembly, from (Pettersson et al., 2009, pp.121).

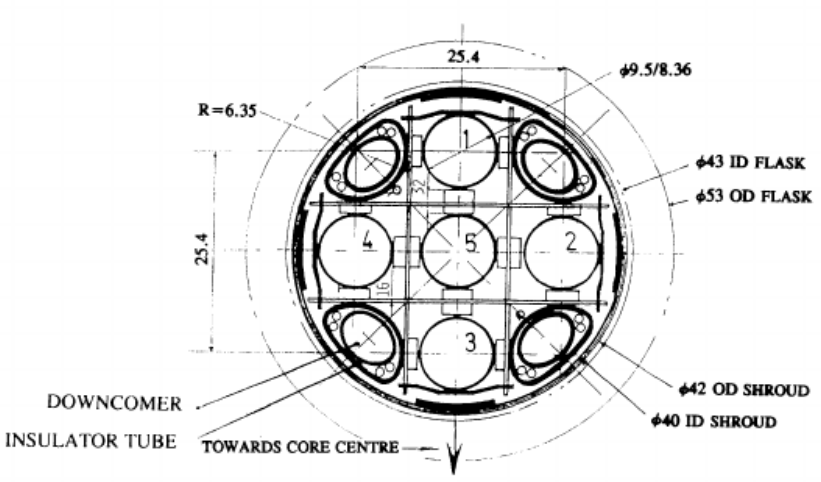

Figure 2.11: Cross section of the IFA-54 assembly, from (Pettersson et al., 2009, pp.121).

electrical heater and a heater just like utilized for the REBEKA test which design is described in the follow of this chapter. During the test without the blowdown phase, the heat-up phase begun once dry condition has already started. In this last condition, the LHGR and the reflood liquid velocity could vary between the 18 and 26 W/cm and between 2.25 and 10.1 cm/s.

IFA-650 test series. The Halden IFA-650 LOCA tests were conducted in 2003. In this thesis are

Table 2.5: Summary of all the test series of the IFA-511X and IFA-54X.

Test series	Heating Elements	Test identification	Test type
IFA-511.2	Nuclear rods	A1-A3,B1-B3, C1-C3	Blowdown-reflood tests
		B4-B9, D1, E1-E7	Blowdown-reflood tests
		F1-F3, G1, H1, H2	Blowdown-reflood tests
		K1-K4, J1, J2	Blowdown-reflood tests
IFA-511.3	Semiscale electrical heater	B5-B9, E5-E7, F1, G1	Blowdown-reflood tests
IFA-511.4	Rebeka elctrical heater	7404-7410	Blowdown-reflood tests
		7822-7829	Reflood test without blowdown
		7830-7832	Reflood test
IFA-511.5	Semiscale electrical heater	9332-9337,9345-9347	Reflood test without blowdown
		9338-9344	Blowdown-reflood tests
IFA-541	Nuclear rods	A1-A10, B1, B2, C1-C4	Blowdown-reflood tests
		D1-D6	Blowdown-reflood tests
		9771-9780	Blowdown-reflood tests
IFA-543	Nuclear rods		Ballooning test
IFA-544	Rebeka electrical heater		Ballooning test
IFA-545	Nuclear rods		Ballooning test
IFA-546	Rebeka electrical heater		Ballooning test
IFA-547	Nuclear rods		Ballooning test

Table 2.6: Summary of the power rod used in the IFA-511X and IFA-54X test series.

	Nuclear Rod (IFA-511)	Nuclear rod (IFA-54X)	Semiscale EH	REBEKA EH
Fuel rod D $[mm]$	9.07	8.196	-	-
Pellet height $[mm]$	9	10.5	-	-
Filler gas	He (bar)	-	-	-
$D_{clad,e}$ $[mm]$	-	10.75	-	-
$D_{clad,i}$ $[mm]$	9.30±0.02	8.37	-	0.75
Heated length $[mm]$	1500±2	1482	1486±10	1500
Aluminia pellet D_e $[mm]$	-	-	-	6.08
Aluminia pellet D_i $[mm]$	-	-	-	6.08

presented the results of the test series 4,9, 10 and 14. The objective of the IFA-650X test series were to evaluate the ballooning size and the consequences of the fuel cladding oxidation, the fuel fragment relocation inside the ballooned region and the "secondary transient hydriding" on the inner side of the cladding (around the burst region). The "in-pile" section of the apparatus is shown in the figure 2.12, figure 2.13 shows a cross section of the device at the height of the heated parts. The length of the inner active rod varied between the 360-480 mm. The fuel rod was surrounded by an electrical heater shroud and a pressure flask. The heater provided to

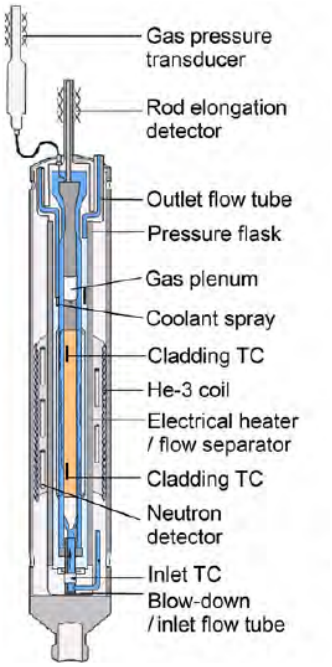

Figure 2.12: "In-pile" section of IFA-650, from (Jernkvik, 2016, pp.6).

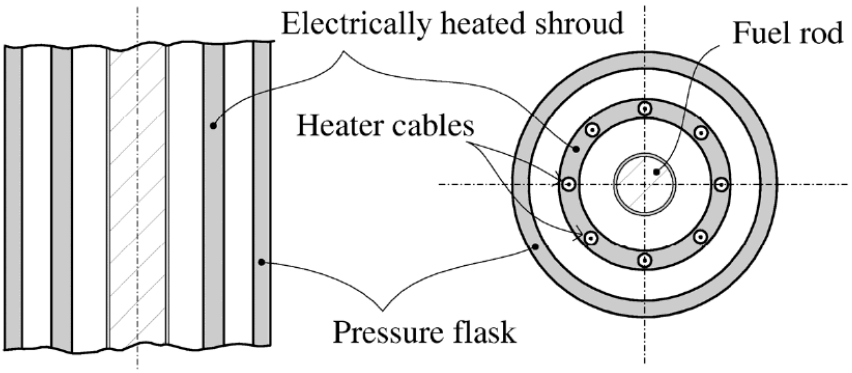

Figure 2.13: Section of the IFA-650, , from (Jernkvik, 2016, pp.7).

simulate the heating effect of the nearby fuels with a similar power. Looking at the hydraulic layout depicted in the figure 2.14, during the nominal condition the device was connected to the loop and filled with heavy water at pressure around 70 *bar* and a temperature of 515 K. Suddenly the apparatus was isolated and the fuel sample was cooled by a natural convection loop. The second stage consisted to detect the total transport activity by bypassing the outer circuit. Once that the correct level of power has reached, the valves that connected the "in-pile" part with the dump tank (TA6301) were opened by depressurizing the entire system. As a result

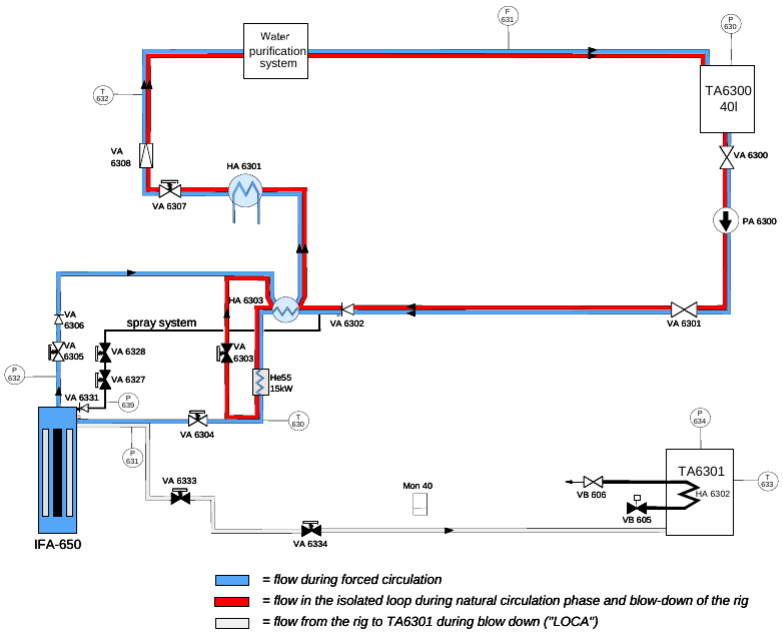

Figure 2.14: Simplified hydraulic layout of the IFA-650, from (Pettersson et al., 2009, pp.122).

of the sharp system depressurization, the coolant immediately flashed and the steam produced was collected inside an external tank where it was condensate. At the end of the transient, the pressure could reach values around the $0.2 \div 0.3$ bar. The time required for the blowdown phase depended on the way to discharge the water form the device, from the bottom part ($65 \div 75$ s) or, simultaneously, from the bottom and the top part ($30 \div 35$ s). In most of the tests performed, to regulate the clad temperature, a small amount of water was sprayed inside the "in-pile" test. Tables 2.7-2.8 summarize the characteristics of the rod utilized and the results obtained from this test campaign.

Table 2.7: Summary of the rod parameters in the IFA-650X test series.

Parameter	IFA-650.4	IFA-650.9	IFA-650.10	IFA-650.14
Active length of sample $[mm]$	480	480	440	360
P_{gap} $[bar]$	40	40	40	20
D_{fuel} $[mm]$	9.13	913	8.19	8.19
Fuel burn-up $[MWd/kg]$	92.3	89.9	61.0	70.8
Cladding material	Zircaloy-4	Zircaloy-4	Zircaloy-4	Zircaloy-2
$D_{fuel,e}$ $[mm]$	10.75	10.75	9.50	9.62
Cladding thickness $[mm]$	0.725	0.725	0.570	0.630
ϖ (mean) $[\mu m]$	10	7	27	32

Table 2.8: Results obtained from the IFA-650X test series.

Parameter	650.4	650.9	650.10	650.14
LHGR (fuel) $[W/cm]$	9.3	26	13.7	9.7
LHGR (heater) $[W/cm]$	15	16	12	15
Max. T_{clad} [K]	1075	1475	1114	1065
Blowdown type [a]	1	2	1	2
Blowdown duration $[s]$	58	35	71	75
t_{fail} $[s]$ [b]	336	133	249	None
t spraying $[s]$ [b]	566	149-175	261	None
Reactor scram $[s]$ [b]	617	316	417	274

[a] Water discharged out from the bottom part (1), from the bottom and top part (2).
[b] Time after the beginning of the blowdown.

Out-of-reactor tests

The REBEKA program The REBEKA (REactor typical Bundle Experiment KArlsruhe) was an experimental device built at the KIT institute. The objective of this facility was to investigate the fuel cladding deformation during the refilling and the reflooding phases. The active length of the rods simulators was of 3900 mm see figure 2.15, the bundle configuration was in a 5x5 and 7x7 square, the figure 2.16 shows the layout loop. The experimental sequences of the device are listed below:

1) With the opening of the valve V1, the water and the steam were injected inside the test section from the bottom. At the same time, the control valve CV was opened. During the first phase, the test bundle was heated and pressurized in order to reach a target cladding temperature of 800 K.

2) The power inside the electrical rods simulators was increased up to reach nearly 9 kW in order to produce a heat-up rate of 7 K/s.

3) With the closure of the control valves, the water was forced to flow up the test section (beginning of the reflooding phase). During this phase the power inside the fuel bundle was reduced to mitigate the greater heat capacity of the electrical heaters (respect to the real fuel rod).

Table 2.9 summarized the results from this test campaign.

MRBT programme At the Oak Ridge National Laboratory (ORNL) a test campaign sponsored by the NRC (Nuclear Regulatory Commission) was conducted with a single and multi-rod test assembly. Figure 2.17 shows the pin simulator placed in a test chamber. The heat-up rate reached was nearly of 28 K/s. In the multi-rod test, the fuel rod simulators were composed by Zircaloy-4 cladding with an external diameter of 10.9 mm. The power generated inside the fuel

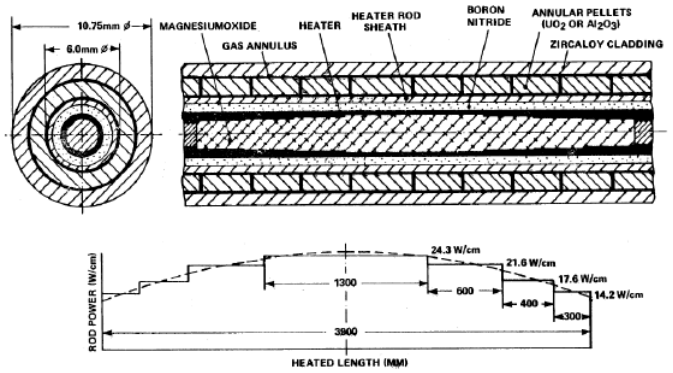

Figure 2.15: REBEKA fuel sample simulator, from (Pettersson et al., 2009, pp.126).

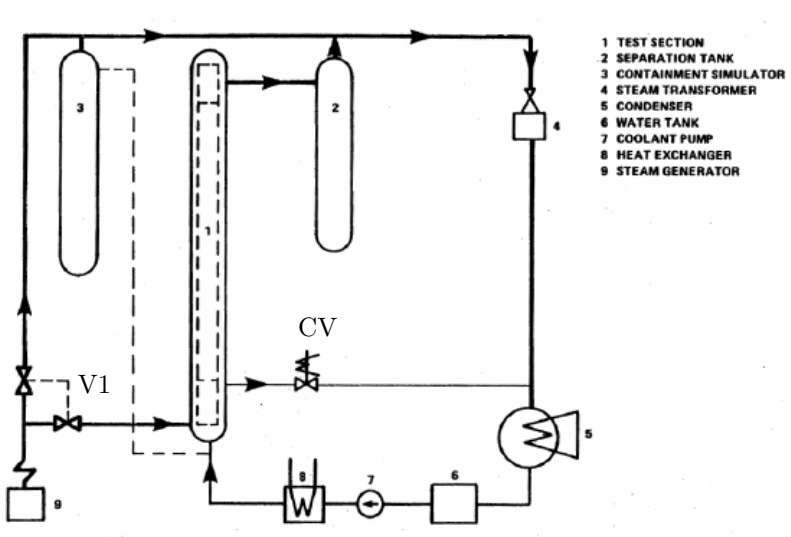

Figure 2.16: Symplified REBEKA loop layout, from (Pettersson et al., 2009, pp.125).

rods was produced by an electrical heater of the same dimension of those utilized in the REBEKA test with an active length of 915 *mm*. To allow a vertical movement, the 8x8 array contained the fuel pins was suspended, see figure 2.18. During the preliminary phase, the electrical heaters were calibrated and a small amount of super-heated steam circulated inside the loop. When the cladding burst, the experience was considered terminated and the fuel simulators were switched off. Some of the objectives of the multi-rod test were to investigate:

- The effects of rod-to-rod interaction on failure behavior;
- The relation between the temperature and pressure rupture;

Table 2.9: Results obtained from the REBEKA test series.

Test number	Bundle size	Λ $[K/s]$	$T^a_{clad,b}$ $[^\circ C]$	$P^a_{gap,b}$ $[bar]$	Circumferential strain [a] [%]	Remarks
1	5x5	7	810	60	28	Only 2 rods burst
2		7	870	55	54	3X3 pressurized
3		7	830	51	44	3X3 pressurized
4		7	830	53	46	3X3 pressurized
5	7x7	7	800	68	49	All rods pressurized
6		7	790	62	42	2 rods not pressurized
7		7	790	57	55	All pressurized

[a] Values averaged on all the rods.

- The flow resistance coefficient as a function of flow blockage;
- The magnitude of the blockage patterns.

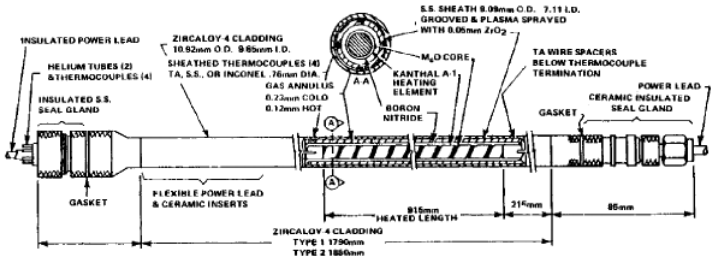

Figure 2.17: MRBT fuel pin simulator, from (Pettersson et al., 2009, pp.129).

Classification of LORELEI

LORELEI is a single rod experimental device with a real fuel sample. The position of LORELEI inside the Jules Horowitz reflector lays this facility half-way between a in-reactor and a out-of-reactor device. The evolution of the dry phase, allows us to study in detail the mechanical behavior of the fuel sample during the accidental and the post-accidental condition. In particular it is possible to investigate some phenomena as the oxidation growth and, how this formed oxide would affect the mechanical behavior of the fuel alloy during the re-flooding phase. LORELEI as in IFA-650, provides an electrical heater placed along the flow separation tube which simulates the heating effect of the nearby fuels. As in IFA-650 test, a preliminary experimental phase is performed in order to create a detectable fission product inventory. As happened in some of the experiences such as IFA-511.4 and IFA-511.5, in LORELEI, the blowdown phase, is not simulated, but the steam required for the dry-phase, is produced indirectly by activating an

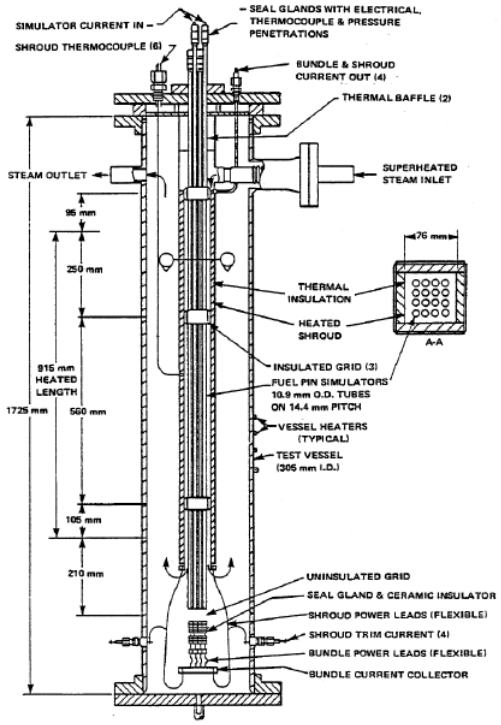

Figure 2.18: 4x4 multi-rod test assembly in the MRBT, from (Pettersson et al., 2009, pp.130).

electrical heater in the bottom of the device. This electrical heater heats up a small amount of water remained from the previous emptying.

Chapter 3

LORELEI test device

3.1 The Jules Horowitz material testing reactor

In the last 50 years, the MTRs (Materials Test Reactor) have been an important way for the development and the qualification of materials and nuclear fuel. Most of these reactors have

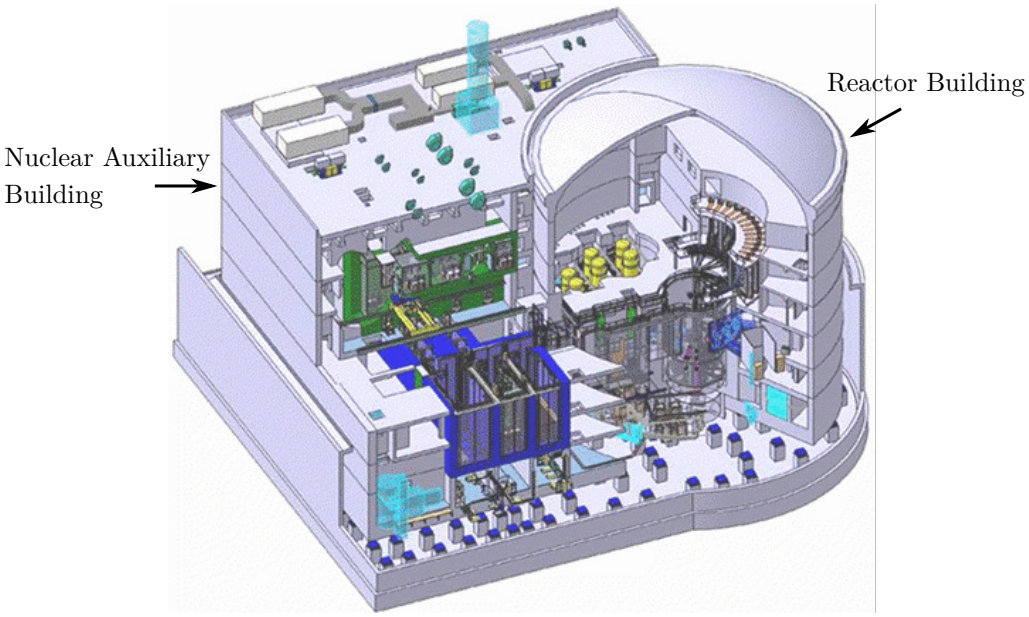

Figure 3.1: Jules Horowitz Reactor building, courtesy of CEA.

reached 50 years of operational life and their shutdown may be imminent, probably not later than 2020. In this contest, the Jules Horowitz Reactor, which has been planned also with the support of the European Commission Research, will be a key factor to improve and show the

safety of existing reactors and the support of new ones. This reactor, which is under construction in Cadarache, is a high flux test reactor, born from the collaboration between various partnership in the nuclear field. It will be an important facility for research and development for the nuclear industry. The planned full power is 100 MWt and it is designed to provide a high neutron flux (5.5 $10^{14} n/cm^2 s$). The Jules Horowitz Reactor (JHR) complex figure 3.1, consists of a reactor building and a nuclear auxiliary building. The first one has a diameter of 37 m and is constructed in reinforced concrete. The reactor building contains three storage pools for spent fuel and irradiated fuel experimental devices. A transfer channel allows to move the spent fuel and experimental devices between these two places. Other infrastructure contains the circuit for cooling and ventilation, the emergency diesel generators and a "cold workshop" which allows to test the experimental devices before moving inside the reactor. The JHR complex includes also some online laboratories which monitor the fuel samples under radiation.

3.1.1 The irradiation devices

Simultaneously to the JHR construction, the CEA has planned to install some experimental loops aiming at testing materials and fuel under irradiation, see figure 3.2. These testing components are composed by one (or a few) samples of limited length, below are briefly described the mains test devices.

MADISON The objective of this device is the study of the fuel under normal working situation (for PWR, BWR and VVER-type reactors). In particular this device allows to investigate the evolution of the fuel proprieties (e.g. the microstructure, the fission gas release etc.) in function of the burn-up or the Linear Heat Generation Rates (LHGR).

ADELINE By using a new or pre-irradiated fuel rod, this device is able to reproduce several scenarios such as (see CEA Nuclear Center, The Irradiation Devices, www-rjh.cea.fr)

- Power ramp test;
- Rod internal over-pressurization of fuel rod;
- Rod internal free volumes gas sweeping in the fuel rod;
- Fuel pellet center melting condition approach

MICA This loop is a capsule experimental device whose objective is to study the behavior of the structural materials under irradiation for LWRs in a temperature range of $300 \div 450 °C$.

MELODIE This apparatus is designed for online bi-axial constrain analysis on materials.

CLOE Loop for the study of the corrosion under radiation for PWR and BWR reactors.

LORELEI Test device whose objective is to analyze the thermal-mechanical behavior of the fuel rod and the radiological consequences during a Loss of Coolant Accident (LOCA). The design and manufacturing of the test device are made in collaboration with the Israel Atomic Energy Commission (IAEC).

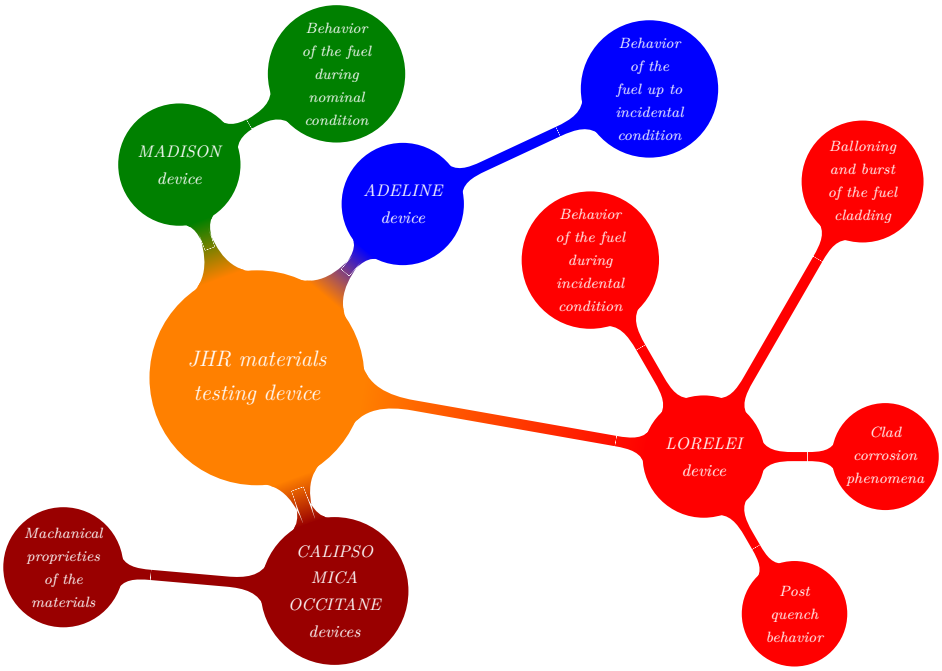

Figure 3.2: Mind map of the experimental devices within the JHR project.

3.2 Objective and motivations of LORELEI

The main objectives of the LORELEI device is to simulate the thermal-mechanical behavior of one LWR (Light Water Reactor) rod during a LOCA accident. The final results are be devoted in prior to: (Moran et al., 2014; Ferry et al., 2014):

(i) Understand the mechanical behavior governing the fuel sample during a LOCA accident (e.g. ballooning, clad burst etc.);

(ii) Understand the corrosion at high temperature, in particular the steam-zirconium oxidation and the clad embrittlement;

(iii) Investigate the fuel rod behavior during the quenching and post-quench phases;

(iv) Quantify the radionuclide released fraction (e.g. gaseous, volatile; semi-and non-volatile, and fissile material);

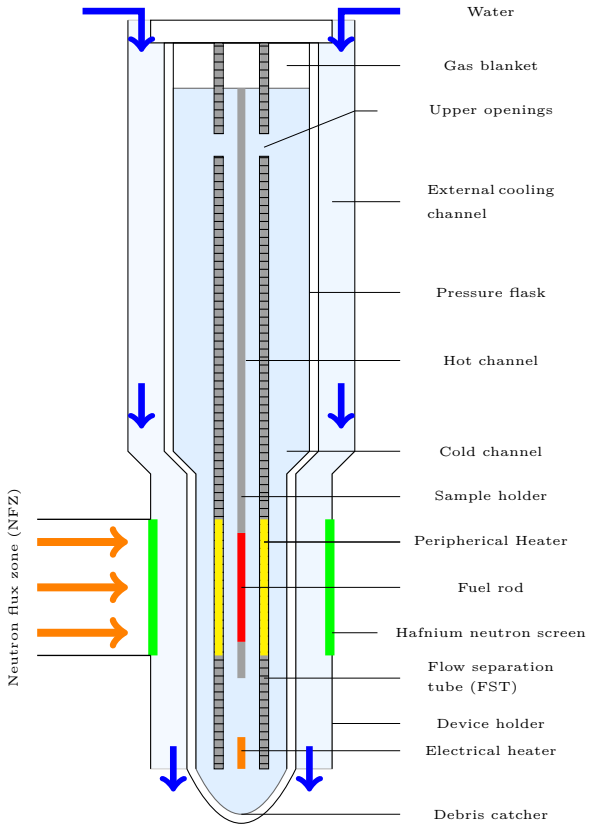

Figure 3.3: Simplified layout of LORELEI.

(v) Supply and validate numerical code and if possible to implement new models and laws.

The LORELEI test device will contribute to characterize new fuel cladding, new fuel (e.g. $U0_2$, MOX and additives) and to design new fuel assemblies. The test campaign will be important to investigate peculiar aspects such as fuel relocation (within the rod and out-of rod), impact of grids on the fuel relocation, etc.

3.3 Description of LORELEI

In the figure 3.3 is depicted a simplified representation of the in-pile device. The in-pile device has been designed to work as a closed capsule where the fuel rod is held by a sample holder. The total height of this closed capsule is about 3.4 m and has a change in diameter in the middle of its vertical axis. In particular, the diameter of the device is smaller at the bottom in order to minimize the gamma power buildup coming from the reactor and bigger at the top to increase the cooling by the cooling channel. The pressure flask is formed by two stainless steel parts: the inner part is designed to withstand the internal pressure, it forms a gas gap

Table 3.1: List of materials

Element	Material
Fuel	UO_2
Cladding	Zircaloy
Sample holder	Zircaloy
Peripheral Heater	Inconel
Flow separation tube	SST
Inner Flask	SST
Outer Flask	SST
Neutron Screen	Hafnium
Device Holder	Zircaloy

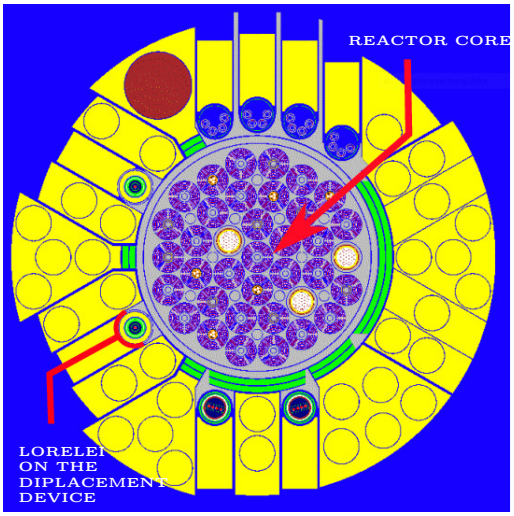

Figure 3.4: Cross section of JHR, courtesy of CEA.

with the second part which ensures the thermal insulation and gives indication of leakage in the flasks. A flow separation tube (FST) forms two concentric channels: a hot channel surrounding the fuel sample and the cold channel between the FST and the internal pressure flask. Due to the FST, a convective (thermosiphon) flow can be formed ensuring the cooling of the fuel rod during the first experimental sequence called the re-irradiation phase. The gap between the device holder and the pressure flask forms a cooling channel, where the water pumped from the reactor pool, flows in a forced convection regime. An hafnium neutron screen is used to flatten the axial fuel flux and to adjust the distance from the reactor core. Placed at the bottom of the hot channel, an electrical heater produces steam during the dry phase. The debris catcher

collects all the fragments of the fuel and the cladding that are expected to come down during the fuel ballooning/burst and during the quenching phase. Table 3.1 shows all the materials of the device. The in-pile part of the device will be installed in the water channel inside the nuclear reflector, see figure 3.4. The dispacement device (DD) allows radial movement toward the core. The total power produced inside the device depends on the value of the linear power produced by the fuel sample whose length is 60 cm and on the gamma power coming from the reactor which will be accumulated inside the materials and water along the NFZ.

3.4 Experimental sequence in LORELEI

Figure 3.5 shows all the experimental sequences which the LORELEI test device undergoes.

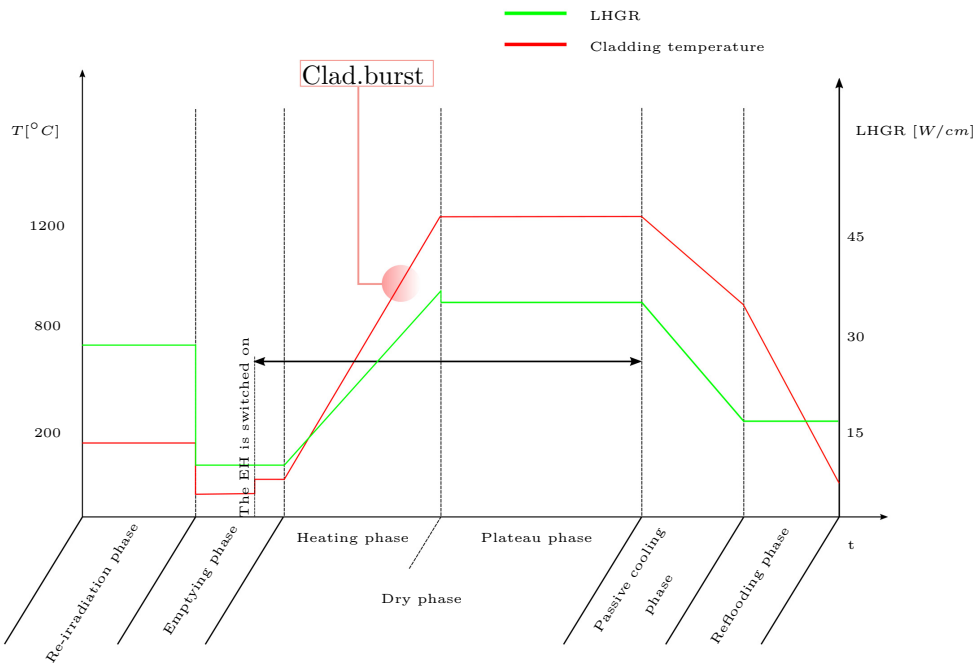

Figure 3.5: Experimental sequences of LORELEI test device.

Re-irradiation phase The irradiation phase occurs before the simulation of the real LOCA transient. During this phase the fuel is re-irradiated for few days in order to generate detectable short lived fission products. The fuel is cooled by single-phase thermosiphon (convective) flow

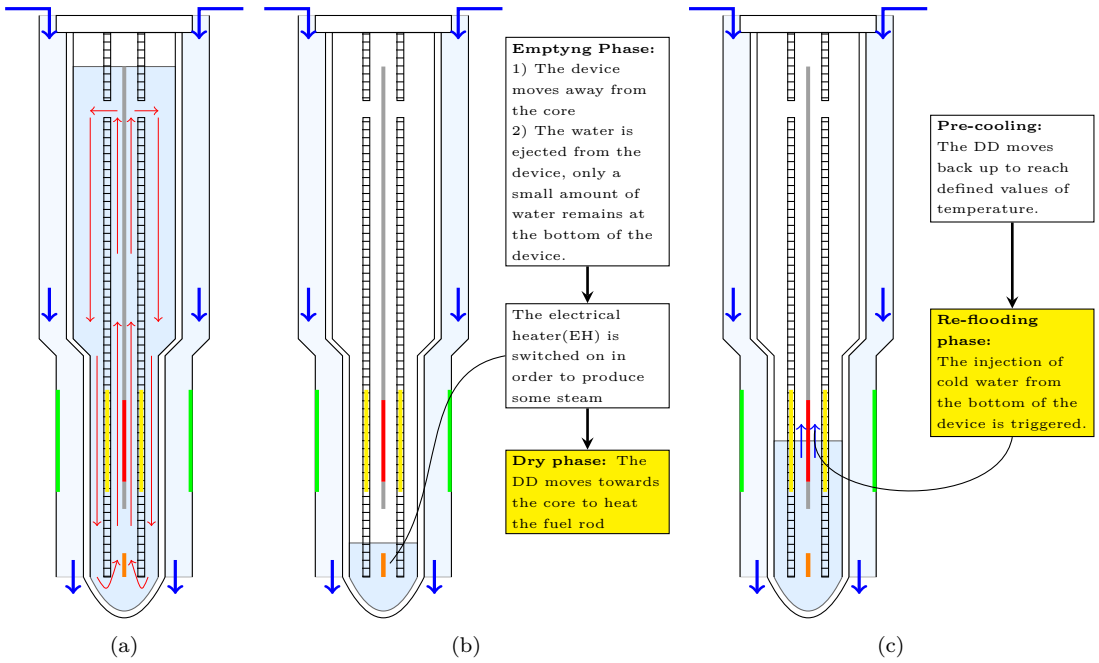

Figure 3.6: Simplified layout of LORELEI test device (a), during the Emptying and Dry phase (b), during the Pre-cooling and Re-flooding phase (c).

and the LHGR is 30 W/cm (the red arrows in the figure 3.6(a) point out the flow direction of the liquid inside the device during this phase). The pressure inside the device is fixed at 70 bar.

Emptying phase During the emptying phase, the device moves away from the core and the LHGR decreases, the water is ejected from the device and helium is injected to take its place. The pressure inside the device decreases to about 3 bar. A small amount of water remains at the bottom of the device in order to provide a saturated steam during the dry phase. At a specific moment, the EH (Electrical Heater) at the bottom of the device is switched on in order to produce some steam for the next phase, see figure 3.6(b).

Dry-phase The dry phase consists, in turn, of two different steps:

Heating phase. The device moves towards the core to heat the fuel sample. During this phase, when the cladding temperature range is 700÷1000 $°C$, the cladding balloons and bursts. This phase ends when the fuel cladding temperature reaches a temperature around 1200$°C$.

Plateau phase. In this phase, the maximum fuel cladding temperature is maintained at 1200$°C$, the equilibrium between the power produced inside the device and the power lost and dissipated by radiation ensure that the temperature of the fuel cladding does not increase.

For high values of temperature, the exothermic oxidation between steam and the zirconium will be studied. The duration of this phase will be set according to the amount of Zirconium oxidized.

Passive cooling phase. This phase is a pre-cooling phase where the device moves back up to reduce the nuclear power and to reach defined values of temperature. The fuel will be cooled passively at a rate of -1 to -10 $°C/s$.

Reflooding phase. In this phase the quenching is studied by injecting cold water from the bottom of the device, see figure 3.6(c). The reflooding will be initiated when reaching a pre-defined cladding temperature between 800 and 1200 $°C$. The internal pressure flask will be designed to resist the pressure peaks associated with this phase.

Chapter 4

Modelling of LORELEI with CATHARE

The modeling by means of CATHARE begins with the geometry description during which are introduced all the constants and chosen the specific modules that best represent each single element of the entire layout. In this phase the User simplifies the layout by finding out which modules are related to the single component, chooses the initial boundary conditions and the appropriate thermal structures. With the introduction of some specific Subroutine, the User may modify the standard calculation or include new physical correlations. An example is the introduction of new materials that may not be present inside the default library or because is necessary to modify some of their physical parameters. For any system that we are interested in studying, there is not a single modeling but the user will provide to give one which appears to be more valid and realistic. Once that the proper modeling has been found, the steady state calculation begins. The real transient part shall be enabled only after a stable steady state is reached.

4.1 Geometry of LORELEI

Figure 4.1 shows a technical drawing of LORELEI. In the table A.1 in a the Appendix A are listed the geometrical values and the materials of all the elements of the device.

4.1.1 Modules utilized for the circuit layout

A schematic layout of the modeling for the LORELEI apparatus is shown in the figure 4.2. The entire layout is composed by two separate circuits: the first circuit consists of the hot and cold channel and the second one of the external cooling channel. The two circuits are coupled

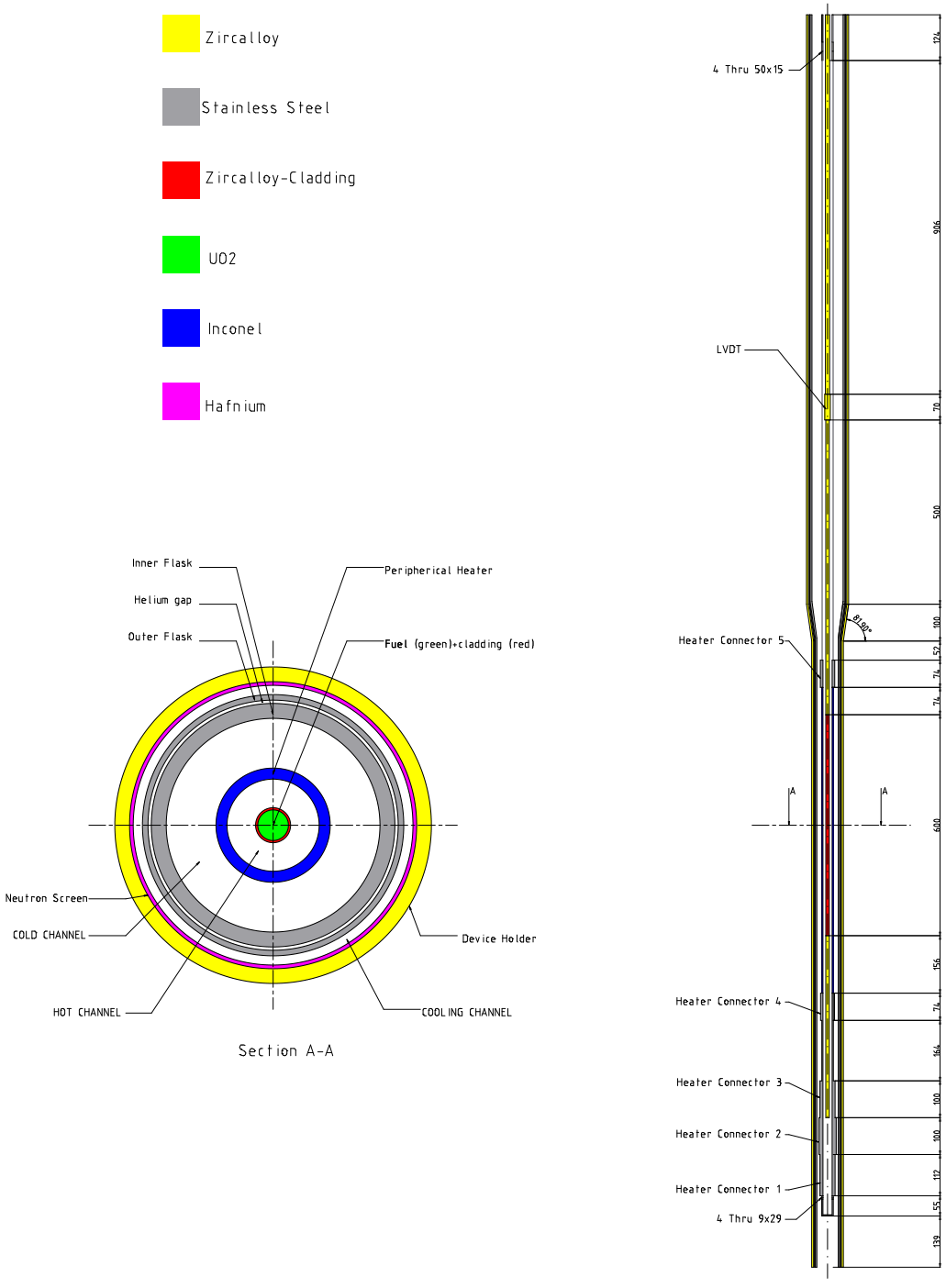

Figure 4.1: LORELEI test device.

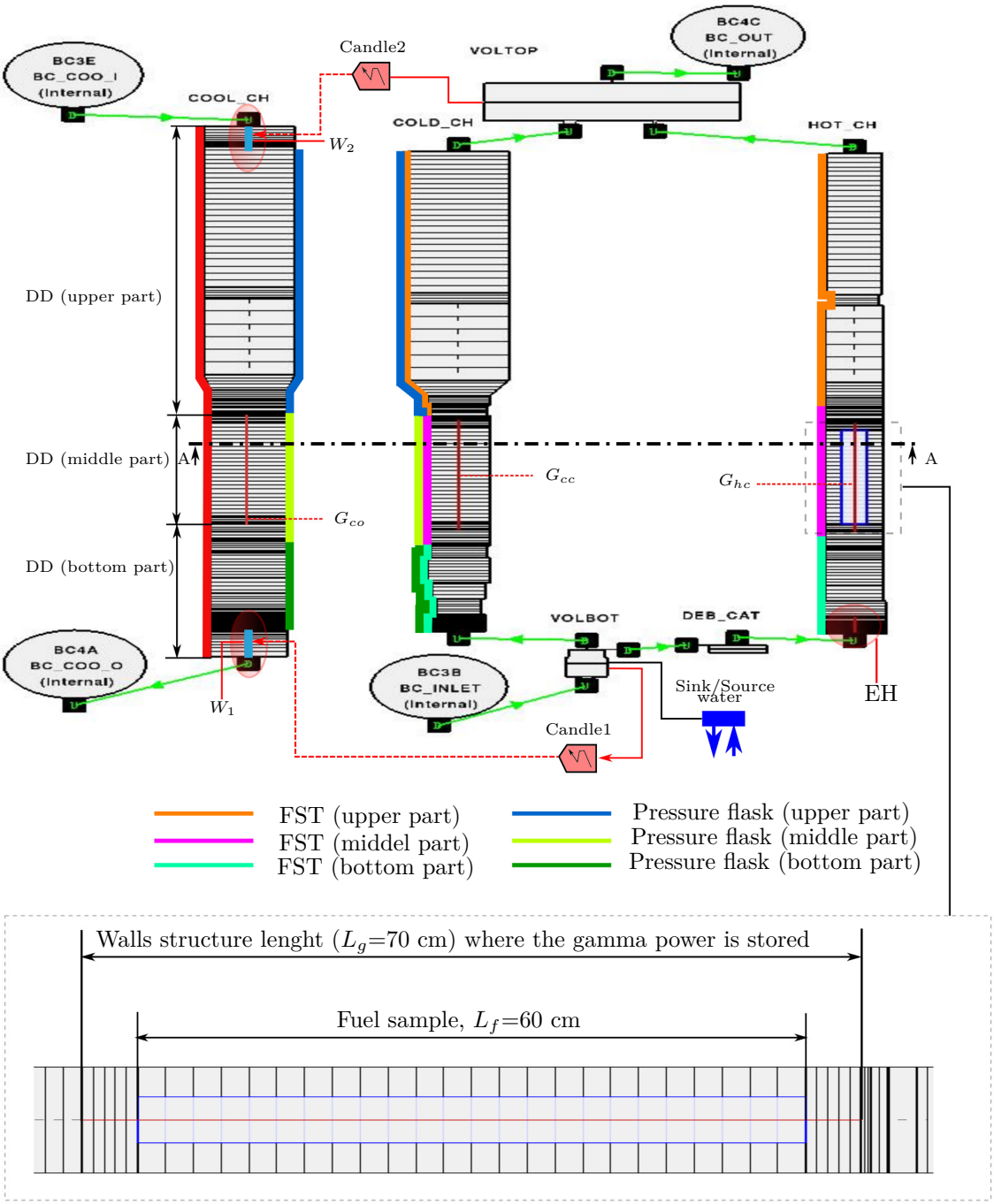

Figure 4.2: Modeling of LORELEI test device with GUITHARE graphic interface.

thermally by a heat exchanger. The hydraulic modules and the boundary conditions are listed below:

- 3 VOLUME elements to module the debris catcher (DEB_CAT) and the lower part (VOLBOT) and the upper part (VOLTOP) of the device. Tables A.2,A.3 and A.4 in the Appendix A summarize the geometrical values for those elements.
- 3 AXIAL elements to model the hot channel (HOT_CH), cold channel (COLD_CH) and the cooling channel (COOL_CH). Tables A.5, A.6 and A.7 in the Appendix A summarize the geometrical values for those elements.
- 4 boundary conditions:
  - BC_OUT connected to the volume VOLTOP and BC_INLET connected to the lower volume VOLTOP.
  - BC_COO_O and BC_COO_I are connected to the cooling channel.

The conditions imposed in the boundary conditions BC_OUT and BC_INLET change according to the experimental phase to simulate. The hydraulic conditions imposed to the cooling channel are a liquid mass flux Q_cool at the BC_COO_I and the external pressure (pool reactor pressure) P_pool at the BC_COO_O, see figure 4.3. A SINK/SOURCE operator is connected to the volume VOLBOT to extract and to inject a certain amount of water during the dry and quenching phase.

```
 BC_COO_I = BCONDIT j_t_co DSTREAM ;
MODEL bc_coo_i BC3E TL ( REALLIST 35.  35.  )
TG ( REALLIST -1.  -1.  )
ALFA ( REALLIST 1.D-5 1.D-5 )
X1 ( REALLIST 1.D-5 1.D-5 )
QL ( REALLIST Q_cool Q_cool )
QG ( REALLIST 1.D-5 1.D-5 )
ABSTIME ( REALLIST 0.0D0 tendf ) ;

BC_COO_O = BCONDIT j_b_co USTREAM ;
MODEL bc_coo_o BC4A
P (REALLIST P_pool P_pool)
ABSTIME (REALLIST 0.  tendf ) ;
```

Figure 4.3: Boundary conditions imposed to the cooling channel.

4.1.2 Modeling of thermal sources

In the table 4.1 all the thermal structures utilized inside the model are shown.

Table 4.1: Thermal structures.

Description	sub module	absolute coordinate	elements associated
Fuel sample	FUEL	0.900-1.500	hot channel
Gamma heating in the water (G_{hc})	WALL	0.850-1.550	hot channel
Gamma heating in the water (G_{cc})	WALL	0.850-1.550	cold channel
Gamma heating in the water (G_{cool})	WALL	0.850-1.550	cooling channel
FST (bottom part)	EXCHANGER	0.194-0.744	hot channel $\longleftrightarrow$ cold channel
FST (middle part)	EXCHANGER	0.744-1.600	hot channel $\longleftrightarrow$ cold channel
FST (upper part)	EXCHANGER	1.600-3.400	hot channel $\longleftrightarrow$ cold channel
Pressure flask (bottom part)	EXCHANGER	0.194-0.744	cold channel $\longleftrightarrow$ cooling channel
Pressure flask (middle part)	EXCHANGER	0.744-1.600	cold channel $\longleftrightarrow$ cooling channel
Pressure flask (upper part)	EXCHANGER	1.600-3.400	cold channel $\longleftrightarrow$ cooling channel
DD (bottom part)	WALL	0.000-0.744	cooling channel
DD (middle part)	WALL	0.744-1.600	cooling channel
DD (upper part)	WALL	1.600-3.400	cooling channel
Electrical heater	WALL	0.194-0.306	hot channel
Wall to recover the power W_1	WALL	0.000-0.194	cooling channel
Wall to recover the power W_2	WALL	3.276-3.400	cooling channel

Linear Heat Generation Rate (LHGR)

The neutronic calculation was performed by means of the Monte Carlo code TRIPOLI4 V4.9 (Brun et al., 2013) by considering the core in equilibrium with the Xenon and the control rods inserted in a position to achieve the critical reactivity. The Linear Heat Generation Rate (LHGR) $[W/cm]$ is model by the following equations

$$LHGR_{water} = 593e^{-0.180x_c}\,, \tag{4.1}$$

$$LHGR_{steam} = 375e^{-0.160x_c}\,. \tag{4.2}$$

They express respectively the value of the LHGR (Linear Heat Generation Rate) produced by the fuel sample as a function of distance from the core x_c, when inside the device (hot-cold channels), is present water or steam. The equations 4.1-4.2 are derived from the total neutron flux inside the fuel sample. The nuclear heating inside the structure is calculated from the energy deposited by the neutron and photons inside the material volume. The normalized LHGR axial fuel profile imposed in the fuel rod expressed by the [4.3], was obtained from neutronic calculation by assuming the x_c=17 cm (LHGR=25 W/cm), with a 1 mm of hafnium screen, see figure 4.4(a).

$$LHGR(z) = 3.501\ 10^{-6}z^4 - 1.402\ 10^{-5}z^3 - 2.375\ 10^{-2}z^2 - 5.662\ 10^{-2}z + 31.33\ \ [W/cm]\,. \tag{4.3}$$

Gamma power sources

The normalized axial profile imposed in the thermal structure takes into account the gamma power along the neutron flux zone and it is fitted with the following symmetric polynomial distribution (Blandin et al., 2013), see figure 4.4-(b).

$$f_\gamma(z) = \begin{cases} (1 - 0.2z - 9.7z'^2 - 15.8z'^3 - 7.4z'^4) \\ \text{for} \quad -0.35\,m \leq z' \leq 0 \\ (1 + 0.2z' - 9.7z'^2 + 15.8z'^3 - 7.4z'^4) \\ \text{for} \quad 0 \leq z' \leq 0.35\,m \end{cases}$$

with $z' = z - 1.2$. The extension of the NFZ is 70 cm and all the specific powers due to the gamma

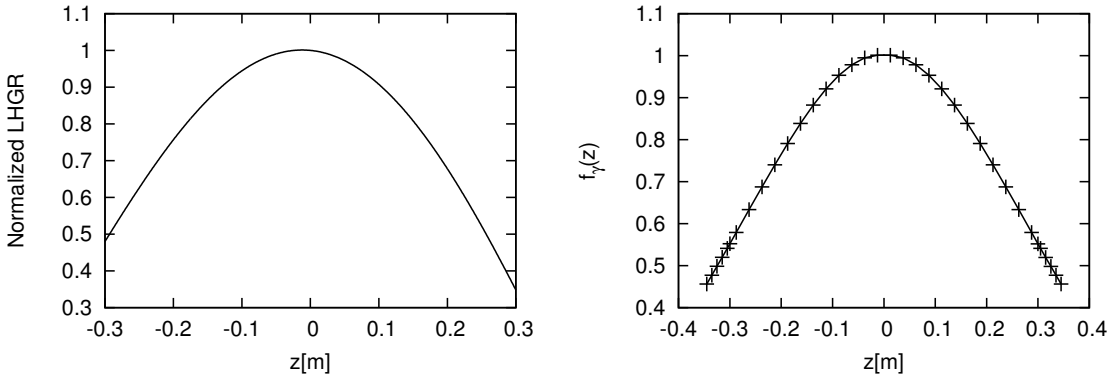

(a) (b)

Figure 4.4: Normalized fuel axial profile (a), normalized gamma power profile (b).

heating inside the materials and the water are averaged on this length. In the tables 4.2-4.3, are listed the values expressed in W/g on 10 peripheral sections when inside the device is present water or steam, see figure 4.5. These values were obtained for an uranium enrichment equals to 4.95 %, a fuel burn up of 80 GWd/t for a core power of 100 MW. During the re-irradiation phase, the volumes VOLTOP and VOLBOT lose a certain amount of power by exchanging with the external cooling channel. In CATHARE is not possible to couple thermally a volume element with an axial one, for this reason an alternative solution has been designed to overcome this problem. In particular, two sinks of power (Candle1 and Candle2), see figure 4.2, are connected respectively to the volume VOLTOP and VOLBOT, two internal walls W_1 and W_2 are placed on the bottom and on the top part of the cooling channel. During the calculation, the total power lost by the dry side through the walls is extracted from the volumes by means of the sinks of power. The liquid temperatures calculated inside the two volumes are then imposed in all the meshes composed the two walls. A thermal wall EH is placed on the bottom of the hot channel

to produce the power required to produce the steam during the dry phase. Figure 4.6 shows the radial nodalization of the thermal structures corresponding to the cross-section A-A defined in figure 4.2.

Table 4.2: Specific gamma power generated inside the device (water environmental).

Angles	108°	144°	180°	216°	252°	288°	324°	0°	36°	72°	Mean value
Fuel cladding	2.8	2.6	2.4	2.6	2.8	2.9	3.1	2.9	3.1	2.9	2.8
Water (hot_ch)	3.8	3.5	3.4	3.2	3.7	4.0	4.1	4.4	4.3	4.1	3.8
FST	2.8	2.6	2.5	2.6	2.8	3.1	3.3	3.4	3.3	3.0	2.9
Water (cold_ch)	3.5	3.1	2.9	3.0	3.6	4.3	4.8	5.0	4.9	4.1	3.9
IPF	2.7	2.3	2.2	2.4	2.8	3.4	3.8	4.0	3.8	3.3	3.1
Helium gap	-	-	-	-	-	-	-	-	-	-	5.1
OPF	2.9	2.3	2.2	2.3	2.9	3.7	4.3	4.5	4.2	3.6	3.3
Water (cool_ch)	4.0	3.2	3.0	3.1	4.1	5.7	6.8	7.6	6.9	5.6	5.0
Hafnium (neutron screen)	5.6	4.5	4.2	4.6	5.9	7.7	9.3	9.7	9. 1	7.5	6.8
Device holder	2.4	1.8	1.7	1.9	2.4	3.3	4.2	4.5	4.1	3.2	2.9

Table 4.3: Specific gamma power generated inside the device (steam environmental).

Angles	108°	144°	180°	216°	252°	288°	324°	0°	36°	72°	Mean value
Fuel cladding	2.5	2.3	2.3	2.3	2.4	2.7	2.7	2.8	2.8	2.6	2.6
Water (hot_ch)	-	-	-	-	-	-	-	-	-	-	5.0
FST	2.6	2.4	2.4	2.4	2.6	2.8	3.0	3.0	2.9	2.8	2.7
Water (cold_ch)	-	-	-	-	-	-	-	-	-	-	4.9
IPF	2.6	2.4	2.3	2.4	2.7	3.1	3.5	3.6	3.5	3.0	2.9
Helium gap	-	-	-	-	-	-	-	-	-	-	5.1
OPF	2.7	2.4	2.3	2.4	2.8	3.4	4.0	4.2	3.9	3.4	3.2
Water (cool_ch)	4.4	3.7	3.6	3.8	4.4	5.6	6.8	7.3	6.7	5.4	5.2
Hafnium (neutron screen)	5.8	4.7	4.5	4.8	5.8	7.3	8.6	9.0	8.4	7.3	6.6
Device holder	2.3	1.9	1.8	1.9	2.4	3.2	4.0	4.3	3.9	3.1	2.9

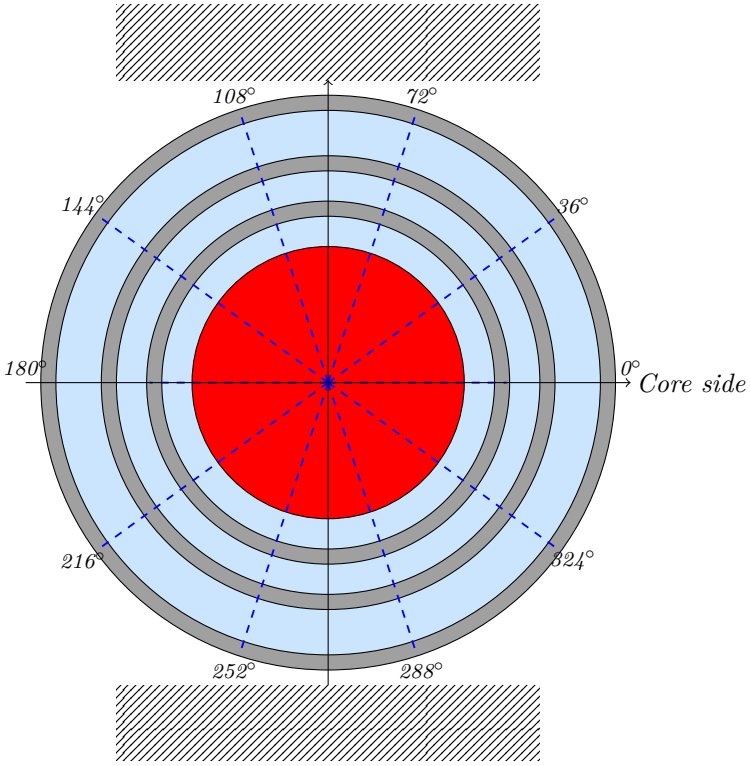

Figure 4.5: Partitions of the device.

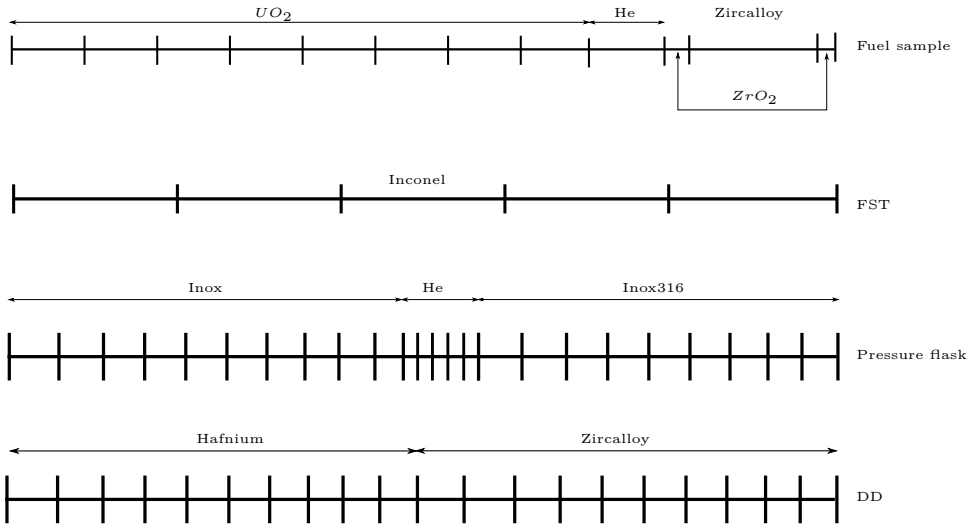

Figure 4.6: Radial nodalization of the thermal structures.

Chapter 5

Analysis of the Re-irradiation phase

In this Chapter, the thermal-hydraulic study of the Re-irradiation phase is described. At first it has been necessary to evaluate the behavior of the device during the nominal condition, in particular, in this situation, the pressure inside the device is maintained constant and the fuel sample is cooled by a natural circulation loop between the hot and cold channel. In this first stage, an assessment of the evolution of the water temperature along the channels and the thermal structures are performed in accordance with the previous CFD studies as well (Gitelman et al., 2014; Korotkin et al., 2014; Ferry et al., 2014). The second part of this chapter is dedicated to the study of some abnormal conditions which provides to answer to some specific questions such as for example, what are the limits of the termosypohon liquid flow (TLF) or how the fuel cladding temperature changes if the natural circulation loop between the hot and cold channel decreases. For this second part, a more representative set of simulations are described. In some case, some simplify mathematical expressions are formulated to better understand the physic problem.

5.1 Nominal condition

As already described in the Chapter 3, during this phase, the fuel sample is cooled by a convection (thermosyphon) liquid flow generated between the hot and cold channel; the pressure of the system is fixed to 70 bar. The results performed and shown in this Manuscript, refer to conservative value for the LHGR=40 W/cm instead of 30 W/cm. Figure 5.1 shows the values of the temperatures of the water and the thermal structures that comprising the apparatus. Looking at the green curve, from the bottom, one can see that the liquid, inside the hot channel, starts to warm up when enters in the neutron zone reaching 144$°C$. Then it cools down slightly by

transferring heat to the liquid inside the cold channel. Following the liquid temperature inside the cold channel (orange curve), from the top, the liquid is at first cooled down by the external cooling channel, then in the gamma zone the liquid warms up to $141°C$ and comes out of the channel at $135°C$. Figure 5.2 shows the temperature of the device holder and of the liquid inside the cooling channel. The liquid enters inside the channel at 35 $°C$ (conservative average temperature of the reactor pool) and it exits the device at 38 $°C$. Figure 5.3 shows the liquid velocity inside the hot, cold, and cooling channel. Analytically, it is possible to estimate the

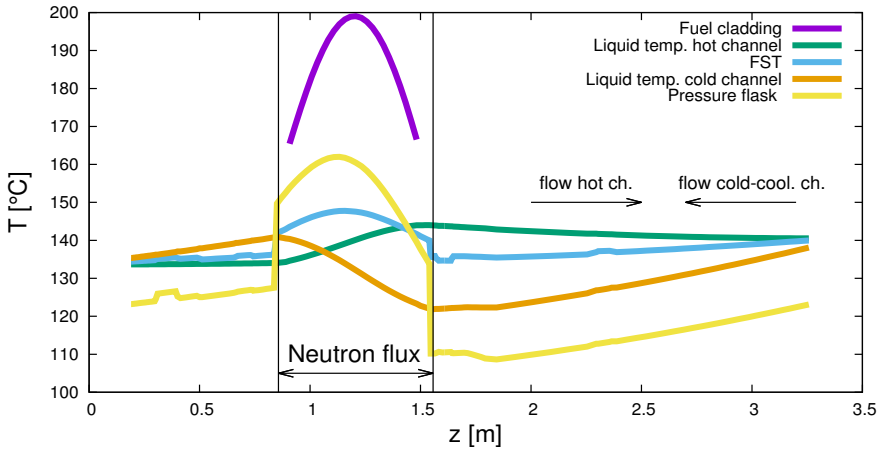

Figure 5.1: Map of temperatures, LHGR=40 W/cm.

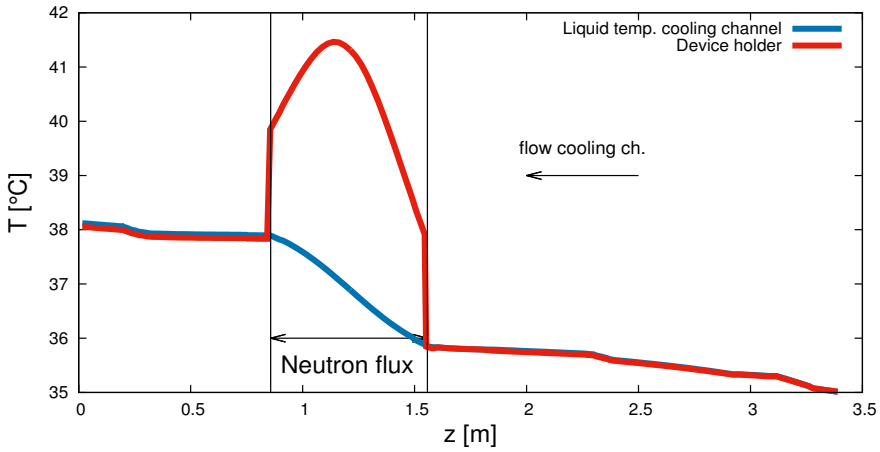

Figure 5.2: Device holder temperature and liquid temperature inside the cooling channel, LHGR=40 W/cm.

temperature $T_l(2)$ of the sub-saturated liquid inside the hot channel outgoing from the fuel zone during the Re-irradiation phase. In particular, it is possible to write the following heat balance

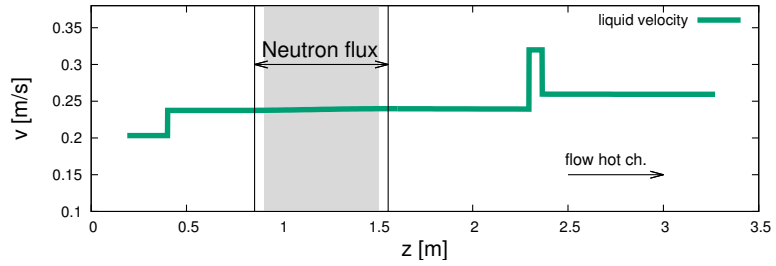

(a)

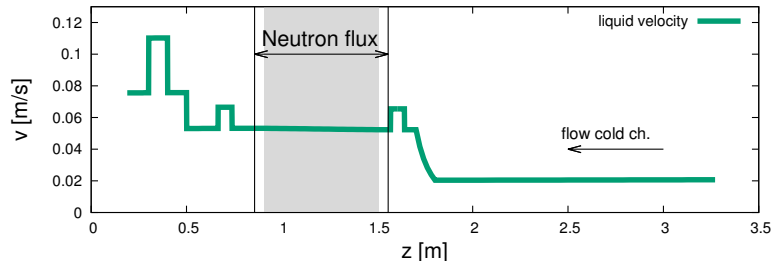

(b)

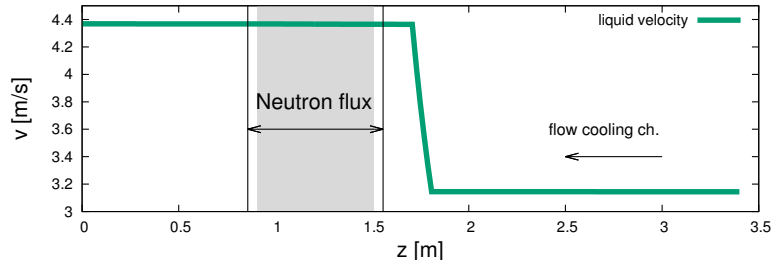

(c)

Figure 5.3: Liquid velocity inside the hot (a) cold (b) and cooling (c) channel, LHGR=40 W/cm. The gray zone marks the fuel zone.

equation

$$2\pi \int_0^z \left(q''_{fuel} R_{fuel} + q''_{FST} R_{FST,i}\right) \mathrm{d}z + \\ + \int_0^z \gamma_{l,hc} \rho_l (R^2_{FST,i} - R^2_{fuel}) \pi \mathrm{d}z - Q_{lost} = \int_{T_l(1)}^{T_l(2)} \dot{m}_l C p_l \mathrm{d}T \ . \tag{5.1}$$

In the eq.[5.1] $T_l(1)$ is the liquid temperature before passing through the fuel zone. γ_{hc} is the specific power $[W/kg]$ released in the water due to the gamma heating, $\dot{m}_l$ is the liquid mass flow $[kg/s]$ and Q_{lost} is the power loss to the cold channel. By neglecting the term Q_{lost}, by resolving

the [5.1] is possible to find the value of $T_l(2)$ as

$$T_l(2) = T_l(1) + z\left(\frac{2\pi(q''_{fuel}R_{fuel} + q''_{FST}R_{FST,i})}{\dot{m}_l Cp_l} + \frac{\gamma\rho_l\pi(R^2_{FST,i} - R^2_{fuel})}{\dot{m}_l Cp_l}\right). \quad (5.2)$$

Let us consider the case just analyzed with CATHARE with a LHGR=40 W/cm, q''_{fuel}=1400000 W/m^2, q''_{FST}=30000 W/m^2, the liquid mass flux $\dot{m}_l$=0.12 kg/s, D_{fuel} and $D_{FST,i}$ respectively 9.5 mm and 25 mm and the $T_l(1)$=136°C. By substituting these values in the [5.2], the value of the liquid temperature outgoing from the fuel zone is given by

$$\frac{(\pi q''_{fuel}D_{fuel}+q''_{FST}D_{FST,i})z}{\dot{m}_l Cp_l} = \frac{(140000)(0.0095)(\pi)(0.6)+(30000)(0.025)(\pi)(0.6)}{0.12\text{x}4270} = 7.65\,°C$$
$$\frac{\gamma\rho_l V_l}{\dot{m}_l Cp_l} = \frac{1.7\,10^6(3.14(0.025^2-0.0095^2)0.6)}{4\text{x}0.12\text{x}4270} = 0.26\,°C$$
$$T_l(2) = 136 + 7.65 + 0.26 = 143.91\,°C.$$

Figure 5.4 presents the water bulk temperature along the thermosyphon loop and the cladding wall temperature for a nominal power of 40 W/cm obtained by a CATHARE and CFD analysis (Gitelman et al., 2014; Korotkin et al., 2014; Ferry et al., 2014) The comparison indicates an acceptable agreement, except for a deviation in the flux zone at the cold channel. In this zone, the main flow direction is downward, where buoyancy forces generated by the gamma power in the structure, generates opposing buoyancy forces. Therefore, the deviation in this zone is expected since the CATHARE software 1D model cannot model the 3D phenomena caused by the opposing buoyancy forces and the 3D power distribution in the system. The 3D model predicts higher water temperatures in flux zone due to the different flow regime.

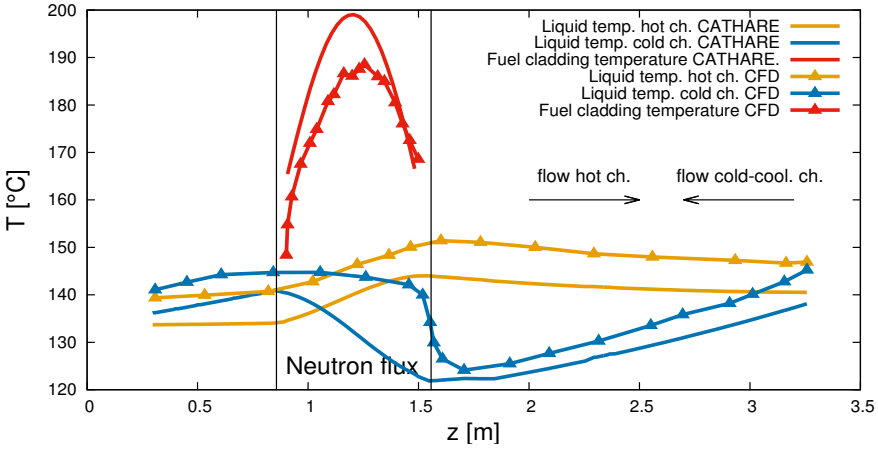

Figure 5.4: Liquid temperature along the in-pile device channels loop and cladding temperature, comparison between CATHARE2 and FLUENT 3D models, LHGR=40 W/cm.

5.1.1 Pressure drop calculation

The CATHARE code does not take into account the singular concentrated pressure drop, for this reason the user will impose the values in accordance with the kind of singularity. These pressure drops correspond to head losses due to geometric changing and they are always the following form (Lavialle, February, 2006):

$$\Delta P_{sing} = \frac{1}{2} k_p \rho \mathrm{v}^2 \ . \tag{5.3}$$

In the [5.3], k_p is the constant pressure drop coefficient given by the user. The user could tune the values of k_p with the pressure drops calculated by a previous CFD analysis. If one cannot determine experimentally the single value of the k_p is possible as a first approximation to evaluate these values by consulting a specific manual. For details see (Idelchik and Friend, 1986). Figure 5.5 shows the pressure drops inside the hot channel due to the presence of a sudden expansion or a sudden contractions during the Re-irradiation phase. In particular, by considering the bottom-up liquid flow inside the hot channel, the liquid encounters two sudden contractions and one sudden expansion. The first two pressure drop appear at the beginning of the fuel holder and when the liquid pass through the Linear Variable Differential Transformer (LVDT). The sudden expansion occurs at the end of the LVDT itself. On the other hand, inside the cold channel the top-bottom liquid flow encounters a numerous cross section variation due to some heater connections along the flow separation tube (FST), see figure 4.1. By comparing the sum total of the pressure loses inside the two channels with the total pressure inside the device ($70\,10^5 Pa$), those can be neglected without making a significant error.

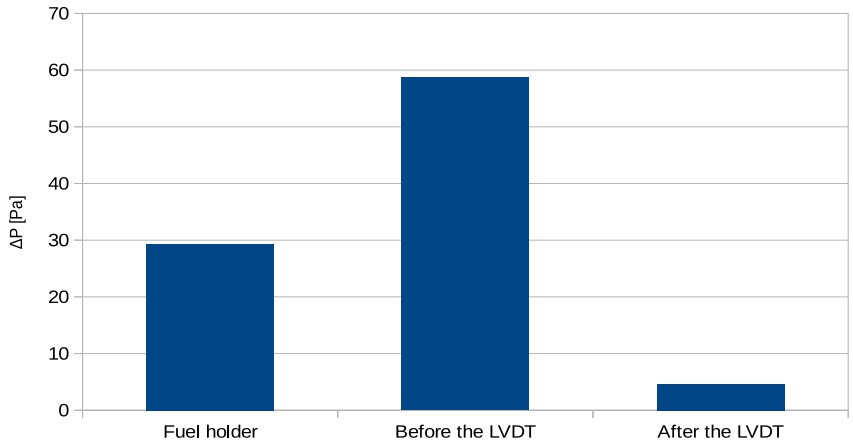

Figure 5.5: Concentrated pressure drop calculation inside the hot channel.

5.1.2 Convective flow at constant pressure

The objective of these first simulations is to understand the limit condition of the device, in particular to study how the thermosiphon liquid flow (TLF) changes as a function of the linear heat generation rate (LHGR) and check a possible threshold value for the LHGR above which the TLF between the hot and cold channel is negligible. The pressure inside the device is artificially maintained constant at 70 *bar* for every value of LHGR. In the real conditions, the device is a closed capsule and the pressure increases in accordance with the internal power source. The results of this simulation show that the ONB occurs after the LHGR reaches nearly 100 W/cm, see figure 5.6. The liquid remains sub-saturated up to 220 W/cm and a limit was found for the TLF for LHGR=260 W/cm. In this case, the steam collected on the top of the device prevents the ingress of water from the hot to the cold channel and TLF stops, see the void fraction in figure 5.7. Table 5.1 summarizes some principals thermal-hydraulic parameters and the figure 5.8 shows the values of the thermosyphon liquid flow as a function of the LHGR. To obtain a estimation of the evolution of the fuel temperature in accordance with different levels of power, below is presented a simplified analysis from the Lumped-Method Theory. This last assumption considers that the temperature of the solid is spatially uniform at any instant during the transient process. Mathematically this assumption is expressed as $Bi << 1$, where Bi is the Biot number. This assumption implies that temperature gradients within the solid are negligible. The absence of a temperature gradient implies the existence of infinite thermal conductivity. By considering the fuel sample in LORELEI and its multilayer materials, such condition is clearly impossible, however, this simple model allows us to illustrate the physic problem in general. We consider that the fuel sample inside the LORELEI apparatus is associated to a cylinder with the same geometrical characteristics. Hypothetically, the liquid cools the cylinder remains single phase. It is possible to write the following heat balance equation

$$\begin{aligned} &\rho V c_p \frac{dT'(t)}{dt} = -hA(T'(t) - T_\infty) + \Delta q_0^{'''} V \ , \\ &\text{with } \ T'(0) = T_1 \ . \end{aligned} \tag{5.4}$$

T_1 is the liquid temperature at infinity distance from the cylinder, $\Delta q_0^{'''}$ is the difference of the volume power between two values of power. The solution of the [5.4] can be written as

$$T(t) = \frac{\Delta q_0^{'''}}{hA}\left(1 - \mathrm{e}^{-\lambda t}\right) + T(1) \ . \tag{5.5}$$

$\lambda = \frac{hA}{\rho CpV}$ is the Characteristic constant of the system. Table 5.2 summarizes some thermal-hydraulic values obtained according to different values of LHGR. T' is the value of the temperature derived by the [5.5]. The values of Re_l and the other values are obtained directly from the CATHARE calculation in a mesh point of the hot channel corresponding to the middle of the fuel sample. The value of h is obtained from the equation 1.24.

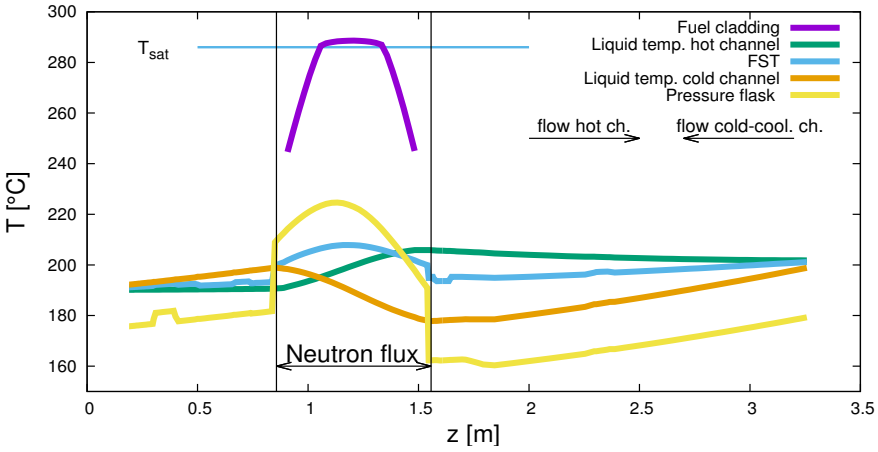

Figure 5.6: Map of temperatures, LHGR=100 $[W/cm]$.

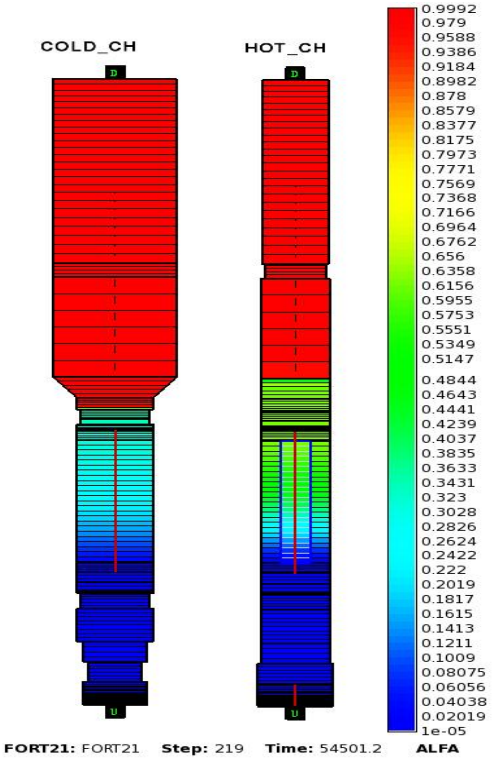

Figure 5.7: Void fraction inside the hot and cold channel.

5.1.3 Convective flow at constant volume

For the analysis of the abnormal condition, the device is assumed closed and isolated from the cubicle. In this case, particular attention must be focused on the helium blanket on the top

Table 5.1: Summary of the mains thermal-hydraulic parameters.

LHGR W/cm	max T_{cl} $°C$	max $T_{l,h}$ $°C$	max $T_{l,c}$ $°C$	max $T_{l,coo}$ $°C$	TLF kg/s
40	198	143	139	38.1	0.093
60	238	167	162	38.8	0.105
80	272	187	181	39.4	0.115
100	288	205	199	40.5	0.124
140	292	236	230	41.5	0.140
180	293	261	255	42.0	0.158
220	295	289	280	42.8	0.198

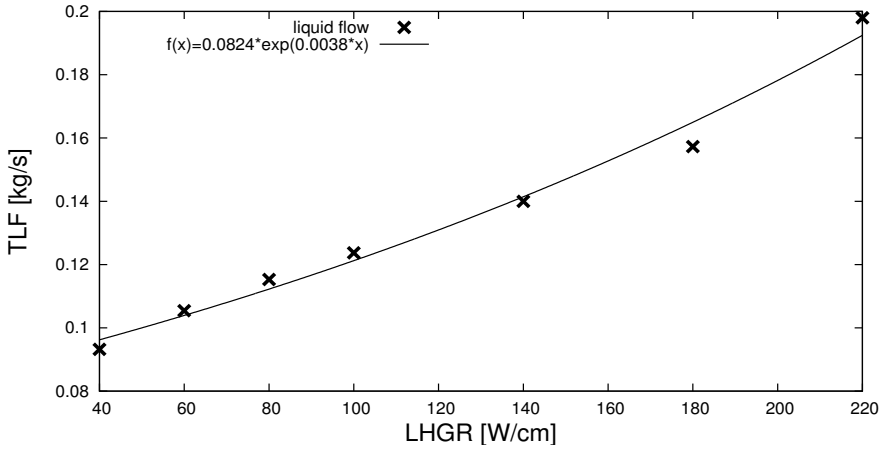

Figure 5.8: TLF in function of LHGR, the pressure inside the system is maintained constant at 70 bar.

Table 5.2: Fuel temperature and summary of the mains physic parameters for three different values of LHGR.

LHGR $[W/cm]$	Re_l	μ_l $[kg/m\,s]$	Cp_l $[J/kg\,K]$	k_l $[W/m\,K]$	Pr_l	h $[W/m^2\,K]$	T' $[°C]$
40	17700	0.000195	4275	0.693	1.203	1439	144
60	23500	0.000166	4328	0.686	1.047	1690	180
80	28850	0.000134	4390	0.676	0.870	1823	200

part of the device that in the CATHARE modeling is placed inside the volume VOLTOP. Let us consider for example an unexpected acceleration of the device towards the core; the power produced inside the device starts to increase and the internal pressure will rise according to the

dilatation of the water inside the device. The increase depends on the initial volume of the He blanket. The objective of the study is to determine the consequences on the pressure evolution. Figure 5.9 shows the value of the internal pressure of the device as a function of the LHGR when inside the volume VOLTOP are present 5 l of helium. It can be seen that the change of internal pressure by varying the LHGR from 40 to 60 W/cm is almost 10 bar; just before the device pressure has reached a value around 90 bar, in accordance with the safety procedures the reactor SCRAM is triggered and for pressure greater than 90 bar, two pressure relief valves (PRV) are set to open.

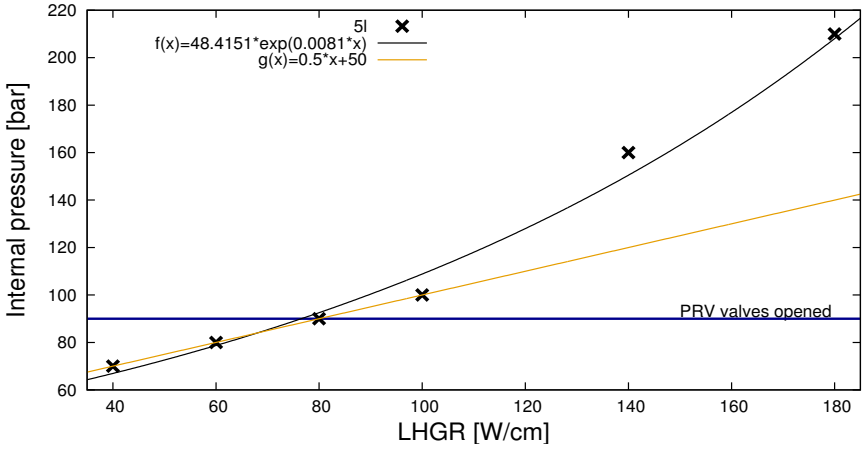

Figure 5.9: Internal pressure of the device in function of LHGR, inside the device are present 5 l of helium.

5.2 Study of some accidental conditions during the Re-irradiation phase

5.2.1 Failure of the displacement device

During this accidental scenario, the displacement device (DD) which allows the movement of the apparatus along the reflector, fails and starts to accelerate towards the core. The DD starts to accelerate towards the core in a time of 2 s up to reach its maximum velocity value of 6.5 mm/s. When the security system detects an incorrect position of the DD, the classified withdrawal is triggered (t_1=2 s) and the heating elements are switched off (t_2=t_1+0.1 s). At t_3=3 s the DD decelerates, stops in in 1 s and starts to move backward by reaching the maximal withdrawal velocity of 5.5 mm/s in a time of 2 s. In this section the case during which the classified withdrawal is defective is analyzed. In this situation, the device continues to move towards the core at its maximal speed until is stopped by a mechanical stop block. In this last case, at t=t_1+5

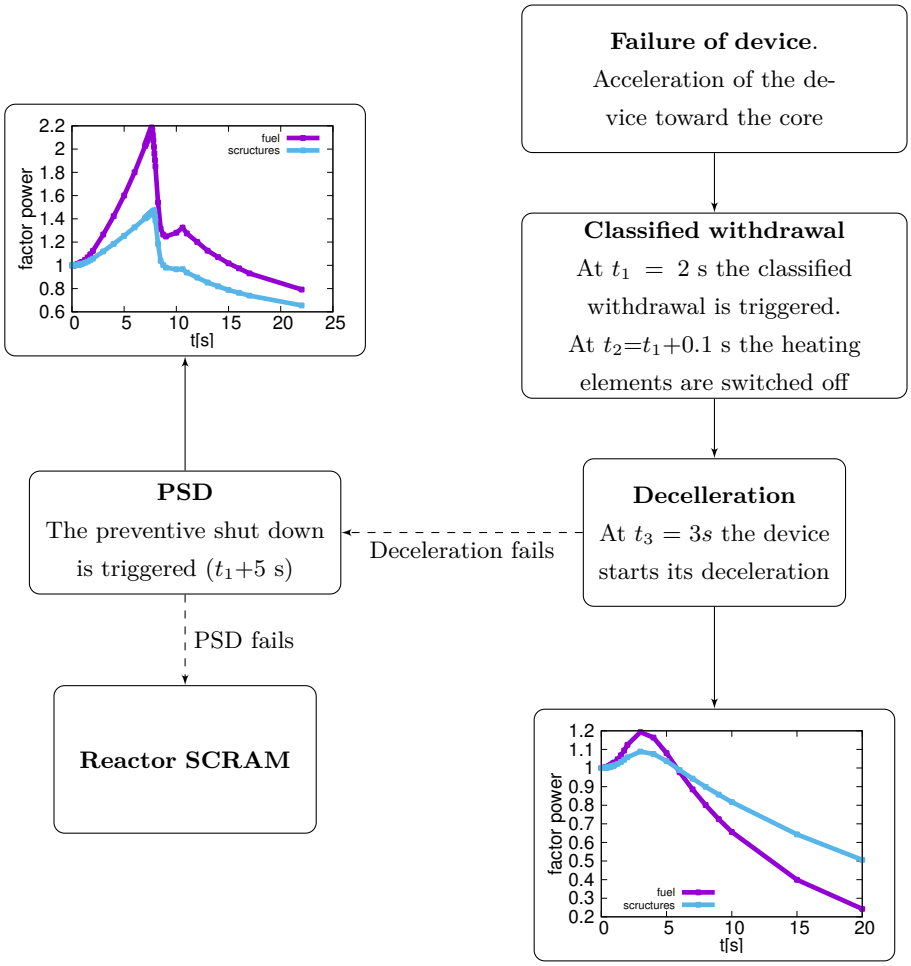

Figure 5.10: Failure ofthe displacement device, events diagram.

s the preventive shut down (PSD) is triggered while the device keeps moving towards the core, see figure 5.10. Figures 5.11(a)-(b) and (c)-(d) show respectively the values of the velocity and the distance covered by the device when the classified withdrawal is triggered and when it is not. During the approach of the DD toward the core, the power generated inside the fuel sample increase up to 2.2 times its initial value according to the [4.1]. The fuel cladding temperature increases about of 30 $°C$, see figure 5.12(a). The power due the gamma heating increases up to 1.4 its initial value, the temperatures calculated in the FST, inner pressure flask and hafnium neutron screen increases by approximately ΔT such that $\Delta T < 10\ °C$, see figures 5.12(b)-(c)-(d).

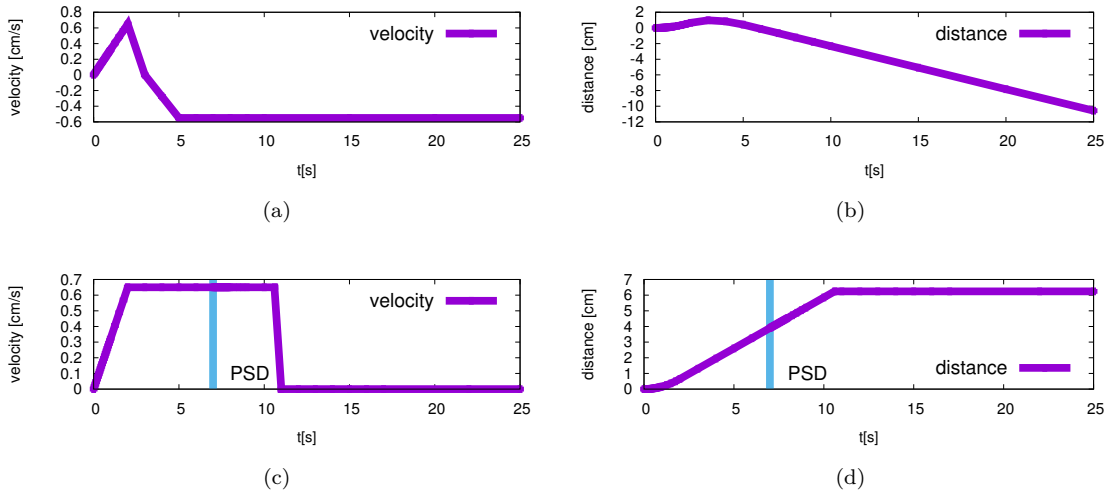

Figure 5.11: Velocity and distance covered by the displacement device when the classified withdrawal is triggered (a)-(b), when the classified withdrawal fails and the PSD is triggered (c)-(d).

5.2.2 Failure of the cooling channel

Once the coolant loop pump has failed, the system which provides to secure the device is triggered. Below is listed the chronological sequences before and after the reactor SCRAM triggering.

Before the SCRAM triggering

1) The pump fails, the inertia of the pump assures a small amount of cooled water inside the channel of the reflector.

2) Once the liquid flow inside the circuit has decreased, the pressure inside the cooling circuit increases.

3) The reactor SCRAM is triggered when the suction pressure increases up to exceed the high pressure threshold (nearly 8 s after the failure).

After the SCRAM triggering If the internal pressure of the cooling loop increases up to a certain limit, some natural convection valves are set to be opened. The new temperature distribution inside the cooling channel shall be such that the liquid inside the cooling channel is reversed In the following sections an analysis of the apparatus after the REP pumps failure, is presented.

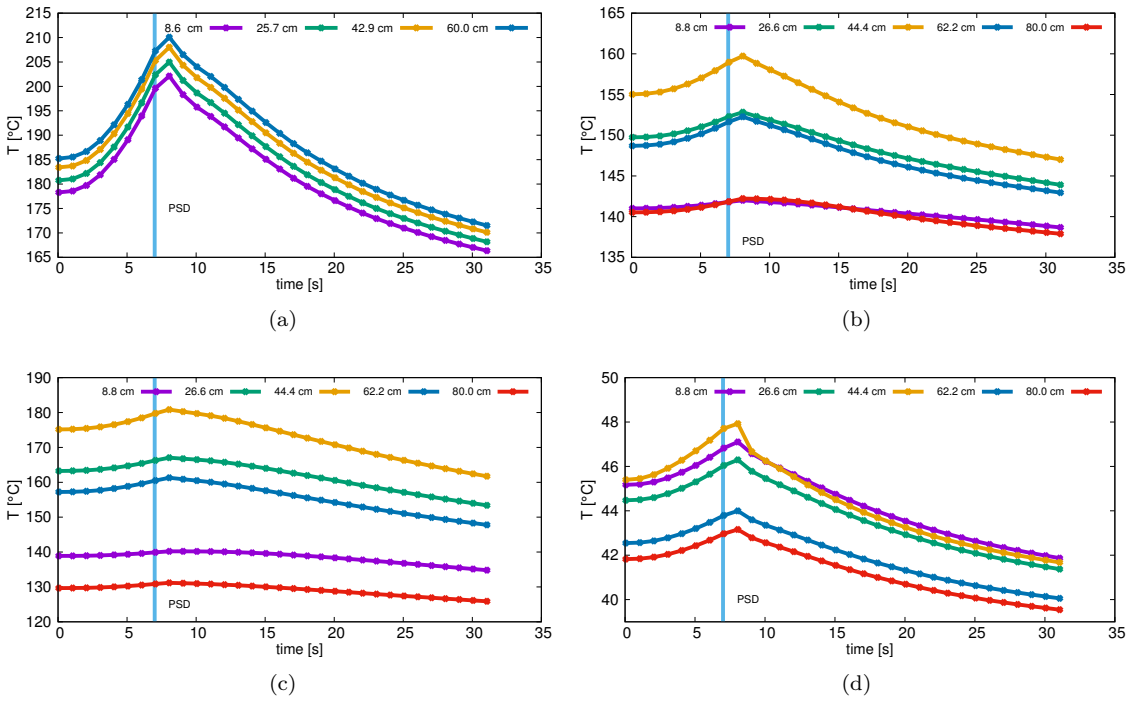

Figure 5.12: Temperature of some thermal structures during the accidental scenario: external fuel cladding (a), FST (b), internal pressure flask (c), hafnium neutron screen (d).

Failure of the REP pumps, reactor SCRAM is not triggered

Without more water that circulates with a certain velocity inside the the cooling channel the heat sink strongly decreases, all the power generated inside the hot and cold channel is no more dissipated inside the JHR reactor pool. In the first 200 *s* from the pumps failure, the thermosyphon liquid flow (TLF) between the hot and the cold channel assures an adequate cooling and maintains the fuel temperature low. After that, the temperatures of the fuel cladding and the internal FST increase. After nearly 100 minutes from the beginning of the accidental scenario, the dry-out condition inside the cooling channel occurs. Figure 5.13 shows the temperature evolution along the fuel cladding, the FST, the inner pressure flask and the hafnium screen. Figure 5.14 shows the behavior of the pressure inside the device.

Failure of the REP pumps, reactor SCRAM is triggered

In this case, after 7 *s* from the failure of the cooling circuit pumps, the reactor SCRAM is triggered. The initial pressure inside the system is fixed at 65 *bar* in the first simulation and 75 *bar* in the second, see figure5.15. Figure 5.16 shows the evolution of the temperature along the thermal structures. In particular, looking at the figure 5.16(a)-(b) the temperature shows

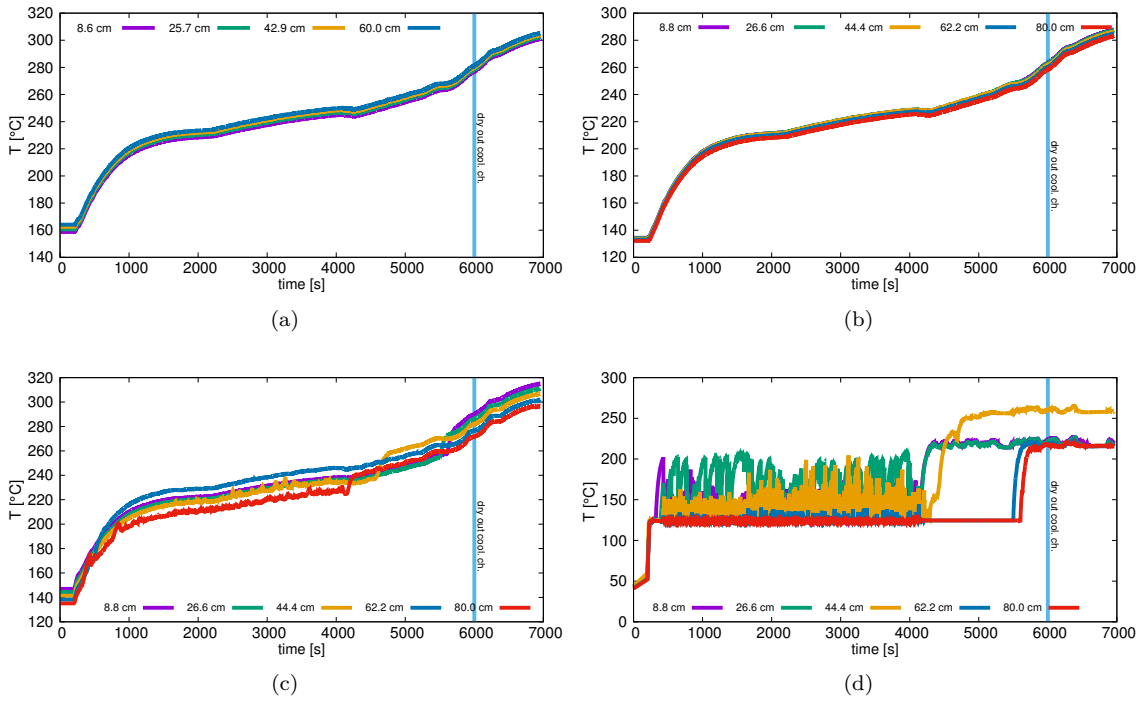

Figure 5.13: Walls temperatures at different heights: fuel cladding (a), inner part of FST (b), inner pressure flask (c), hafnium neutron screen (d).

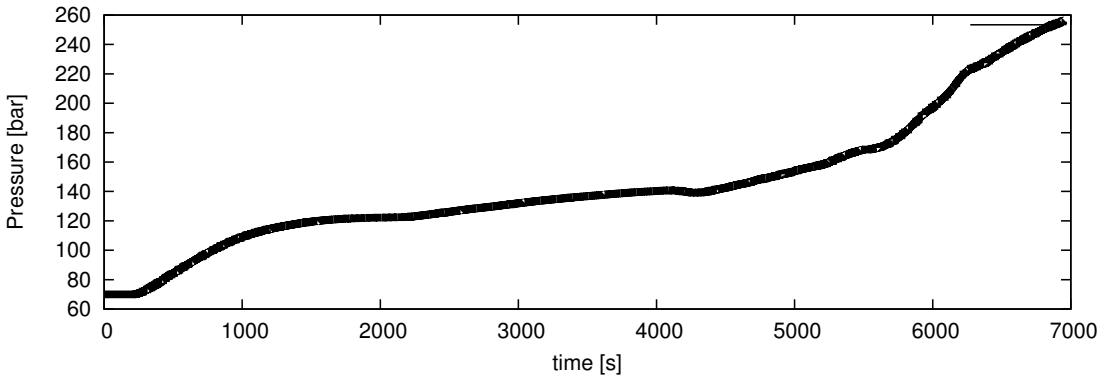

Figure 5.14: Internal pressure.

a stable behavior due to the thermal inertia of the TLF which, after the first seconds from the accidental scenario, does not decreases sharply. In particular, after 500 s the TLF stabilizes at nearly 0.025 kg/s, see 5.17. Inside the cooling channel Once the pumps has failed, the mass flow decreases immediately, the heat transfer coefficient between the water and the outer pressure flask reduces significantly as demonstrated looking at the small temperature spike figure5.16(c)

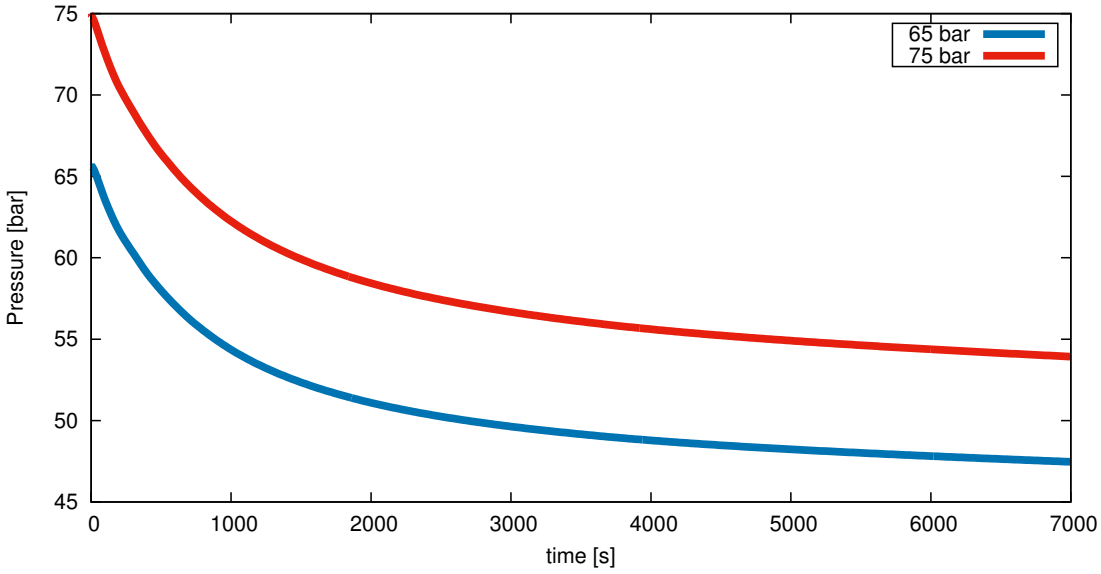

Figure 5.15: Internal pressure.

and the temperature along the hafnium neutron screen figure5.16(d). The liquid temperature inside the cooling channel does not reach the saturation temperature and no bubbles are formed inside it.

5.3 Conclusion

The results derived from the analysis on the working limits of the TLF (thermosyphon liquid flow) confirms a stable behavior of the device even for high LHGR values. By considering the in-pile pressure inside the device as a constant, fixed at 70 bar, the results show a stable behavior of the TLF even for LHGR of the order of 220 W/cm. If the device is considered as a closed capsule, an important role is played by the cushion of helium on the top part of the device. In this chapter the case when a volume of 5 l of helium is considered. In particular, the results suggest that for this specific amount of gas, between the 40 and 100 W/cm, the internal pressure inside the in-pile device increases almost linearly of order of 0.5 bar for every W/cm of linear power (LHGR) injected inside the fuel sample, see figure 5.9. As a first accidental scenario, the case during which the classified withdrawal is defective, is analyzed. In this condition, as a result of an increasing of the fuel factor of 2.2 times its initial value, the fuel temperature could increases its value of 2.7 $°C/s$ in the first 9 s after the beginning of the transient. The fuel temperature starts to decrease of nearly -2 $°C/s$ after 2 s the triggering of the preventive shut down (PSD), see figure 5.12. The temperature decreasing ratio depends on the thermal structure analyzed and the axial coordinate where the temperature is computed. The second accidental scenario

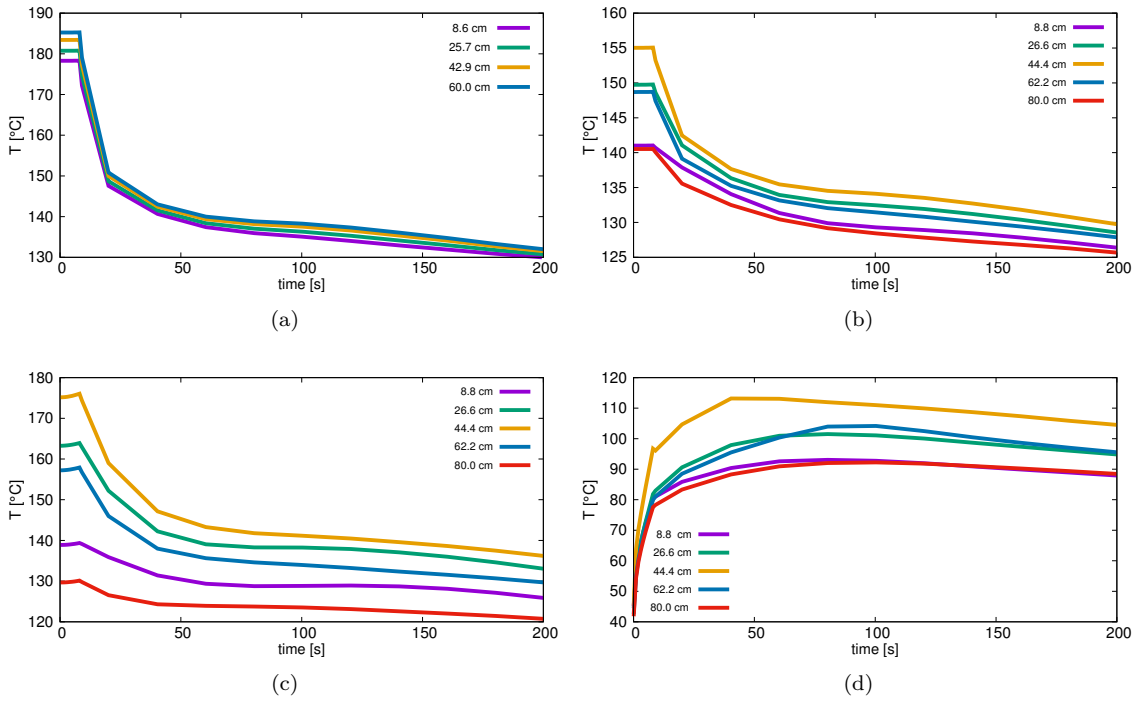

Figure 5.16: Walls temperatures at different heights: fuel cladding (a), inner part of FST (b), inner pressure flask (c), hafnium neutron screen (d).

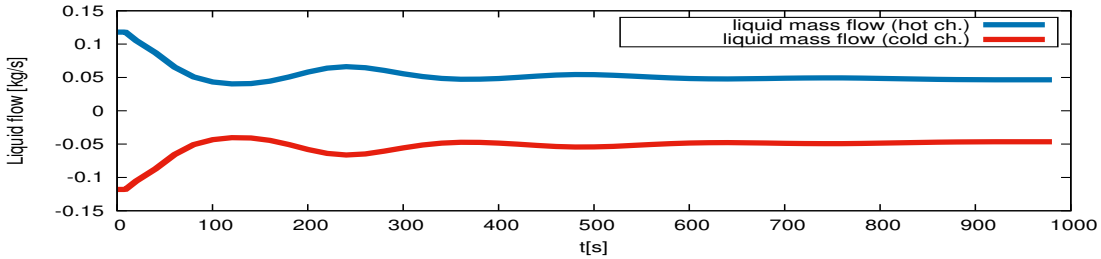

Figure 5.17: Liquid mass flow inside the hot and cold channel.

presented in this chapter, shows a more critical case. In this situation, the heat sink produced by the cooling channel ceases (for example, failure of the re-circulating pump) and the preventive shut down (PSD) is not detected. The results derived from this simulation suggest that the time before which the dry-out condition occurs is approximately of 6000 s. The aim of this simulation is to investigate the evolution of the in-pile pressure, for this reason, the opening of the pressure relief valves (PRV) are not covered. In this condition, as the figure 5.14 shows, the internal pressure of the in-pile device reaches the 90 *bar* in a matter of 500 s. In this case, it is quite interesting to observe the evolution of the temperature of the thermal structures computed along

the fuel, the flow separation tube (FST) and the inner pressure flask (IPF), those do not increase immediately but they remain at the same temperature for nearly 200 s. After this initial time, the increasing of temperature along the fuel cladding and the flow separation tube (FST) varies between $0.075 \div 0.085$ $°C/s$ and nearly 0.1 $°C/s$ for the IPF. The last scenario presented, shows the evolution of the temperature of the thermal structures if the preventive shout down (PSD) is detected. In this condition, the triggering of the PSD prevents the formation of boils inside the cooling channel. Looking at the thermosyphon liquid flow (TLF) between the cold and hot channel, this ensures a big thermal inertia for the fuel cladding and the flow separation tube (FST), which temperature do not increase during the transient. A small increase of temperature in visible along the inner pressure flask. The temperature computed along the hafnium screen increase in the fist 50 s and subsequently remains quite stable.

Chapter 6

Analysis of the Dry and Quenching phase

The aim of this Chapter is to understand the behavior of the device during the Dry phase and to obtain a preliminary assessment of the Quenching phase. The first part of this chapter shows the results obtained by the thermal and mechanical analysis of the dry phase. At the end of the re-irradiation phase, the device empties, only a small amount of water remains at the bottom of the device. In order to produce some steam necessary to perform the dry phase, the EH placed on the bottom of the device is switched on. Once the vapor has been generated, the device (DD) can move toward the core (Heating phase). For this first part a set of simulations are studied in order to understand the best conditions to perform the Dry-phase correctly. For this purpose, different initial conditions with different fuel sample configurations are set to determine the evolution of the system and the fuel sample itself. In the second part of this chapter, a preliminary study of the behavior of the device during the re-flooding phase, is analyzed. In particular the evolution of the internal pressure and the behavior of the cladding temperature are investigated.

6.1 Dry phase

6.1.1 Hypothesis and initial conditions

Radiation model

During the CATHARE calculation of the dry phase, a special subroutine is implemented to the standard input file to take into account the radiative heat transfer between the structures. For each mesh located along the fuel zone, the radiative transfer is activated when the local void fraction calculated in the hot and the cold channel, is greater than a threshold value imposed

by the user. To better understand the modus operandi of this subroutine, the figure 6.1 shows a view of the LORELEI apparatus at the height where the fuel sample is located. From the point of view of calculation, once the subroutine has been activated, at every time step, for the $j-th$ mesh composing the innermost and outermost radial mesh of the thermal structures involved (marked in gray in the figure 6.1), the total powers exchanged by radiation are calculated as follows

$$
\begin{aligned}
P_{r,fuel} &= -\sigma_{sb}\sum_j \left[\frac{(T^4_{clad}-T^4_{FST,i})}{\frac{1}{\epsilon_{ZR}}+\frac{(1-\epsilon_{IN})R_{clad}}{\epsilon_{ZR}R_{FST,i}}}S_{clad}\right]_j \ , \\
P_{r,FST} &= \sigma_{sb}\sum_j \left[\frac{(T^4_{clad}-T^4_{FST,i})}{\frac{1}{\epsilon_{ZR}}+\frac{(1-\epsilon_{IN})R_{clad}}{\epsilon_{ZR}R_{FST,i}}}S_{FST,i}-\frac{(T^4_{FST,e}-T^4_{IPF,i})}{\frac{1}{\epsilon_{IN}}+\frac{(1-\epsilon_{SS})R_{FST,e}}{\epsilon_{IN}R_{IPF,i}}}S_{FST,e}\right]_j \ , \\
P_{r,IPF} &= \sigma_{sb}\sum_j \left[\frac{(T^4_{FST,e}-T^4_{IPF,i})}{\frac{1}{\epsilon_{IN}}+\frac{(1-\epsilon_{SS})R_{FST,e}}{\epsilon_{IN}R_{IPF,i}}}S_{IPF,i}-\frac{(T^4_{IPF,e}-T^4_{OPF,i})}{\frac{1}{\epsilon_{SS}}+\frac{(1-\epsilon_{SS})R_{IPF,e}}{\epsilon_{SS}R_{OPF,i}}}S_{IPF,e}\right]_j \ , \\
P_{r,OPF} &= \sigma_{sb}\sum_j \left[\frac{(T^4_{IPF,e}-T^4_{OPF,i})}{\frac{1}{\epsilon_{SS}}+\frac{(1-\epsilon_{SS})R_{IPF,e}}{\epsilon_{SS}R_{OPF,i}}}S_{OPF,i}\right]_j \ ,
\end{aligned}
\tag{6.1}
$$

with

$$
\begin{aligned}
S_{clad}|_j &= 2\pi R_{clad}|_j h_j \\
S_{FST,i}|_j &= 2\pi R_{FST,i} h_j \\
S_{FST,e}|_j &= 2\pi R_{FST,e} h_j \\
S_{IPF,i}|_j &= 2\pi R_{IPF,i} h_j \\
S_{IPF,e}|_j &= 2\pi R_{IPF,e} h_j \\
S_{OPF,i}|_j &= 2\pi R_{OPF,i} h_j \ .
\end{aligned}
\tag{6.2}
$$

In the [6.2] are expressed the external and internal surfaces S with the related radius R, see figure 6.1. During the calculation, if the FUEL sub-module is activated, the fuel cladding radius $R_{clad}|_j$ may changes in accordance with the thermal expansion ([1.50]). The values of $\alpha_{hc}|_j$ and $\alpha_{cc}|_j$ are stabilized by the user, in general the choice of those values is done in accordance with the physic of the problem.

Fuel sample configuration and control of the displacement device

For this phase some simulations have been performed. Table 6.1 divides the simulations in accordance with the initial conditions of the fuel utilized. At the beginning, a new fuel sample with a low initial pressure gap and a minimum value of the cladding oxide, is used. For a second type of simulation, a fuel with a thicker external oxidation and higher internal gap pressure is utilized. At first, the case during which the displacement device (DD) remains at fixed position

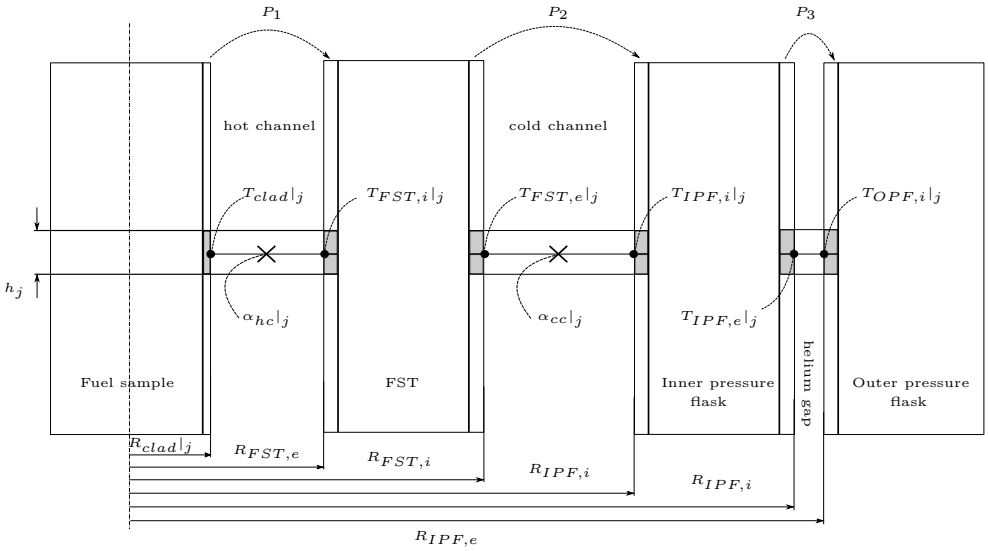

Figure 6.1: Schematic description of the calculation model implemented in the radiation heat transfer subroutine.

Table 6.1: Initial condition of the fuel sample.

Fuel sample configuration	1	2
R_{fuel} $[mm]$	4.15	4.15
ζ_{gap} $[\mu m]$	1	1
$R_{clad,e}$ $[mm]$	4.75	4.75
$\zeta_{oxy,e}$ $[\mu m]$	5	5
$\zeta_{oxy,i}$ $[\mu m]$	5	100
P_{gap} $[bar]$	10	50
Fuel sample type	ZRCEA	ZRCEA

once the cladding temperature has reached a target value, is analyzed. Other simulations analyze the behavior of the DD when this can move in accordance with the target value of the fuel cladding temperature. For this last case, an ON/OFF type-regulator was implemented to maintain the middle of the fuel cladding at 1200 $°C$ (set point value) with a maximum permissible error of $\pm$ 50 $°C$. Some specific velocities of the displacement device (u_{DD}) are chosen in order to verify the maximum fuel heat-up rate. For all the simulation analyzed, the power generated inside the electrical heater P_{EH} can vary between three different values 1-1.5-2 kW. In particular, by setting $P_{EH} < 0.8kW$, the calculations suggest that the steam does not penetrate inside the hot channel and the dry phase cannot be studied. In a benchmark simulation, in order to evaluate the impact of power produced by the cladding oxidation, the activation of the electrical heater placed at the bottom of the device is activated after the approach of the device toward the core

(heating phase). In the simulations performed, the dry phase lasts nearly 25 minutes. Actually, when the device becomes operational, the whole dry phase lasts in accordance with the level of the clad oxidized reached.

Limit of the heat-up of the fuel cladding

During the approach of the device toward the core, in order to minimize the non-homogeneous peripheral temperature distribution around the fuel sample, an electrical heater is placed on the flow separation tube (FST) along the total height of the fuel sample. The use of this electrical heater is required to take into account the heating effect of the nearby fuels which surrounded the rod in a real fuel bundle. However, the change of power over the time of this electrical heater, has a technological limit above which it cannot go. The IAEC (Israel Atomic Energy Commission), which is in charge of the design the apparatus, has planned to install an electrical heater which temperature heat-up rate shall not exceed the 20 $°C/s$ (before the clad burst). For this reason the fuel sample heat-up rate, shall not exceed this threshold limit as well. The heat-up rate Λ may be expressed as the derivative of the fuel cladding temperature over the time.

6.1.2 Simulations

Introduction

Table 6.2 summarized the characteristics of the four simulations which has been performed for the dry phase. In particular each simulation differs from the other by the fuel sample configuration, if the ON/OFF fuel temperature regulator is activated, at what time and at how much power is injected inside the electrical heater (EH) to produce the steam required. For all the simulations performed, the threshold value imposed for the void fraction inside the hot and cold channel, is such that $\alpha_{hc}|_j = \alpha_{cc}|_j = 0.98$. The choice of this value is done according to the physic of the problem. In this case, as it will be discussed afterwards, some steam tends to condense not only in the coldest zone inside the device but also inside the channel in zone 2, see figure 6.2. In particular, the zone 2 could include the top part of the fuel zone and some liquid could cool a part of the fuel sample. The constant values of the emissivity coefficient for the materials are listed in the table 6.3.

Simulation 1

Within 20 minutes from the beginning of the transient and the activation of the electrical heater (EH), all the steam produced in the hot channel has pushed the helium above the fuel zone. After that, the nodes which comprise the fuel cladding reach the saturation temperature and the system pressure stabilizes. At this point the device moves towards the core (t=1000 s). In the first calculation performed, once the DD has reached the position corresponding to the

Table 6.2: Characteristcs of the simulations for the Dry phase.

Simulation n°	1	2	3	4
Fuel sample configuration	1	1	2	2
Temperature Regulator	No	Yes	Yes	Yes
Steam production[a]	Before	Before	Before	After
P_{EH} $[kW]$	1-1.5	1-1.5-2	1-1.5-2	1

[a] The steam production necessary for the dry phase can occur before or after the approach of the displacement device (DD) towards the reactor core

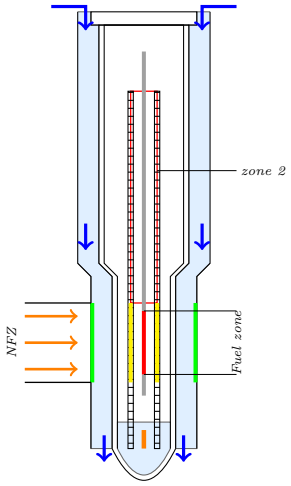

Figure 6.2: Zone 2 along the hot channel.

Table 6.3: Emissivity.

Zircaloy	Inconel	SS
ϵ_{ZR}	ϵ_{IN}	ϵ_{SS}
0.8	0.7	0.5

target value of temperature, it remains there for all the duration of the plateau phase. For this specific calculation, the initial pressure inside the system is fixed to 3 bar and some water (1.2 l) remains at the bottom of the device to produce the required steam. For this simulation we set the LHGR=25 W/cm and P_{EH}=1 kW. The results obtained from this calculation reveal two phenomena which might modify the cladding temperature profile during the dry phase.

1. The first phenomenon occurs at the beginning of the dry phase. When the device starts to

move towards the core, the cladding surface on the top of the fuel sample remains too wet and its temperature equals the saturation temperature of the system. The code suggests that the temperature in the two last nodes is computed by nucleated boiling mechanism. Figure 6.3 shows the behavior of the fuel cladding temperatures in some points along the fuel sample. In particular the cladding temperature computed between the points 1-22 (0-55 cm) increases according to x_c (12 $°C/s$) while the temperature calculated in the last 5 cm remains low.

2. The second phenomenon occurs during the plateau phase, when the zone 2 includes all or a part of the fuel zone and some liquid cools the cladding surface. In figure 6.4 the gray bands mark the zone 2 where the gas and the liquid mass flow determine the cycles of vaporization and condensation along the hot channel; the negative values of the liquid mass flow indicates the liquid direction which goes from the top towards the bottom of the hot channel. Between the water level and the zone 2 a stagnant zone is formed where only the gas phase is present. In the first 300 s the liquid flow remains at the top part of the fuel sample, see figure 6.4(a), after nearly 450 s the liquid front covers and cools all the fuel sample. For the remaining time of the dry phase, the liquid remains along all the fuel length, as shown in figure 6.4(b)-(c)-(d) and the cooling effects do not decrease.

When the P_{EH} is changed from 1 to 1.5 kW, the effects of the condensation increase, see figure 6.5. The results have shown that, when the DD remains at fixed position for all the duration of the dry phase, for any P_{EH} chosen, these cooling effects make the cladding temperature profile very sensible to these phenomena. It should be noted that if the activation of the EH is delayed with respect to the approach of the device towards the core, the steam could start to cover the fuel cladding when this is already hot (above 1000 $°C$) by producing a peak in power due to steam-zicalloy reaction which could lead to a temperature disturbances on the fuel cladding.

Simulation 2

A second way of functioning for the DD corresponds to a movement in accordance with the target value of the fuel cladding temperature. The ON/OFF controller measures the error between the set point and the temperature in the middle of the fuel cladding. The regulation should be done by changing the distance of the DD and consequently by varying the LGHR in agreement with [4.1]. The velocity of the DD is set to 6 mm/s. Figure 6.6 and figure 6.7 show respectively the distance of the device from the core and the corresponding value of the LHRG during all the dry phase for P_{EH}=1-1.5-2 kW. In this case the minimum value allowable for x_c is 10 cm. The figures 6.8(a)-(b)-(c) show the fuel cladding profile for three different values of P_{EH}=1-1.5-2 kW after 500-1000-1500 s from the approach of the device towards the core. The best condition is found for P_{EH}=1kW where the cladding temperature profile is uniform along all the fuel length. The general cooling at the beginning of the dry phase becomes evident for P_{EH} ≈1.5 kW. The

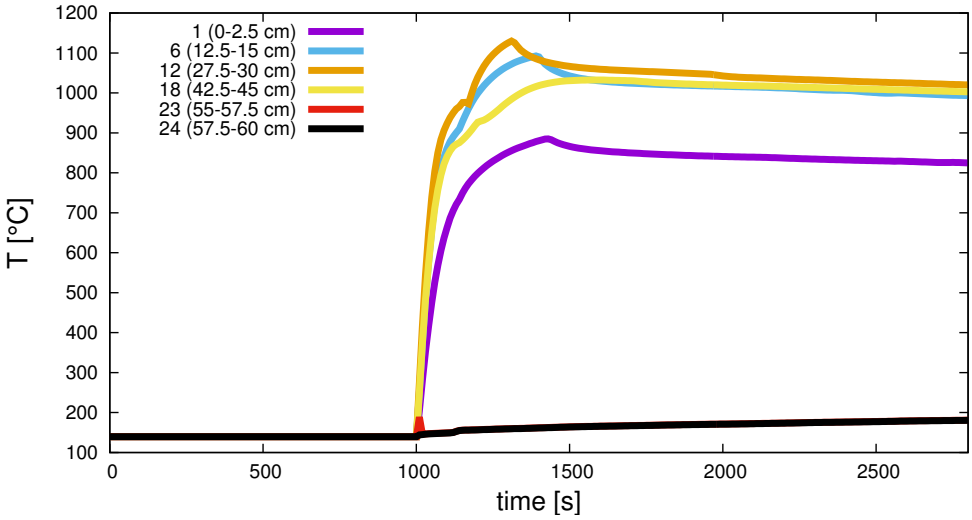

Figure 6.3: Cladding temperature in six different nodes.

temperature calculated on the top of the fuel sample, for P_{EH}=2 kW, shows that the extension of the cladding surface that remains wet, involves nearly the last 7 cm of fuel length. The second problem related to the cooling effects during the dry phase appears for the P_{EH}=1.5 kW when the liquid tends to cool down the last nodes. By increasing the P_{EH} up to 2 kW the last 20 cm of the fuel sample are cooled. Despite some condensation phenomena for $1.5kW \leq P_{EH} \leq 2kW$, the cladding temperature profile meets the necessary requirements. For the entire dry phase, the cladding temperature remains quite uniform over 40 cm, i.e. from 1 to 1.4 m where the fuel ballooning is expected.

Gas distribution inside the device The figures 6.9-6.10-6.11 show the evolution of the steam and the non-condesible gases mass inside the hot channel (HOT_CH), the upper volume (VOLTOP) and the cold channel (COLD_CH).

Hot channel. Once the Dry phase has begun, the steam produced inside the hot channel increases in accordance with the value of P_{EH}. For P_{EH}=1-1.5 kW, all the helium introduced inside the channel during the emptying phase, is pushed upward from the steam flow (for P_{EH}=2 kW all the helium is ejected from the hot channel before the dry phase has started). When the fuel cladding temperature has reached a temperature around 1000 $°C$, the zirconium in the fuel alloy reacts with the steam as demonstrated looking at the hydrogen mass produced. For P_{EH}=2 kW, the continuous phenomena of condensation-vaporization are visible looking at the the steam fluctuation which occurs with a constant frequency after 600 s from the beginning of the transient. The same steam decreasing before nearly 600 s is always produced as a results of the condensation. The magnitude and the frequency of the spikes in m_{H_2} in the first 200 s are

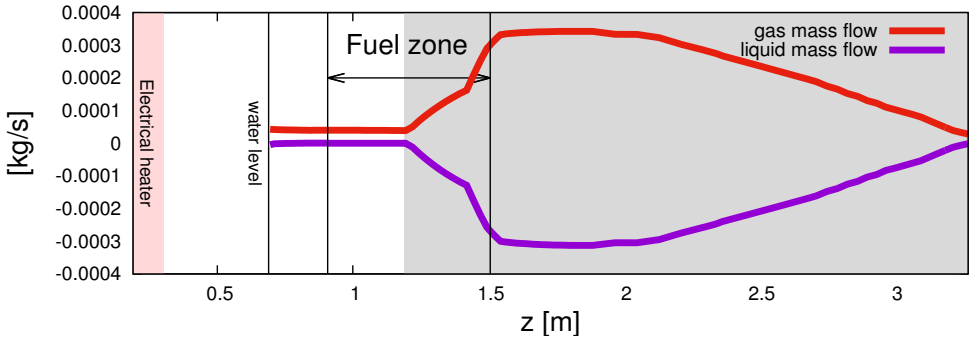

(a)

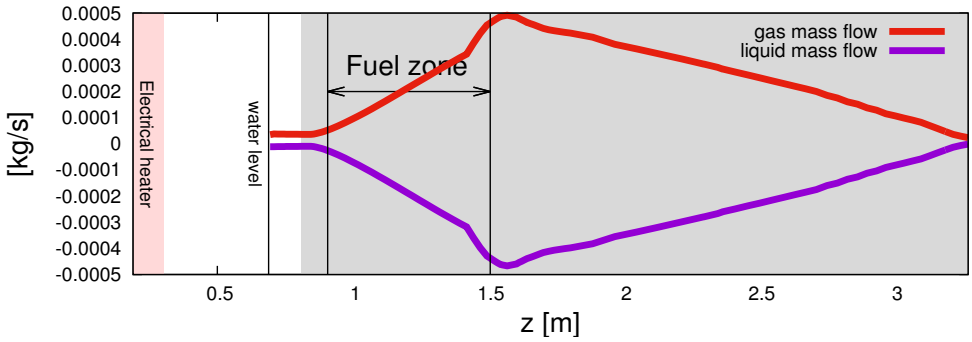

(b)

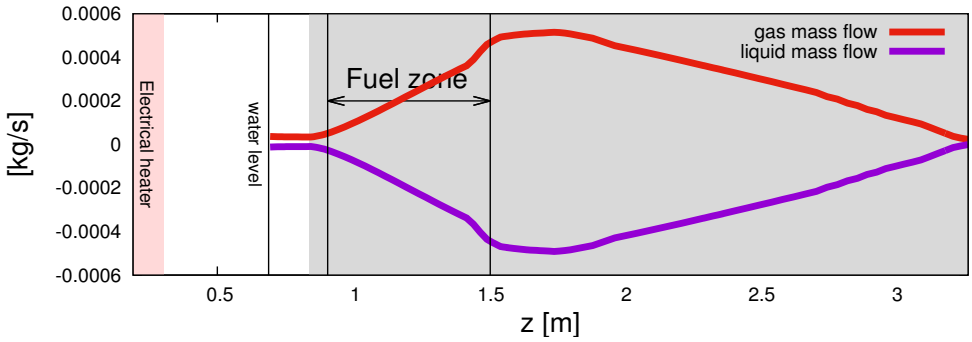

(c)

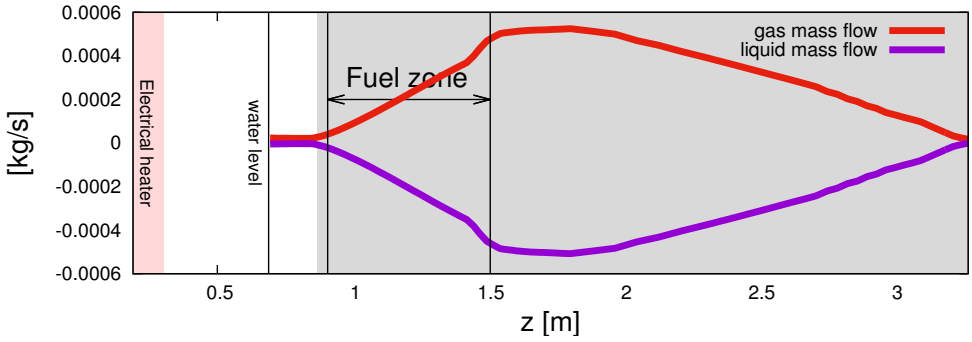

(d)

Figure 6.4: Gas and liquid mass flow inside the hot channel after 300 s (a), 600 s (b), 1200 s (c) and 1800 s after the approach of the device towards the core.

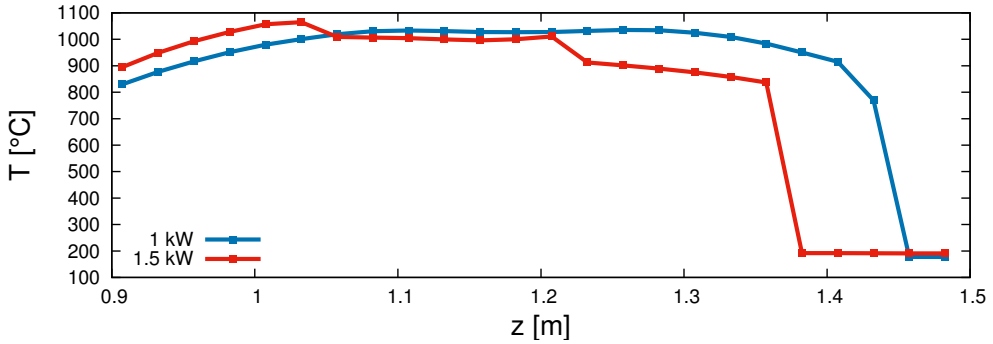

Figure 6.5: Cladding temperature profile after 1500 s from the approach of the device towards the core.

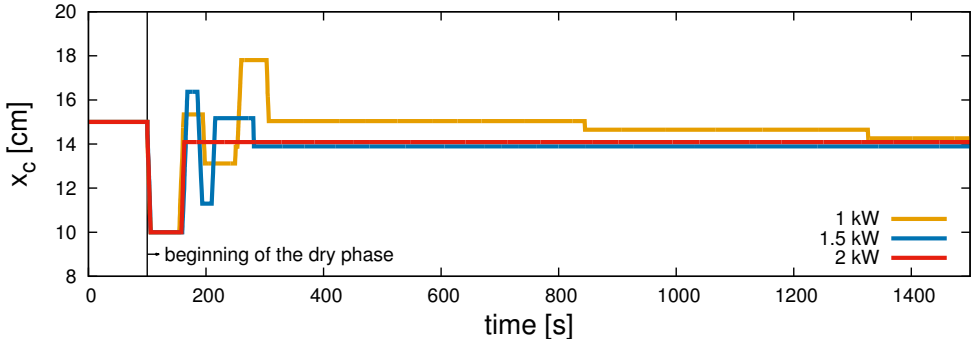

Figure 6.6: x_c during the dry phase.

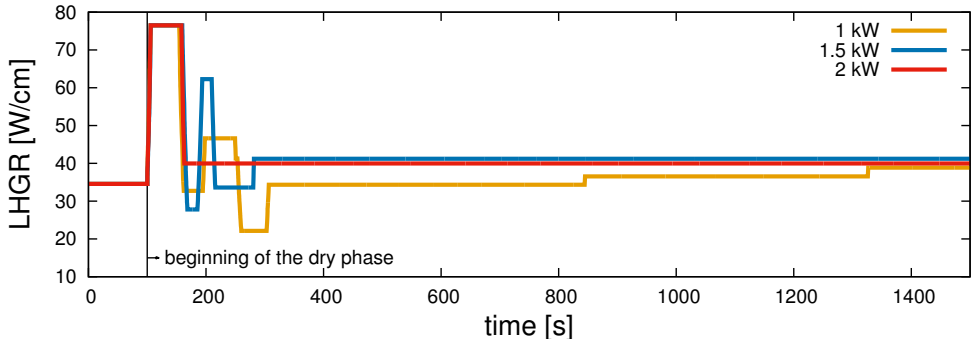

Figure 6.7: LHGR during the dry phase.

mainly due to two phenomena:

- The oscillation of the cladding temperature during its regulation (see the fuel temperature in the middle of the fuel sample in the following of this thesis).

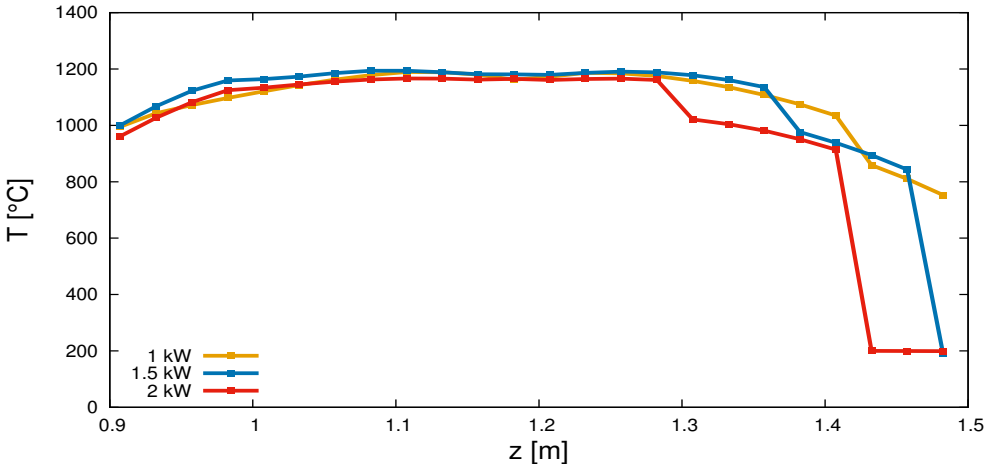

(a)

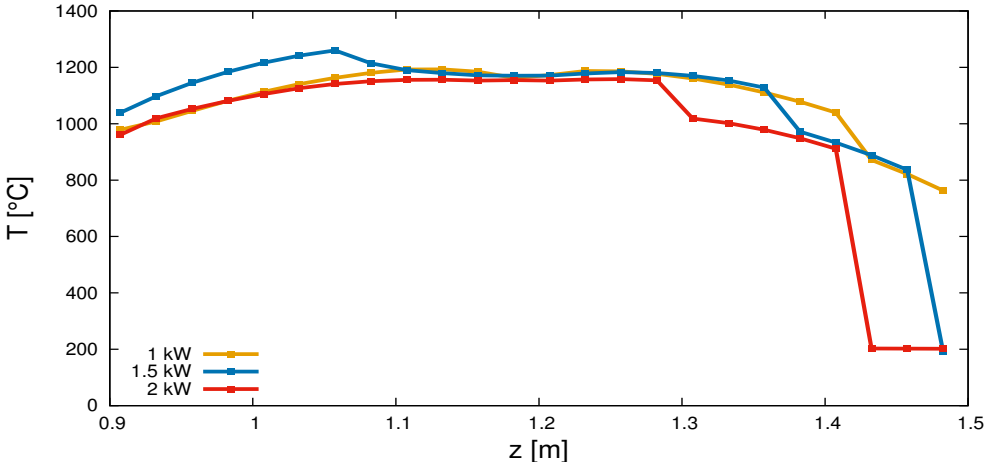

(b)

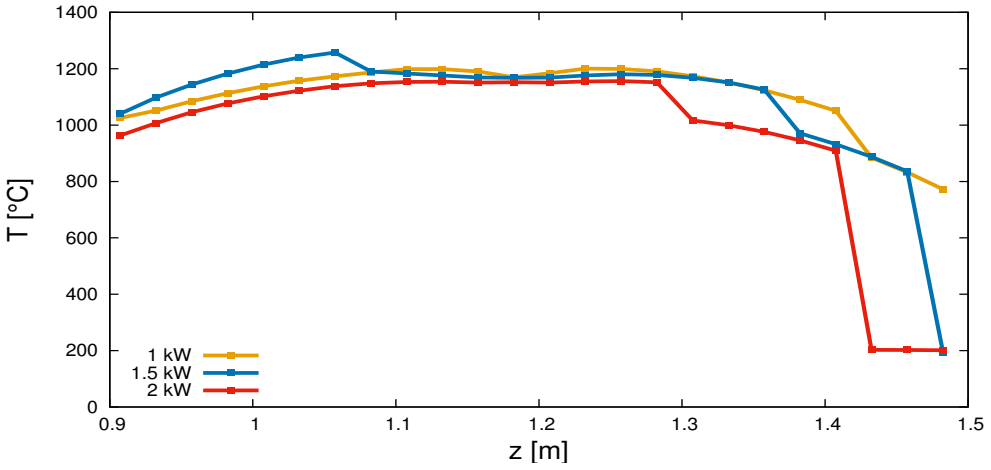

(c)

Figure 6.8: Cladding temperature profile after 500 (a), 1000 (b), 1500 (c) s from the approach of the device towards the core.

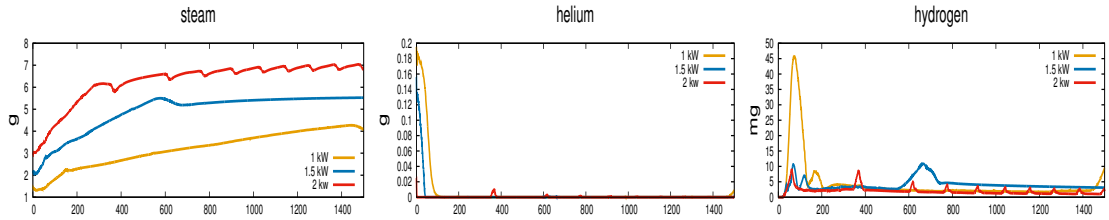

Figure 6.9: Gases flow inside the hot channel during the dry phase.

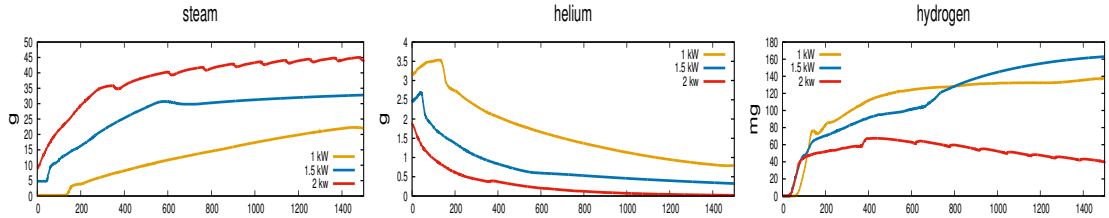

Figure 6.10: Gases flow inside the upper volume during the dry phase.

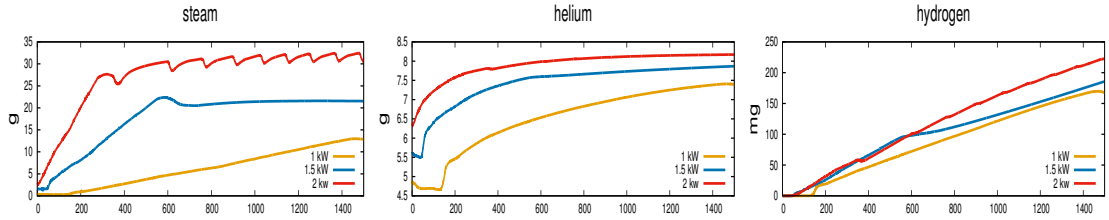

Figure 6.11: Gases flow inside the cold channel during the dry phase.

- The different gas stratification at the beginning of the dry phase. In particular, for P_{EH}=1 kW the grater concentration of helium in the top of part of the device, coupled with a less steam production, shall be such that the hydrogen produced remains longer inside the hot channel, by increasing its mass concentration (firs peak at nearly 75 s after the beginning of the Dry-phase). This phenomena does not appear for P_{EH}=1.5-2 kW where the hydrogen produced is immediately ejected from the hot channel.

Upper volume (gas blanket). In this volume, the steam produced inside the hot channel tends to accumulate. For P_{EH}=1-1.5 kW, the helium present at the beginning of the dry phase, increases its concentration because receives other gas dragged by the steam produced in the hot channel. When the steam increases, the helium is dragged in the upper part of the cold channel. The hydrogen in this upper volume tends to be accumulated.

Cold channel. Figure 6.12 shows the gas fraction distribution inside the cold channel at the end of the dry-phase for P_{EH}=1 kW, a similar gas distribution is observed for P_{EH}=1.5-2 kW. As

it can be seen, the steam covers all the neutron flux zone (NFZ) up to reach a height of nearly 1.8 m. Between 1.8 m and 2.5 m a mix of steam and helium fills the channel. Starting from 2.5 m up to the end of the channel, the hydrogen produced increases its concentration. The largest percentage of helium is accumulated in this channel (83 % of the total m_{He} for P_{EH}=2 kW). The mass of hydrogen increases up to the end of the transient (m_{H_2} is more the 200 mg for P_{EH}=2 kW).

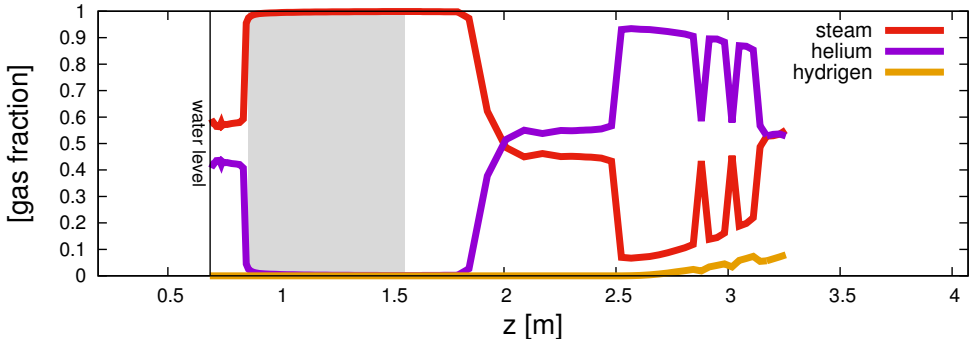

Figure 6.12: Gas fraction inside the cold channel at end of the dry phase t=1500 s, P_{EH}=1 kW. The gray zone marks the neutron flux zone (NFZ).

Oxidation process When the cladding temperature has reached a temperature of order of $\approx 1000°C$, the exothermic reaction between the steam and the zirconium in the fuel cladding can be studied. In this thesis, the Cathcart-Pawel law (Cathcart et al., 1977) has been utilized for the calculation of the oxidation process. Figure 6.13 correlates the power released by the cladding oxidation with the cladding temperature calculated in the middle of the fuel sample, for P_{EH}=1-1.5-2 kW. For all the three cases analyzed, the peak of power varies between 220 and 250 W. Figure 6.14(a)-(b)-(c) shows the thickness of the external cladding oxidized. As mentioned before, the low levels of the thickness in the top of the fuel sample for P_{EH}=1.5-2 kW are due to low value of temperature in the upper part of the fuel alloy. For P_{EH}=1.5 kW, at the end of the dry phase, the maximum thickness of fuel cladding oxidize is reached at the height of nearly 15 cm of the fuel alloy. In this last case, a thickness of 140μm i.e. 23% of the initial cladding thickness, is reached.

Thermal-mechanical behavior of the fuel cladding Figure 6.15 shows the pressure inside the fuel gap P_{gap}, the times $t_1 < t_2 < t_3$ are the instants when the fuel cladding bursts. For P_{EH}=1.5-2 kW, the lower value of the pressure in the fuel cladding gap is due to the low level of temperature reached in the top of the fuel sample in accordance with the [1.57]. For P_{EH}=1 kW the rupture of the fuel alloy occurs faster and the condition [1.58] is reached quickly. Figure 6.16 shows the average value of the cladding temperature weighed over all the radial points

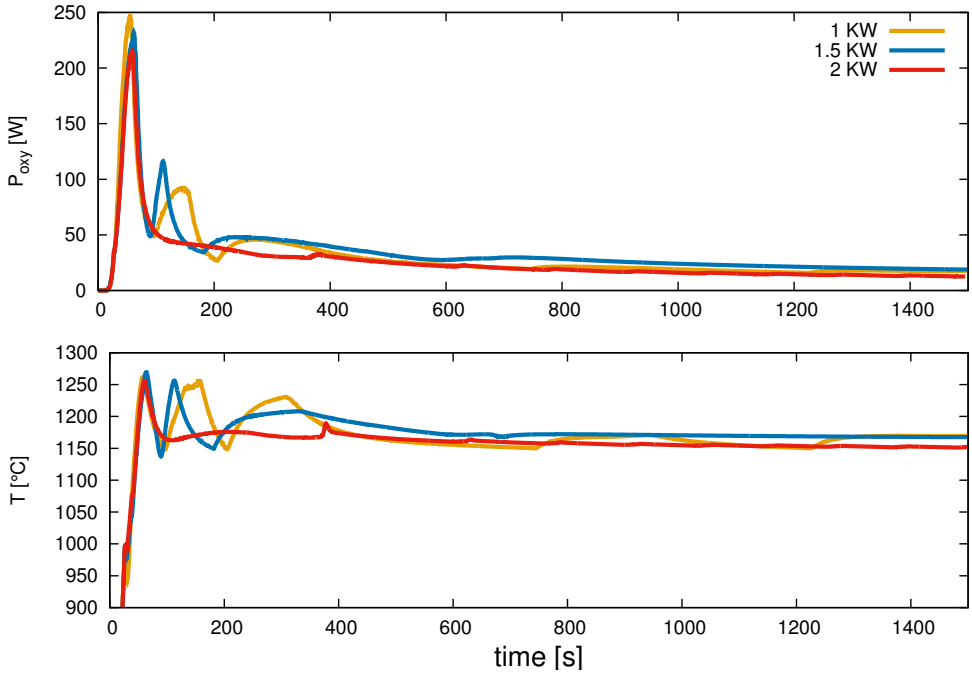

Figure 6.13: Power due to the cladding oxidation for P_{EH}=1-1.5-2 kW (top), fuel cladding temperature computed in the middle of the fuel sample (bottom).

Table 6.4: Results obtained by considering a velocity of the displacement device of 6 cm/s.

P_{EH} $[kW]$	t_b $[s]$	$T_{clad,b}$	Λ $[°C/s]$	ϖ^a [%]	$\zeta^a_{oxy,m}$ $[\mu m]$	$m^a_{H_2,tot}$ $[g]$	max P_{oxy} $[W]$
1	27.5	964	30	23.6	86.6	0.31	250
1.5	37.2	1045	24	34.8	91.6	0.35	241
2	39.4	1075	23	25.8	70.8	0.26	220

[a] Values refereed at the end of the transient.

for a given height of the fuel, and the cladding radius in the first instants of time after the beginning of the dry phase. Always looking at the figure 6.16, the red vertical line marks the axial coordinate where the cladding rupture occurs. The figures 6.17-6.18, show the values of the cladding temperature at the same time steps. For P_{EH}=1.5-2 kW the zone of fuel ballooning zone involves nearly 40 cm i.e. from 1 to 1.4 m, for P_{EH}=1 kW the area affected is reduced at 30 cm, i.e. from 1.05 to 1.35 m. The maximum cladding elongation of nearly 34.8 % the initial radius, occurs for P_{EH}=1.5 kW. In all the three simulations performed, the rupture of the cladding occurs in the middle of the fuel sample. Table 6.4 summarizes some result obtained with this second simulation. As written before, for a conservative calculation, the velocity of the displacement device (DD) is those maximum of 6 cm/s. As it can be seen, by looking at

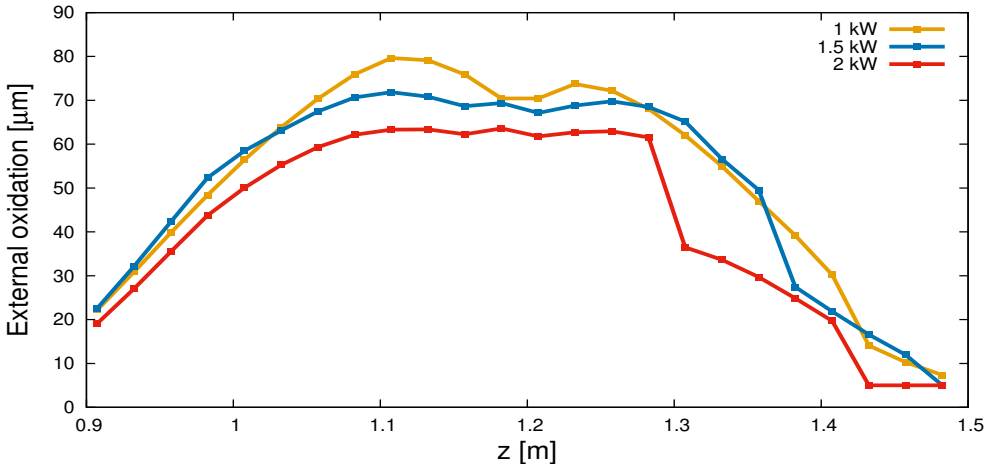

(a)

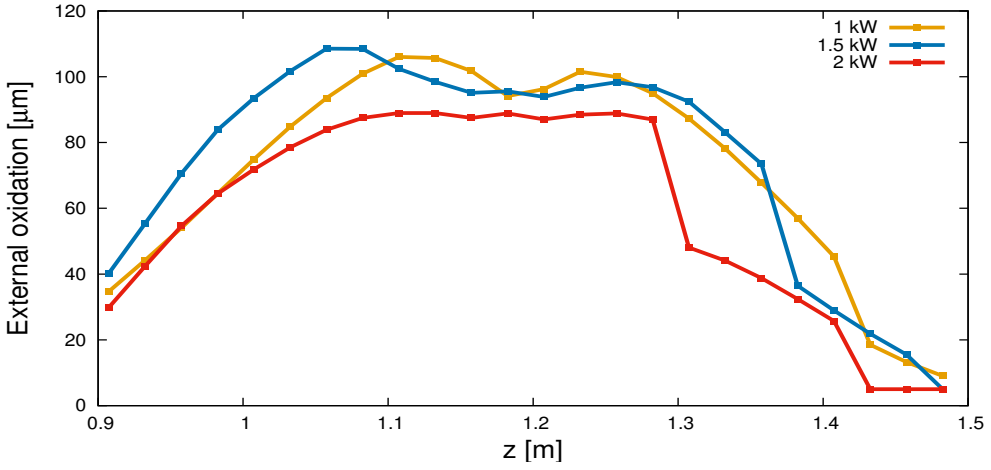

(b)

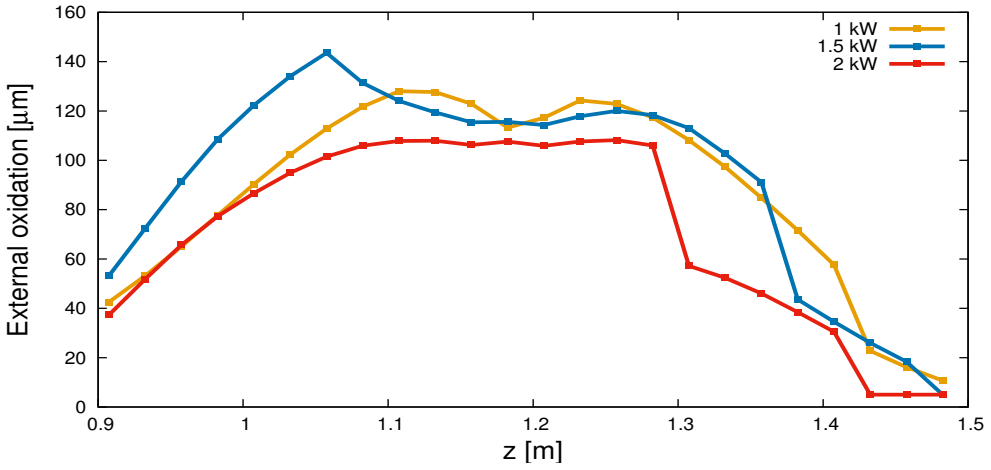

(c)

Figure 6.14: External thickness of cladding oxide after 500 (a), 1000 (b), 1500 (c) s from the approach of the device towards the core.

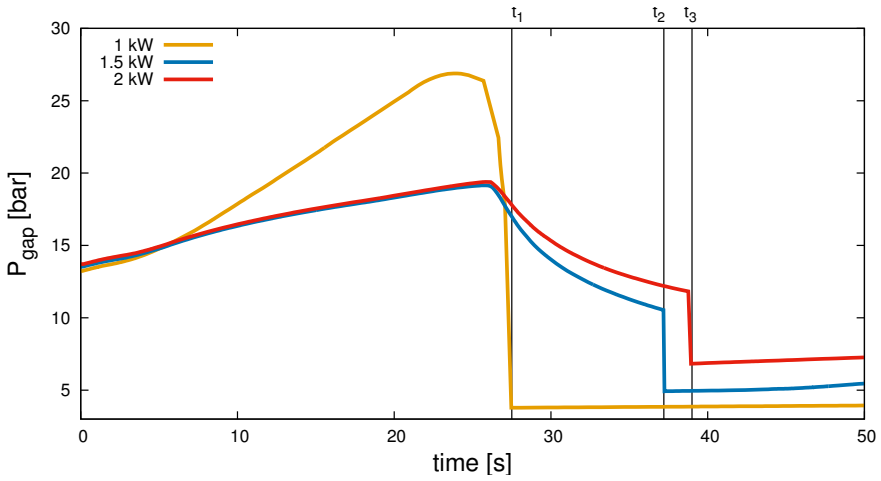

Figure 6.15: Pressure inside the fuel gap in the first 50 s from the beginning of the dry phase.

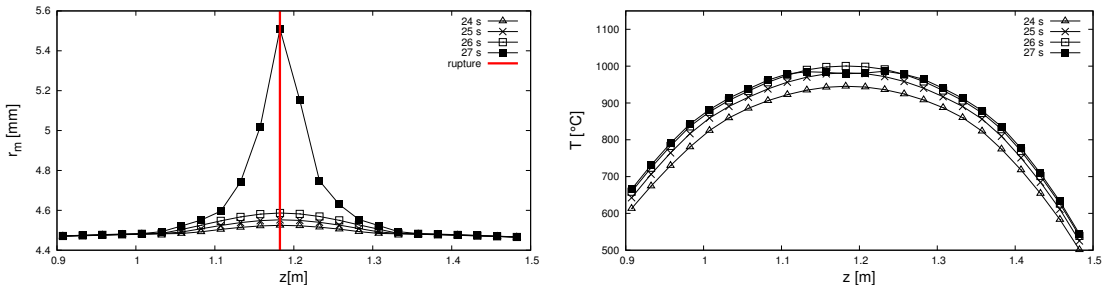

(a) (b)

Figure 6.16: Average fuel cladding radius (a) and corresponding fuel cladding temperature (b), P_{EH}=1kW.

the fourth column of the table 6.4, by considering this displacement device velocity, Λ is always greater than the limit required ($23°C/s<\Lambda<30°C/s$), for all the three cases analyzed. In the table 6.5 are listed the values of Λ for different lower values for the DD velocity, the numbers marked in bold are the values acceptable. The results show that Λ depends not only on the DD velocity but also on the P_{EH}, in fact for the same DD velocity, the heat-up rate decreases in accordance with the increase of P_{EH}. Indeed, greater is the P_{EH} and hence the steam production, faster is the time required for the steam to drag the mass of gases along the fuel sample. This phenomenon increases the average gas velocity along the fuel sample $\hat{v}_{gas}$, and hence the heat transfer coefficient. This phenomenon is more evident switching the P_{EH} from 1 kW to 1.5 kW.

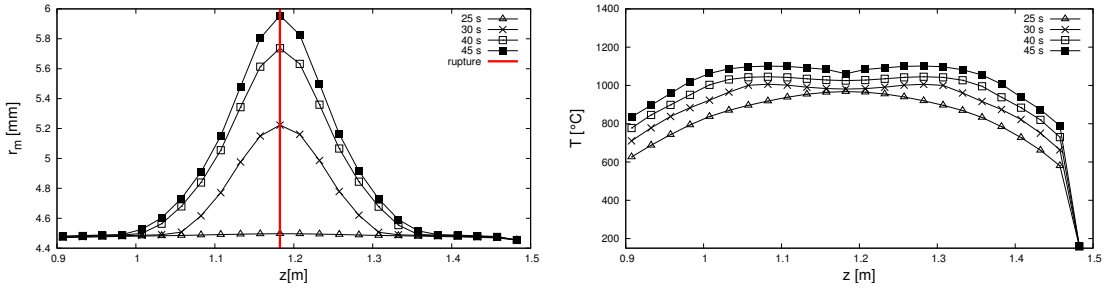

(a) (b)

Figure 6.17: Average fuel cladding radius (a) and corresponding fuel cladding temperature (b), P_{EH}=1.5kW.

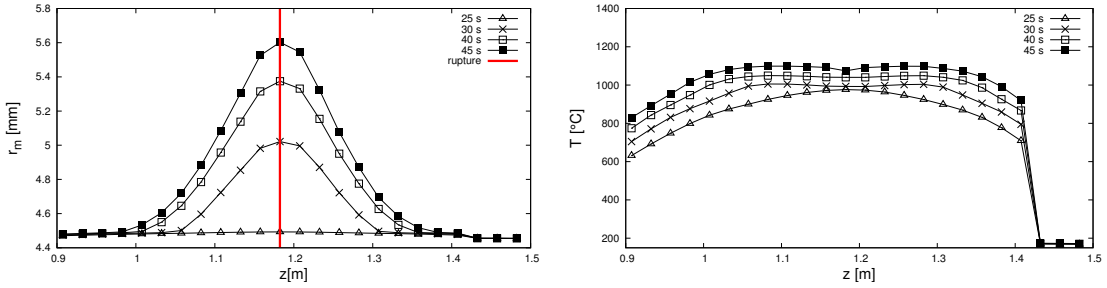

(a) (b)

Figure 6.18: Average fuel cladding radius (a) and corresponding fuel cladding temperature (b), P_{EH}=2kW.

Simulation 3

For this simulation a fuel with the second type of configuration has been utilized (see table 6.2). The thermal-hydraulic behavior of the device is quite similar to the Simulation 2. Figure 6.19 shows the temperature along the fuel sample. As happened in the Simulation 2, for a P_{EH}=2 kW, the temperature calculated in the last nodes remain low, as well as the thickness of the external oxidation, see figure 6.20. The mechanical ballooning of the fuel sample remains asymmetric respect to the mid point of the fuel sample as demonstrated looking at the cladding radius and the respectively cladding temperatures, see figures 6.21,6.22 and 6.23. The average value of the cladding temperature is certainly lower respect to the Simulation 2 due to the lowest power generated by the cladding oxidation. As the simulation 2, the rupture of the fuel cladding occurs always in the middle of the fuel sample. Figure 6.24 shows the evolution of the pressure inside the fuel gap.

Table 6.5: Results obtained by considering a velocity of the displacement device which varies between 0.5 and 1.5 cm/s.

P_{EH}	u_{DD} $[cm/s]$	t_b $[s]$	$T_{clad,b}$	Λ $[°C/s]$	$\hat{u}_g^a$ $[m/s]$
	0.5	58	1030	**15.3**	
1 kW	1.0	43	1006	20.1	0.175
	1.5	37	980	22.7	
	0.5	62	1055	**14.6**	
1.5 kW	1.0	48	1050	**18.7**	0.350
	1.5	44	1050	20.4	
	0.5	69	1075	**13.4**	
2 kW	1.0	52	1077	**18.0**	0.375
	1.5	46	1070	20.0	

[a] $\hat{v}_g$ is the gas velocity inside the hot channel calculated at the height of the middle of the fuel sample, averaged over the first 40 s.

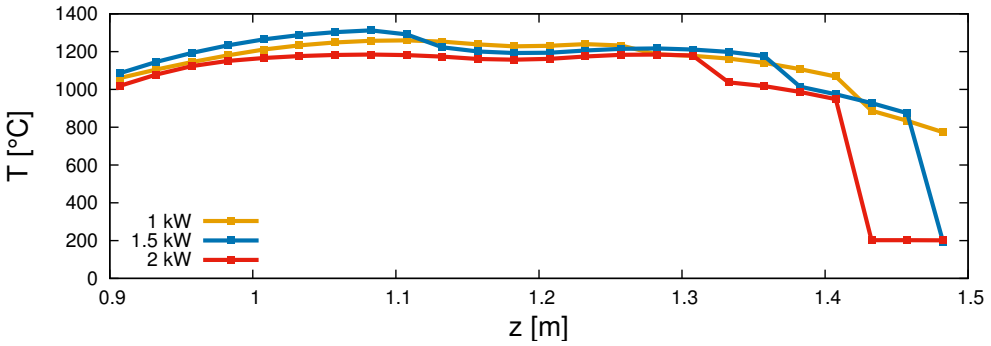

Figure 6.19: Wall temperature along the fuel cladding after 1500 s from the approach of the device towards the core.

Simulation 4

Figure 6.25 shows the cladding temperature in the middle of the fuel cladding when the steam produced by the EH is produced after that the fuel cladding temperature has reached a value of 1200 $°C$. At time t=700 s, the steam generated reaches the fuel sample and the oxidation starts. The power generated by the oxidation increases the cladding temperature and the temperature regulator system moves the device back at nearly x_c=22 cm from the core, see figure 6.26.

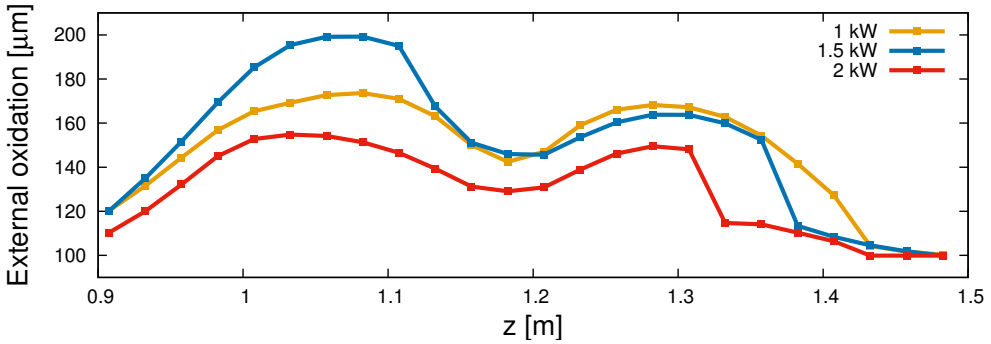

Figure 6.20: External thickness of cladding oxide after 1500 s from the approach of the device towards the core.

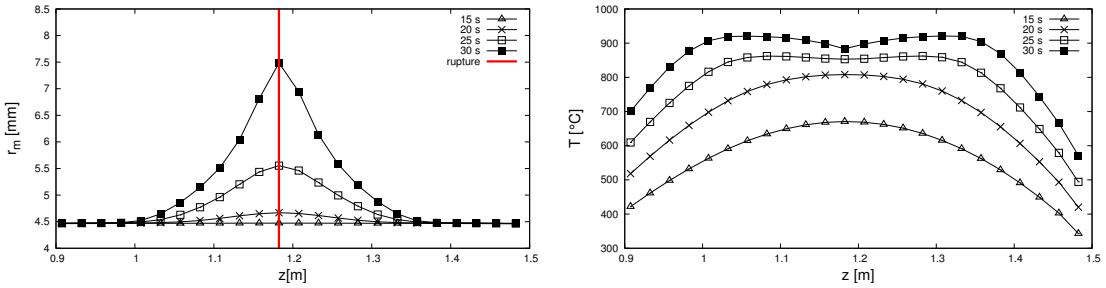

(a) (b)

Figure 6.21: Average fuel cladding radius (a) and corresponding fuel cladding temperature (b), P_{EH}=1kW.

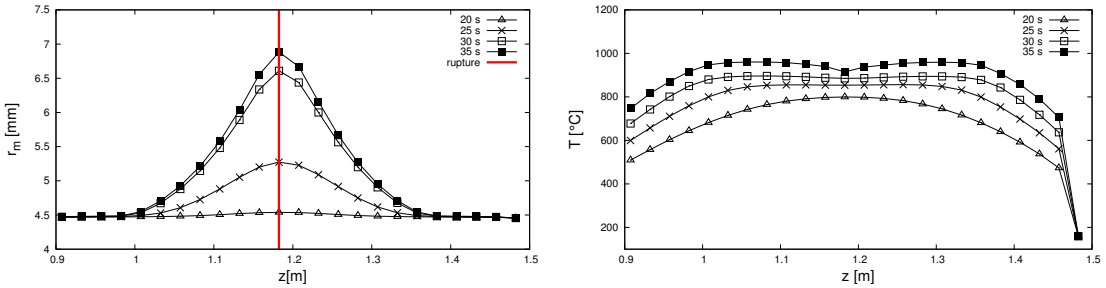

(a) (b)

Figure 6.22: Average fuel cladding radius (a) and corresponding fuel cladding temperature (b), P_{EH}=1.5kW.

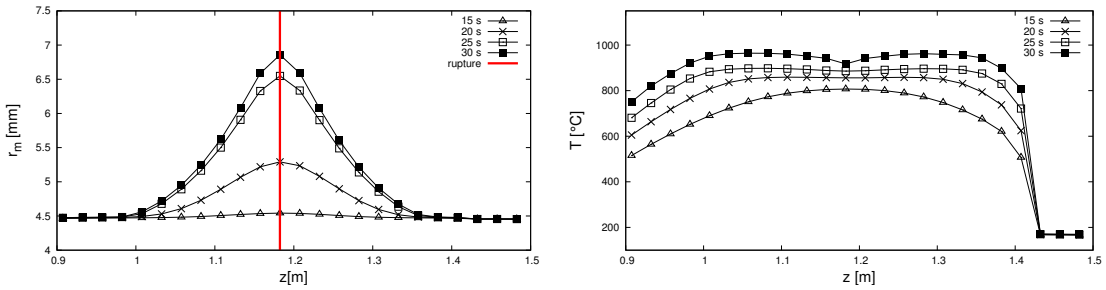

(a) (b)

Figure 6.23: Average fuel cladding radius (a) and corresponding fuel cladding temperature (b), P_{EH}=2kW.

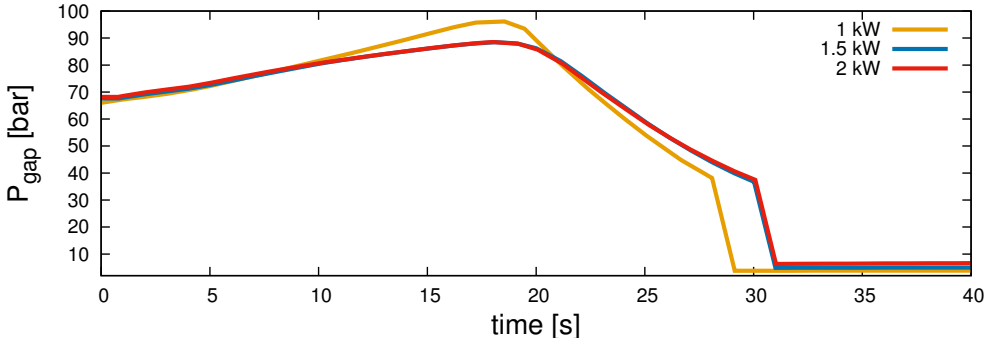

Figure 6.24: Pressure inside the fuel gap in the first 40 s from the beginning of the dry phase.

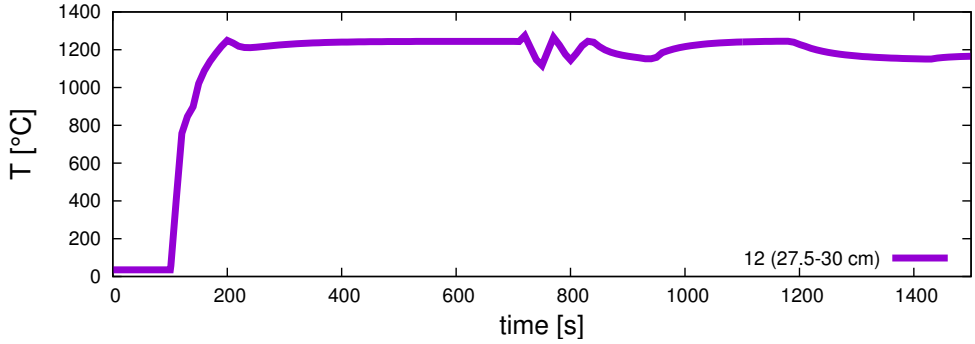

Figure 6.25: Evolution of the cladding temperature in the middle of the fuel sample.

6.1.3 Proposed improvements

When the device will be in operation, some differences between the calculations and the experimental measurements can be expected. In particular some phenomena of condensation, which

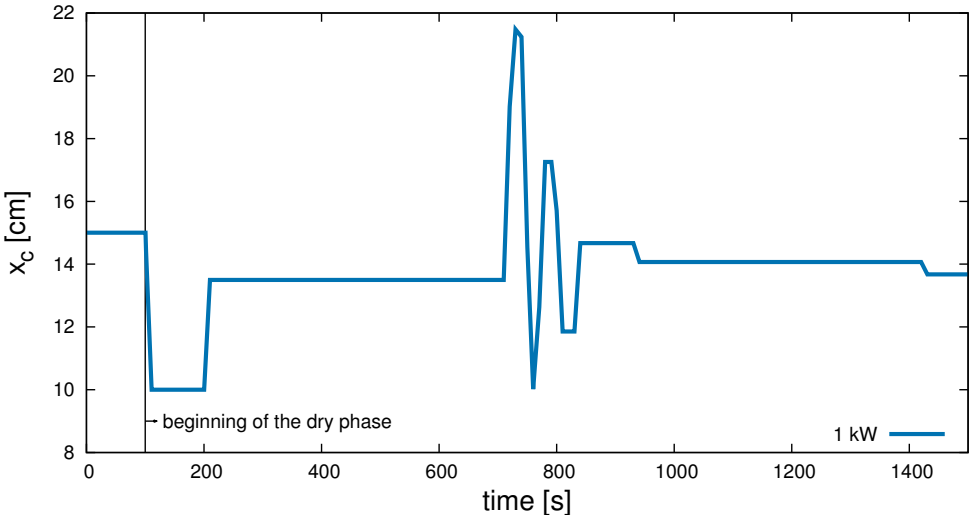

Figure 6.26: x_c during the dry phase.

might occur on the top of the fuel sample, should be taken into account. For this reason it is important to devise some technical solutions which can increase the range of operation of the dry phase. A solution that could prevent the phenomena related to the cladding surface too wet at the beginning of the dry phase, could be to divide this phase in two parts, see figure 6.27. In the first part the device moves towards the core to reach an appropriate cladding temperature T' such that the mechanical properties of the entire fuel sample are maintained unaltered, at this point the electrical heater (EH) can be activated. This procedure could maintain the surface of the cladding hot enough to reduce the condensation. This specific transient is still under investigation, in particular the results concerning the fuel ballooning need to be investigated. A technical solution that could increase the operating range of the P_{EH} by ensuring a suitable cladding temperature profile, is the introduction of a new electrical heater (EH1) on the FST above the NFZ, as shown in figure 6.28. This EH1 will maintain dry the top part of the fuel at the beginning of the dry phase and, according to its length, it will increase the stagnant zone along the fuel zone by reducing the liquid cooling during the plateau phase, see figure 6.29. The EH1 should be activated at the beginning of the dry phase; for P_{EH}=2 kW, the minimal length found for the EH1 to reach an acceptable value of cladding temperature profile was found for nearly 20 cm, see figure 6.30 while to exclude completely the zone 2 along the fuel zone is necessary a EH1 nearly 60 cm length. In the CATHARE calculation, the regulation of the EH1 can be done by a ON/OFF-type regulator, in particular the variable controlled is the temperature of the EH1 which is maintained at 50 $°C$ above $T_{sat}(P)$. The regulator should be activated by injecting 2 kW of power every time the temperature condition is not satisfied.

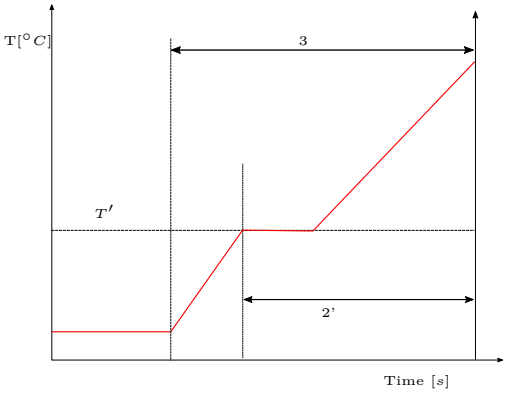

Figure 6.27: Beginning of the dry phase in the new configuration.

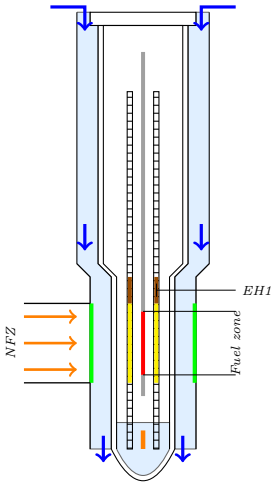

Figure 6.28: Position of the EH1 around the FST.

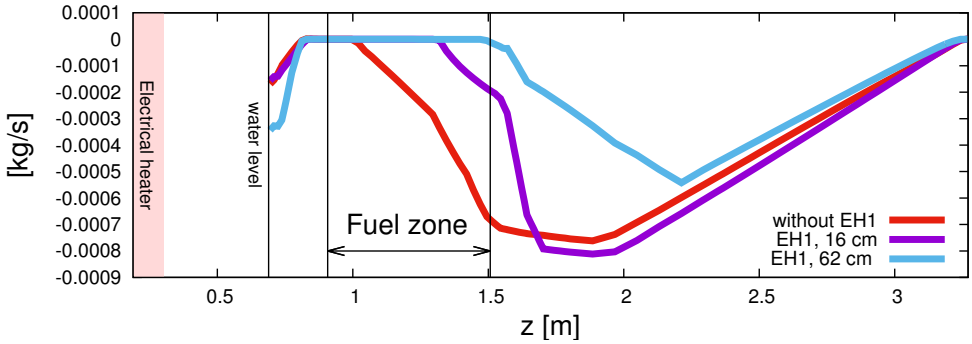

Figure 6.29: Liquid flow inside the hot channel for P_{EH}=2 kW.

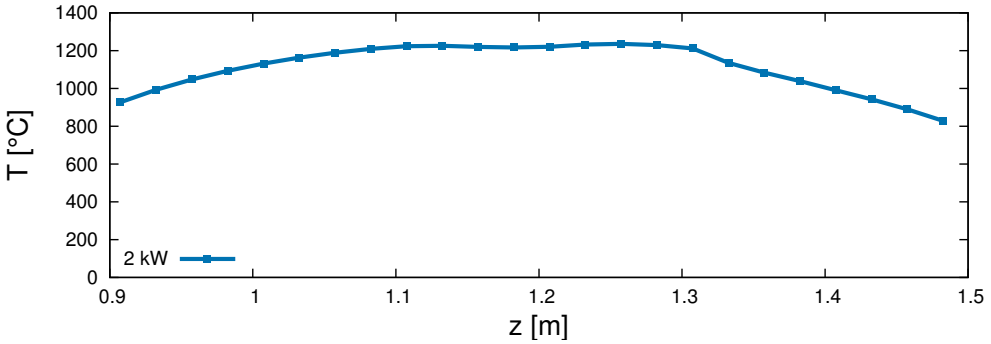

Figure 6.30: Cladding temperature profile for P_{EH}=2 kW.

6.2 Quenching phase

6.2.1 Re-flooding phase

In this last experimental phase, the water is injected from the bottom part of the device, the experimental device remains closed for all the duration of this phase and no water is discharged out of the cubicle. The case studied in this paper analyses the case during which the liquid mass flow injected inside the device is 0.45 kg/s and its inlet temperature is 35°C. The water injection shall be carried out by a SOURCE operator placed in the bottom of the device, see figure 4.2. The end of the re-flooding phase occurs when the liquid front has covered the upper opening and the thermosyphon flow (convective) between the two channels is formed. The first calculation analyzes the case when the Re-flooding phase is preceded by a Pre-cooling phase and the displacement device (DD) moves away from the reactor before the water injection occurs. The second case studied, investigates the injecting of the cold water inside the device immediately after the dry phase. Both the analysis performed consider the fuel axial temperature profile obtained at the end of the dry phase by considering a P_{EH}=1 kW.

6.2.2 Re-flooding preceded by the Pre-cooling phase

In this case, at the end of the dry phase, the DD moves away from the reactor core to reduce the LHGR and hence to decrease the fuel cladding temperature. The duration of the pre-cooling is set in accordance to the regulation of the fuel cladding temperature which is maintained in the middle point at 800 °C (±50 °C). Figure 6.31 shows the evolution of the cladding temperature (middle height of fuel sample) and the internal pressure of the system during the entirely duration of the dry, pre-cooling and re-flooding phase. The internal pressure varies from 3.5 bar (initial pressure once the steam has produced by the EH) to nearly 9 bar at the end of the dry phase. During the pre-cooling phase, the DD moves away from the core and the temperature computed in the middle of the fuel cladding varies in the order of 4 °C/s. The internal pressure reaches

a plateau around 7 *bar* in around 200*s*. The immediate vaporization of the water that covers the hot walls in the NFZ, produces a peak of pressure of approximately 25 *bar* in around 227 *s* before stabilizing at 16 *bar* in 13 minutes. At 1300 *s* from the beginning of the pre-cooling phase, the fuel sample is cooled by a thermosyphon liquid flow (TLF) formed between the hot and cold channel. The liquid mass flow between the hot and the cold channel stabilizes at 0.5 kg/s after nearly 800 *s*, see figure 6.32.

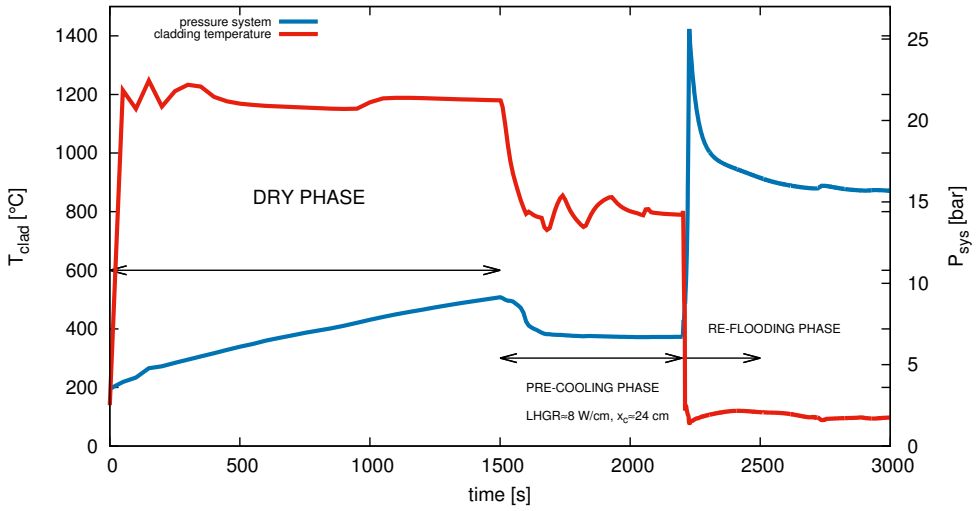

Figure 6.31: Evolution of the cladding temperature and the internal pressure of the system during the dry, pre-cooling and re-flooding phase.

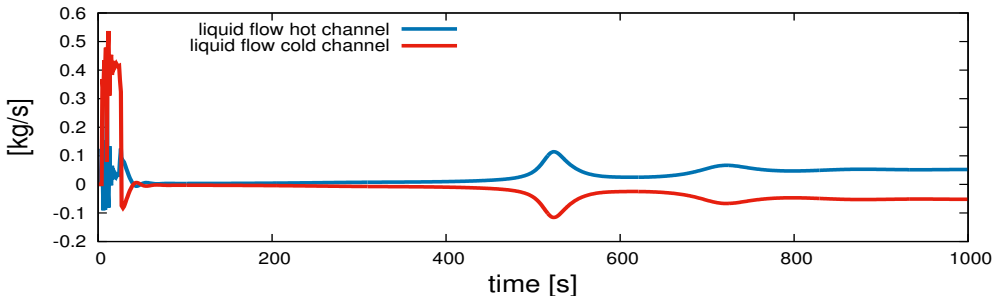

Figure 6.32: Mass liquid flow in the hot and cold channel during the re-flooding phase, the negative sign means the opposite flow direction.

6.2.3 Re-flooding phase without the Pre-cooling phase

In this case the water injection occurs immediately after the dry phase, when the maximum fuel cladding temperature reaches approximately 1200 $°C$. In this situation, the peak of pressure

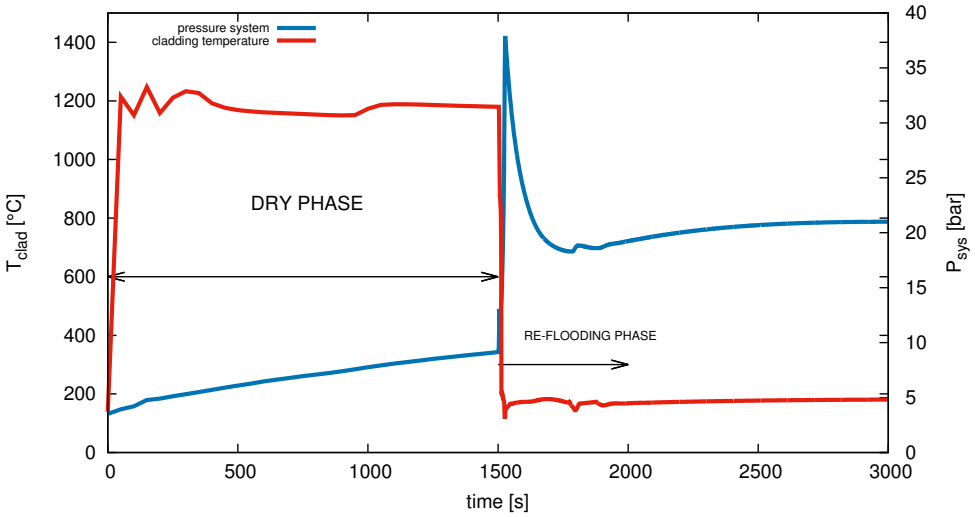

Figure 6.33: Evolution of the cladding temperature and the internal pressure of the system during the dry and re-flooding phase.

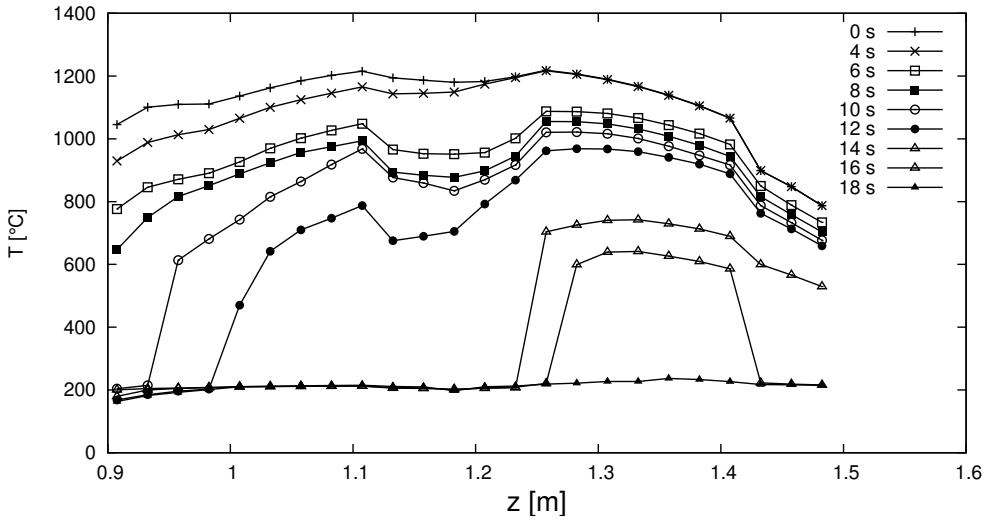

Figure 6.34: Fuel temperature during the re-flooding phase.

generated by the steam production, reaches approximately 38 *bar* in 27 *s* before stabilizing in 200 *s*, see figure 6.33. The variation of the cladding temperature computed in the middle of the fuel sample, following the beginning of the water injection, is nearly 77 $°C/s$. Figure 6.34 shows the profile of the fuel temperature for several instants of time. It can be seen that the clad starts to quench after 4 *s* and it is completely quenched after 18 *s*. Figure 6.35 shows the values of the void fraction computed inside the hot channel during the first seconds after the re-flooding.

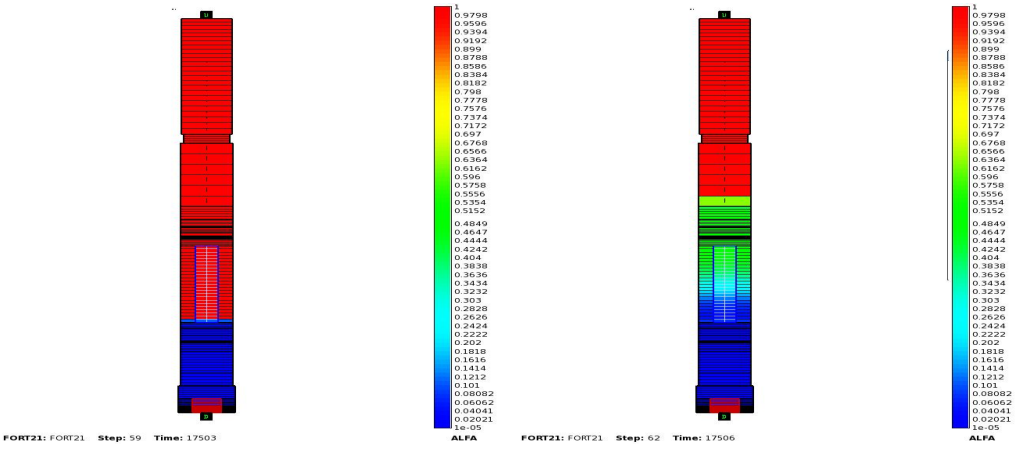

Figure 6.35: Void fraction inside the hot channel after 3 s (a), 6 s (b), 9 s (c), 12 s (d), 15 s (e), 18 s (f).

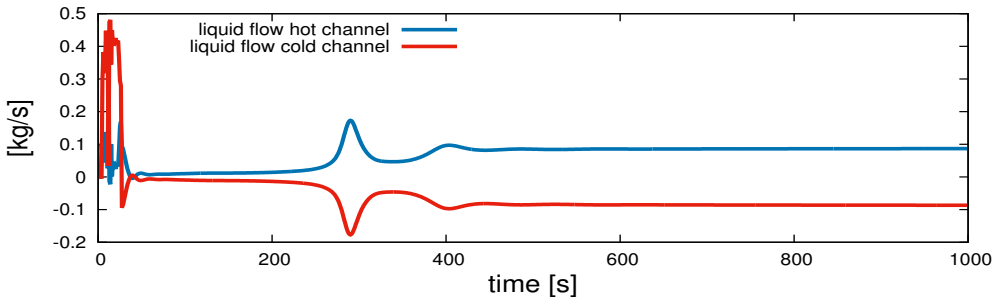

Figure 6.36: Mass liquid flow in the hot and cold channel during the re-flooding phase, the negative sign means the opposite flow direction.

In particular, after 3 s the water level arrives up to the bottom of the fuel sample. Once the cold water has touched the hot fuel cladding temperature (T_{clad} $\approx$1000°C on the bottom part of the fuel sample) a mix of steam and water cools down the bottom part of the fuel sample. When the liquid front covers all the length of the fuel sample, the mechanism of heat exchange between the fuel sample and the external environmental passes from the natural convection in gas to sub-cooled film boiling. In this last condition, some vapor patch can be formed on the hot surface of the cladding by preventing the quenching, see the temperature profile after 16 s from the beginning of transient. The liquid mass flow between the hot and the cold channel stabilizes at 0.9 kg/s after nearly 450 s, see figure 6.36 for details.

6.3 Conclusion

In this chapter a set of simulations are investigated to conduct the dry phase as well possible. The first simulation proposed, analyzes the behavior of the displacement device during which, any sort of temperature regulation is set up. The importance of this first benchmark simulation is to analyze the general behavior of the device, in particular the physic condition inside the hot channel and cold channel. The results have showed that, if the displacement device remains at a predefined distance from the core, then some thermal-hydraulic conditions make the device sensitive to the phenomena of condensation which make difficult the achievement of an uniform fuel cladding profile. By considering other different type of configurations for the fuel sample, we have imposed other working conditions on the device. In this case, we have assume that the displacement device can move according to the cladding temperature target. In this case the cooling effects due to the presence of liquid inside the hot channel, are obstructed by the LHGR which changes according to the position of the displacement device. At the beginning, for a conservative analysis, the maximum velocity of the displacement device (6 mm/s) has been considered. For both these two types of fuel utilized, the results have suggested that, for $P_{EH} = 1kW$ the cladding temperature profile is uniform along all the fuel length. For

$P_{EH} \geq 1.5kW$, the top of fuel remains wet and the cladding temperature low. For $P_{EH} = 1kW$, the homogeneous cladding temperature distribution ensures a greater pressure inside the fuel gap and the fuel burst takes place prematurely. An important result, shown for all the cases analyzed, is that the clad ballooning and cladding rupture are not perturbed by these possible condensation phenomena. The total amount of hydrogen produced, which varies between from $0.25 \div 0.35g$ and $0.20 \div 0.26g$ in accordance with the fuel, is accumulated mainly in the top of the cold channel and in the upper volume. The total power produced by the cladding oxidation is nearly $4W/cm$. For the both of type of fuel sample analyzed, the maximum thickness of oxide is reached for P_{EH}=$1.5kW$. A benchmark calculation has been analyzed to evaluate the consequences of the steam production once the cladding temperature have reached the target value of 1200 $°C$. The results have showed that, as a consequence of the exothermic reaction steam-zirconium, the increase of the fuel temperature is offset by the temperature regulator which moves the device away from the core by perturbing the fuel cladding temperature. In the real condition the velocity of the displacement device is related to the maximum heat-up rate of the electrical heater surrounded the fuel sample on the FST (Λ<20 $°C/s$). By considering three different values of DD velocities and a new fuel, the results have shown that for a P_{EH} =$1kW$, the velocity of the DD should not be greater than $0.5cm/s$ and less then $1.0cm/s$ for P_{EH} =1.5-2kW.

The last part of this final chapter, has been devoted to investigated the behavior of the fuel cladding temperature and the evolution of the internal pressure of the system following the re-flooding phase. In this analysis two cases has been considered. In the first one, the DD moves away from the core to reach a intermediate value around 800 $°C$ before the water injection occurs. This case considers that the liquid mass flow injected inside the device is 0.45 kg/s and its inlet temperature nearly 35 $°C$ (11.7 l of the total amount of water injected). The results have been showed that the water starts to cover the bottom part of the fuel sample after nearly $3s$. In the second case we have that the peak of pressure due to the liquid vaporization reaches approximately 25 bar in around 227 s and 35 bar. After 24 s the water level reaches the upper holes and the convective (thermosyphon) flow between the hot and cold channel is formed again.

Conclusions

In this thesis we have developed a detailed analysis of the LORELEI apparatus by using computational tools. We have first introduced the characteristics of the code CATHARE and the mathematical equations implemented in the code with regard to the main closure laws for a single and a double phases system flow. An analysis of the equations implemented for the sub-module FUEL, have been written in order to clarify the sensitive parameters which are interest for us to analysis the dry phase. A short chapter has been devoted to describe the facility and a typical LOCA scenario by emphasizing the structure of an Emergency Core Cooling System. The layout analysis has revealed that LORELEI presents some similarities with the the IFA-650X apparatus. For example one can find the electrical heater placed around the fuel sample which is necessary to recreate the adiabatic condition during the heating phase. As it has happened in the IFA-650X, a preliminary experimental phase is needed to be performed in order to create a fission product inventory. After an accurate description of the geometry of the in-pile device, we have described all the possible experimental phases.

The first research objective of this Ph.D Thesis is the implementation and the simulation of the CATHARE model for LORELEI. All the geometrical values of any elements of the apparatus, have been obtained from the Israel Atomic Energy Commission (IAEC). The IAEC also performed a preliminary CFD analysis of the re-irradiation and the dry phase in accordance with some specific initial conditions. This has allowed us, without experimental data available, to match the results with those obtained with CATHARE. The results derived from the analysis on the working limits of the thermosyphon liquid flow have confirmed a stable behavior of the device even for high LHGR values. Furthermore, another analysis of the evolution of the pressure of the system has been performed in order to evaluate the behavior of the device during abnormal working conditions. For a safe point of view, to verify the stability of the system, it has been necessary to perform an analysis of some accidental conditions that may verify during the normal operation of the re-irradiation phase.

A comprehensive analysis of the dry phase has been crucial to determined the thermal behavior of the fuel cladding. If one consider valid the CATHARE modeling proposed then, in some specific conditions, some thermal-hydraulic phenomena might lead the fuel cladding profile to reach unsafe limits.

All these benchmark cases exposed in this thesis, starting from the study of the Re-irradiation phase up to the Dry-phase, are important for us to predict the general behavior of LORELEI test design. In addition, when the real test device will be in fact active, all the results obtained from its experimental campaign will be of considerable importance on the validation of the results obtained and discussed in this Thesis. In this context, it will be very interesting to verify the discrepancy between the real behavior of the fuel sample during the dry phase, such as the time which leads to the clad ballooning and burst with the results presented.

Bibliography

Phebus sfd prpgram. Thecnical report, Institute de Protection et de la Sûreté Nucléaire, CEA.

Status and trends of nuclear technologies. Report of the international project on innovative nuclear reactors and fuel cycles (inpro), IAEA, 2009.

B Adroguer, C Hueber, and M Trotabas. Behavior of PWR fuel in LOCA conditions Phebus Test 215P. *International working group on fuel performance and technology for water reactors*, page 38, 1983.

A Arnaud and A Makkovina. Objectives, Test Matrix and Represetativity of the PHEBUS-FP Experimental Programme. In *Proc. Conf. Chateau Cadarache, St. Paul-Les-Durance*, 1991.

Louis Baker and Louis C Just. Studies of metal-water reactions at high temperatures iii. experimental and theoretical studies of the zirconium-water reaction. *ANL-6548*, 86, 1962.

A. Barletta. *Introduzione matematica alla trasmissione del calore*. Pitagora Editrice, Bologna, 2005.

P Battistoni. *Validazione di un modello numerico con il codice di sistema CATHARE2 di un sistema passivo di rimozione del calore residuo*. Master in Energy Engineering, School of Engineering and Architecture, Bologna, 2015.

A Bentaïb, B Hervé, G Cénérino, B Clément, F Corenwinder, M Cranga, G Ducros, F Fichot, D Jacquemain, C Journeau, V Koundy, D Leteinturier, D Magallon, R Meignen, F Monroig, G Nahas, F Pichereau, E Raimondn, J M Seiler, B Tourniaire, and J P Van-Dorsselaere. *Nuclear Power Reactor Core Melt Accidents*. EDP Sciences-Collection: Institute de Radioprotection et de Sureté Nucléaire, 2015.

PJ Berenson. Film-boiling heat transfer from a horizontal surface. *Journal of Heat Transfer*, 83(3): 351–356, 1961.

Theodore L Bergman, Frank P Incropera, David P DeWitt, and Adrienne S Lavine. *Fundamentals of heat and mass transfer*. John Wiley & Sons, 2011a.

Theodore L Bergman, Frank P Incropera, and Adrienne S Lavine. *Fundamentals of heat and mass transfer*. John Wiley & Sons, 2011b.

G Bignan. The Key role of Research Reactors in support to the development of nuclear energy: example of the JHR Project, a new Material Testing Reactor working as a European and International Users Facility in support to Research Institutes and Nuclear Industry. In *Proc. Int. Conf. Nuclear Energy for New Europe (NENE)*, 2016.

C Blandin, J Estrade, C Colin, T Dousson, L Ferry, J Pierre, P Roux, and C Gonnier. Fuel and material irradiation hosting systems in the Jules Horowitz Reactor. In *Proc. Int. Conf. IGORR*, 2013.

Yvonne Broy, Wolfgang Wiesenack, and Lise A Moen. The oecd halden reactor project–international research on safety and reliability of nuclear power generation. *Atw. Internationale Zeitschrift fuer Kernenergie*, 45(4):229–233, 2000.

E. Brun, E Damian, FX Hugot, YK Lee, F Malvagi, A Mazzolo, O Petit, JC Trama, T Visonneau, and A Zoia. *TRIPOLI9-4 Version 9 User Manual*, 2013.

JV Cathcart, RE Pawel, RA McKee, RE Druschel, GJ Yurek, JJ Campbell, and SH Jury. Zirconium metal-water oxidation kinetics. iv. reaction rate studies. Technical report, Oak Ridge National Lab., 1977.

CEA Nuclear Center. The Irradiation Devices. `www-rjh.cea.fr/irradiation-devices.html`.

CEN. Phebus loca program. Institute de Protection et de la Sûreté Nucléaire, Lecture.

J Chao, A Singh, R Henry, M Plys, and C Paik. The maap code: What is it, what has it accomplished, and how can it be used in the future? *Transactions of the American Nuclear Society*, 74(CONF-9606116–), 1996.

B Clément, N Hanniet-Girault, G Repetto, D Jacquemain, AV Jones, MP Kissane, and P Von der Hardt. LWR severe accident simulation: synthesis of the results and interpretation of the first Phebus FP experiment FPT0. *Nuclear Engineering and Design*, 226(1):5–82, 2003.

John G Collier and John R Thome. *Convective boiling and condensation*. Clarendon Press, 1994.

Jean-Marc Delhaye. *Thermohydraulique des réacteurs*. EDP sciences, 2012.

FW Dittus and LMK Boelter. Heat transfer in automobile radiators of the tubular type. *International Communications in Heat and Mass Transfer*, 12(1):3–22, 1985.

L. Ferry, D. Parrat, C. Gonnier, C. Blandin, Y. Weiss, and A. Sasson. The LORELEI Test Device for LOCA Experiments in the Jules Horowitz Reactor. In *Water Reactor Fuel Performed Meeting, WRFPM*, 2014.

T Forgeron, JC Brachet, F Barcelo, A Castaing, J Hivroz, JP Mardon, and Bernaudat C. Experiment and modeling of advanced fuel rod cladding behavior under loca conditions: Alpha-beta phase transformation kinetics and edgar methodology. In *Zirconium in the nuclear industry: twelfth international symposium*. ASTM International, 2000.

G Geffraye, O Antoni, M Farvacque, D Kadri, G Lavialle, B Rameau, and A Ruby. CATHARE 2 V2. 5_2: a single version for various applications. *Nuclear Engineering and Design*, 241(11):4456–4463, 2011.

A Ghione. *Improvement of the nuclear safety code CATHARE based on thermal-hydraulic experiments for the Jules Horowitz Reactor*. Department of Applied Physics, Chalmers University of Technology Göteborg, Sweden, 2015.

D Gitelman, H Shenha, Ch Gonnier, D Tarabelli, A Sasson, Y Weiss, and M Katz. Numerical Simulation of a Single-Phase Closed-Loop Thermo-Siphon in LORELEI Test Device. In *European Research Reactor Conference, RRFM*, 2014.

C Gonnier, G Repetto, and G Geoffroy. Pheabus severe accident fuel damage program: main experimental results and instrmentation behevior. In *The Pheabus fission product project:presentation of the experimental programme and test facility*.

DC Groeneveld, SC Cheng, and T Doan. 1986 aecl-uo critical heat flux lookup table. *Heat Transfer Engineering*, 7(1-2):46–62, 1986.

Hewitt, G F. Loss-of-coolant accident (loca) phenomena. NTEC Module: Water Reactor Performance and Safety, Lecture 8.

RA Holta. The beta to alpha phase transformation in Zircaloy-4. *Journal of Nuclear Materials*, 35(3): 322–334, 1970.

L.L Humphries, R.K Cole, D.L Louie, V.G Figueroa, and M.F Young. *MELCOR Computer Code Manual*, 2015.

Isaak E Idelchik and Erwing Friend. *Handbook of hydraulic resistence*. Hemisphere Publishing, New York, NY, 1986.

Lars Olof Jernkvik. *Computational assessment of LOCA simulation tests on high burnup fuel rods in Halden and Studsvik*. Swedish Radiation Safety Authority, 2016.

EH Karb, L Sepold, P Hofmann, C Petersen, G Schanz, and H Zimmermann. Lwr fuel rod behavior during reactor tests under loss-of-coolant conditions: Results of the fr2 in-pile tests. *Journal of Nuclear Materials*, 107(1):55–77, 1982.

Hyoung Tae Kim, Bo Wook Rhee, and Joo Hwan Park. Application of a zircaloy/steam oxidation model to a cfd code and its validation against a candu fuel channel experiment: Cs28-2. *Journal of nuclear science and technology*, 44(11):1385–1394, 2007.

S Korotkin, Y Kaufman, E Grosman, B Guttmann, S Levy, D Amidan, B Gdalyho, T Cahana, A Ellenbogen, M Arad, et al. Preliminary I&C Design for LORELEI. In *Conference of the Nuclear Societies in Israel*, 2014.

G. Lavialle. *CATHARE 2 V2.5_1: User guidelines*. CEA Grenoble, Francia, February, 2006.

S Leistikow and G Schanz. Oxidation kinetics and related phenomena of zircaloy-4 fuel cladding exposed to high temperature steam and hydrogen-steam mixtures under pwr accident conditions. *Nuclear engineering and design*, 103(1):65–84, 1987.

A. Massih R. and Jernkvist L. *Assessment of data and criteria for cladding burst in loss-of-coolant accident*. Swedish Radiation Safety Authority, 2015.

RK McCardell and PE MacDonald. Power Burst Facility Severe Fuel Damage Test Program. *Irradiation Technology*, pages 213–230, 1983.

N Moran, L Ferry, A Azulay, O Mileguir, Y Weiss, and M Szanto. Concept of the LORELEI Test Device for LOCA Experiment in the JHR Reactor. 2014.

A.L Nicholas and C Hueber. Fission-product chemistry in severe reactor accidents: Review of relevant integral experiments. In *The Pheabus fission product project:presentation of the experimental programme and test facility.*

P D Parson, E D Hindle, and C A Mann. PWR fuel behavior in design basis accident conditions. State-of-the-art Report. Technical report, Task Group on Fuel Behavior of Principal Working Group No. 2 (Committee on the safaty of nuclear installations OECD nuclear energy agency), 1986.

K Pettersson, M Billone, T Fuketa, C Grandjean, G Hache, L Heins, Z Hózer, J de Betou, S Kelppe, R Mayer, F Nagase, J Papin, H Scott, H Sonnenburg, S Sunder, M Valach, J Volglewede, V Vrtilkova, N Waeckel, W Wiesenack, and M Zimmermann. Nuclear Fuel Behaviour in Loss-of-coolant Accident (LOCA) Conditions. State-of-the-art Report. Technical report, Nuclear Energy Agency, 2009.

L Sabotinov. *Experimental investigation of the void fraction at subcooled boiling for different heat flux profiles along the channel*. Phd Thesis, Moscov Power Engineering Institute, Russia, 1974.

P Saha and Novak Zuber. Point of net vapor generation and vapor void fraction in subcooled boiling. In *Heat transfer, 1974. Vol. 4*. 1974.

R. Scardovelli and S. Manservisi. *Termoidraulica dei flussi bifase*. Esculapio, 2012. ISBN 9788874884803.

H Shenha, D Gitelman, I Preker, M Arbel-Haddad, L Ferry, A Sasson, Y Weiss, and M Katz. Thermal design of the lorelei test device using a comsol inverse solver. In *European Research Reactor Conference, RRFM*, 2014.

Jin Ho Song and Tae Woon Kim. Severe accident issues raised by the fukushima accident and improvements suggested. *Nuclear Engineering and Technology*, 46(2):207–216, 2014.

JRS Thom, WM Walker, TA Fallon, and GFS Reising. Boiling in sub-cooled water during flow up heated tubes or annuli. Technical report, Babcock and Wilcox Ltd., Renfrew, Eng., 1967.

L. S. Tong and Y. S Tang. *Boiling Heat Transfer and Two-phase Flow*. Taylor and Francis, 1997.

VF Urbanic and TR Heidrick. High-temperature oxidation of zircaloy-2 and zircaloy-4 in steam. *Journal of nuclear materials*, 75(2):251–261, 1978.

Utited States Nuclear Regulatory Commission. Pressurized Water Reactor (PWR) system. `https://www.nrc.gov/reading-rm/basic-ref/students/for-educators/04.pdf`, a.

Utited States Nuclear Regulatory Commission. Acceptance criteria for emergency core cooling systems for light-water nuclear power reactors. `https://www.nrc.gov/reading-rm/doc-collections/cfr/part050/part050-0046.html`, b.

Utited States Nuclear Regulatory Commission. Appendix K to Part 50-ECCS Evaluation Models. `https://www.nrc.gov/reading-rm/doc-collections/cfr/part050/part050-appk.html`, c.

JP Van Dorsselaere, C Seropian, P Chatelard, F Jacq, J Fleurot, P Giordano, N Reinke, B Schwinges, HJ Allelein, and W Luther. The astec integral code for severe accident simulation. *Nuclear Technology*, 165(3):293–307, 2009.

W Wiesenack. Summary of the Halden Reactor Project LOCA test series IFA-650. *IFE-OECD Halden Reactor Project, HPR-380*, 2013.

Appendices

Appendix A

Constant values of the Device

Table A.1: In-pile device geometry.

Element	Material	D_{int} $[mm]$	D_{ext} $[mm]$	Length $[mm]$	Refer. Coordinate $[mm]$
Lower Extension	Zircaloy	-	9.5	494	406 - 900
Fuel	UO_2	-	8.3	600	900 - 1500
Cladding	Zircaloy	8.3	9.5	600	900 - 1500
Upper Extension	Zircaloy	-	9.5	800	1500 - 2300
LVDT	Zircaloy	-	15	70	2300 - 2370
Sample holder	Zircaloy	-	11.5	1030	2370 - 3400
Debris Catcher	STST	25	31	46	139 - 185
4 Lower Openings (9x29)	-	-	-	-	185 - 194
Lower Instrumental Holder	STST	35	31	565	194 - 744
Heater connector 1	STST	31	41	112	194 - 306
Heater connector 2	STST	31	47	100	306 - 406
Heater connector 3	STST	31	41	100	406 - 506
Heater connector 4	STST	31	38	74	670 - 744
Peripheral Heater	Inconel	25	31	830	744 - 1574
Heater connector 5	STST	25	38	74	1574 - 1648
Upper Instrumental Holder	STST	25	31	1628	1648 - 3276
4 Upper Openings (50x15)	-	-	-	-	3276 - 3326
Inner pressure flask (bottom part)	STST	58	66.1	1708	0 - 1708
Inner pressure flask (upper part)	STST	84.4	95	1592	1808 - 3400
Outer pressure flask (bottom part)	STST	67.9	70.92	1700	0 - 1700
Outer pressure flask (upper part)	STST	96.38	99.4	1600	1800 - 3400
Neutron Screen	Hafnium	75.92	77.92	800	800 - 1600
Displacement device (bottom part)	Zircaloy	75.92	85.92	1700	0 - 1700
Displacement device (upper part)	Zircaloy	104.4	114.4	1600	1800 - 3400

Table A.2: Bottom volume (VOLBOT) and its geometrical values.

height $[m]$				section $[m^2]$		
0-0.139				$2.64\ 10^{-3}$		
0.139-0.194				$1.88\ 10^{-3}$		
junction (name)	height $[m]$	section $[m^2]$	perimeter $[m]$	size $[m]$	length $[m]$	orientation	weight
j_b_cc	0.0	$1.32\ 10^{-3}$	0.311	0.058	0	vertical	1
j_t_dc_2	0.194	$2.61\ 10^{-4}$	0.076	$1.377\ 10^{-3}$	0	horizontal	4
j_b_vb	0.194	0.06	0.265	0.084	0	vertical	1

Table A.3: Debris catcher volume (DEB_CAT) and its geometrical values.

height $[m]$				section $[m^2]$		
0-0.055				$4.90\ 10^{-4}$		
junction (name)	height $[m]$	section $[m^2]$	perimeter $[m]$	size $[m]$	length $[m]$	orientation	weight
j_b_hc	0.052	$4.90\ 10^{-4}$	0.078	0.025	0.0	vertical	1
j_t_dc_2	0.052	$2.61\ 10^{-4}$	0.076	$1.377\ 10^{-3}$	$3\ 10^{-3}$	horizontal	4

Table A.4: Upper volume (VOLTOP) and its geometrical values.

height $[m]$				section $[m^2]$		
0-1.09				$5.59\ 10^{-3}$		
junction (name)	height $[m]$	section $[m^2]$	perimeter $[m]$	size $[m]$	length $[m]$	orientation	weight
j_t_hc	0.0	$3.87\ 10^{-4}$	0.114	0.025	0.0	vertical	1
j_t_cc	0.0	$4.83\ 10^{-3}$	0.362	0.084	0.0	vertical	1
j_t_vt	1.09	0.06	0.265	0.084	0.0	vertical	1

Table A.5: Hot channel (HOT_CH) and its geometrical values.

axial coordinate $[m]$		section $[m^2]$		perimeter $[m]$		size $[m]$	
0.0-0.211		$4.90\ 10^{-4}$		0.078		0.025	
0.212-2.106		$3.14\ 10^{-4}$		0.108		0.025	
2.107-2.175		$3.14\ 10^{-4}$		0.125		0.025	
2.176-3.082		$3.87\ 10^{-4}$		0.114		0.025	
junction (name)	height $[m]$	section $[m^2]$	perimeter $[m]$	size $[m]$	length $[m]$	orientation	weight
j_b_hc	0.0	$4.90\ 10^{-4}$	0.078	0.025	0.0	vertical	1
j_t_hc	3.4	$4.83\ 10^{-3}$	0.362	0.084	0.0	vertical	1

Table A.6: Cold channel (COLD_CH) and its geometrical values.

axial coordinate $[m]$	section $[m^2]$	perimeter $[m]$	size $[m]$
0-0.112	$1.32\ 10^{-3}$	0.311	0.058
0.113-0.211	$9.07\ 10^{-4}$	0.329	0.058
0.212-0.311	$1.32\ 10^{-3}$	0.311	0.058
0.312-0.476	$1.88\ 10^{-3}$	0.279	0.058
0.477-0.549	$1.50\ 10^{-3}$	0.301	0.058
0.550-1.380	$1.88\ 10^{-3}$	0.279	0.058
1.318-1.453	$1.50\ 10^{-3}$	0.301	0.058
1.454-1.514	$1.88\ 10^{-3}$	0.279	0.058
1.614-3.082	$4.83\ 10^{-3}$	0.365	0.084

junction (name)	height	section $[m^2]$	perimeter $[m]$	size $[m]$	length $[m]$	orientation	weight
j_b_cc	0.0	$1.32\ 10^{-3}$	0.311	0.058	0.0	vertical	1
j_t_cc	3.4	$4.83\ 10^{-3}$	0.362	0.084	0.0	vertical	1

Table A.7: Cooling channel (COOL_CH) and its geometrical values.

axial coordinate $[m]$	section $[m^2]$	perimeter $[m]$	size $[m]$
0-1.708	$5.76\ 10^{-4}$	0.461	0.075
1.808-3.4	$8.00\ 10^{-4}$	0.640	0.104

junction (name)	height	section $[m^2]$	perimeter $[m]$	size $[m]$	length $[m]$	orientation	weight
j_b_co	0.0	$5.76\ 10^{-4}$	0.461	0.075	0.0	vertical	1
j_t_co	3.4	$8.00\ 10^{-4}$	0.640	0.104	0.0	vertical	1

Appendix B

LORELEI input file

B.1 Steady State input of LORELEI

```
*
* LORELEI - TEST SECTION
* STEADY STATE OF LORELEI BEFORE THE DRY PHASE STARTS
*
* 1) DEVICE IS EMPTIED BY
*    LEAVING ONLY HELIUM AND
*    A SMALL AMOUNT OF STEAM

* 2) A SMALL AMOUNT OF WATER (1.2 l)
* IS INJECTED INSIDE THE DEVICE
* INITIAL PRESSURE 3.0 bar
*
* CREATED BY PAOLO BATTISTONI
*
****************************************
* adpated geometry as proposed by
* Thermohydraulic Design
* of the LORELEI Test Device
* CDR Version 1.4.2016

* REFERIMENT STEADY STATE
*
BEGIN DATA ;
*
TITLE ' LORELEI - TEST SECTION' ;
*
PI = 3.141592654D0 ;
list_gaz = NONCOND 2 HELIUM HYDROGEN                          ;
tendf = 10000.0  ;

****************************************
* LIST OF HEATERS CONNECTORS INSIDE THE
* COLD CHANNEL
****************************************
* HEATER CONNECTORS1
z_he_1 = 306.E-3 ;
d_he_1_e = 41.E-3 ;

* HEATER CONNECTORS2
z_he_2 = 406.E-3 ;
d_he_2_e = 47.E-3 ;

* HEATER CONNECTORS3
z_he_3 = 506.E-3 ;
d_he_3_e = d_he_1_e ;

* HEATER CONNECTORS4
z_he_4_b = 670.E-3 ;
z_he_4_t = 744.E-3 ;
d_he_4_e = 38.E-3 ;

* PERIPHERAL HEATER
z_hea_b = 759.E-3 ;
z_hea_t = 1559.E-3 ;

* HEATER CONNECTORS5
z_he_5_b = 1574.E-3 ;
z_he_5_t = 1648.E-3 ;
d_he_5_e = d_he_4_e ;


****************************************
* FUEL GEOMETRY
****************************************
d_fuel = 8.3E-3 ;
z_fuel_b = 900.E-3 ;
z_fuel_t = 1500.E-3 ;
h_fuel = z_fuel_t - z_fuel_b ;

d_clad_i = d_fuel ;
d_clad_e = 9.5E-3 ;


****************************************
* INNER FLASK GEOMETRY
****************************************

* HEIGHT OF DIVERGENT PART
z_if_b = 1708.E-3 ;
z_if_t = 1808.E-3 ;

* INNER FLASK BOTTOM (INTERNAL-EXTERNAL)
d_if_b_i = 58.E-3 ;
d_if_b_e = 66.1E-3 ;

* INNER FLASK TOP (INTERNAL-EXTERNAL)
d_if_t_i = 84.4E-3 ;
d_if_t_e = 95.E-3 ;

****************************************
```

```
* OUTER FLASK GEOMETRY
****************************************

* HEIGHT OF DIVERGENT PART
z_of_b = 1700.E-3 ;
z_of_t = 1800.E-3 ;

*OUTER FLASK BOTTOM (INTERNAL-EXTERNAL)
d_of_b_i = 67.9E-3 ;
d_of_b_e = 70.92E-3 ;

* OUTER FLASK TOP (INTERNAL-EXTERNAL)
d_of_t_i = 96.38E-3 ;
d_of_t_e = 99.4E-3 ;

* -35/+35 cm for the gamma power z-profile
* along the structures (averaged along 70 cm)
z_po_b = 850.E-3 ;
z_po_t = 1550.E-3 ;

* difference diameters inner flask bottom part
dd_if_b = d_if_b_e - d_if_b_i ;
dd_if_t = d_if_t_e - d_if_t_i ;

*difference diameters inner flask top part
dd_of_b =  d_of_b_e - d_of_b_i ;
dd_of_t = d_of_t_e - d_of_t_i ;

****************************************
* GEOMETRY OF LVDT
****************************************

d_lvdt = 15.E-3;
z_lvdt_b = 2300.E-3 ;
z_lvdt_t = 2370.E-3 ;


****************************************
* SAMPLE HOLDER + TC WIRING
****************************************
d_wir = 11.5E-3 ;


****************************************
* BEGINNING OF UPPER OPENINGS
****************************************
z_u_open = 3276.E-3 ;


****************************************
* DEVICE HOLDER
****************************************
z_de = 3400.E-3 ;

*DEVICE HOLDER BOTTOM (INTERNAL-EXTERNAL)
d_de_b_i = 75.92E-3 ;
d_de_b_e = 85.92E-3 ;

*DEVICE HOLDER TOP (INTERNAL-EXTERNAL)
d_de_t_i = 104.4E-3 ;
d_de_t_e = 114.4E-3 ;


****************************************
* HAFNIUM NEUTRON SCREEN
****************************************
d_ha_i = 75.92E-3 ;
d_ha_e = 77.92E-3 ;

z_ha_b = 800.E-3 ;
z_ha_t = 1600.0E-3 ;

****************************************
* GEOMETRY OF THE ELECTRICAL HEATER (EH)
* PLACED ON THE BOTTOM OF THE DEVICE
* TO PRODUCE STEAM DURING THE DRY PHASE
****************************************
DE_HEAT1 = 27.E-3                                                    ;
H_HEAT1 = 0.112      ;

****************************************
*****GEOMETRY HOT CHANNEL
****************************************
d_hc_e = 31.E-3 ;
d_hc = 25.E-3 ;
s_hc = (pi/4.)*(d_hc)**2. ;
p_hc = pi*d_hc ;

s_hc_1 = (pi/4.)*(d_hc**2.-d_clad_e**2.) ;
p_hc_1 = pi*(d_hc+d_clad_e) ;

s_hc_2 = (pi/4.)*(d_hc**2.-d_lvdt**2.) ;
p_hc_2 = pi*(d_hc+d_lvdt) ;

s_hc_3 = (pi/4.)*(d_hc**2.-d_wir**2.) ;
p_hc_3 = pi*(d_hc+d_wir) ;


************************************
* GEOMETRIA COLD CHANNEL
************************************
* BEFORE DIVERGENT (BOTTOM)
d_cc_b = d_if_b_i ;
p_cc_b = PI*(d_cc_b+d_hc_e) ;
s_cc_b = (PI/4.)*(d_cc_b)**2. ;
s_cc_b_1 = (PI/4.)*(d_cc_b**2. - d_hc_e**2.) ;

* AFTER DIVERGENT (TOP)
d_cc_t = d_if_t_i ;
p_cc_t = PI*(d_cc_t+d_hc_e) ;
s_cc_t = (PI/4.)*(d_cc_t)**2. ;
s_cc_t_1 = (PI/4.)*(d_cc_t**2. - d_hc_e**2.) ;

*  CROSS SECTION VARIATION - HEATER CONNECTOR 1
s_cc_1 = (PI/4.)*(d_if_b_i**2.-d_he_1_e**2.) ;
p_cc_1 = PI*(d_if_b_i + d_he_1_e) ;

*  CROSS SECTION VARIATION -HEATER CONNECTOR 2
s_cc_2 = (PI/4.)*(d_if_b_i**2.-d_he_2_e**2.) ;
p_cc_2 = PI*(d_if_b_i + d_he_2_e) ;

*  CROSS SECTION VARIATION -HEATER CONNECTOR 3
s_cc_3 = (PI/4.)*(d_if_b_i**2.-d_he_3_e**2.) ;
p_cc_3 = PI*(d_if_b_i + d_he_3_e) ;

*  CROSS SECTION VARIATION -HEATER CONNECTOR 4
s_cc_4 = (PI/4.)*(d_if_b_i**2.-d_he_4_e**2.) ;
p_cc_4 = PI*(d_if_b_i + d_he_4_e) ;

* CROSS SECTION VARIATION -HEATER CONNECTOR 5
s_cc_5 = (PI/4.)*(d_if_b_i**2.-d_he_5_e**2.) ;
p_cc_5 = PI*(d_if_b_i + d_he_5_e) ;


************************************
* GEOMETRIA COOLING CHANNEL
************************************
* BEFORE DIVERGENT (BOTTOM)
d_co_b = d_de_b_i ;
p_co_b = PI*(d_of_b_e + d_de_b_i) ;
s_co_b =(PI/4.)*(d_de_b_i**2. - d_of_b_e**2. ) ;

* AFTER DIVERGENT (TOP)
d_co_t = d_de_t_i ;
p_co_t = PI*( d_of_t_e + d_de_t_i) ;
s_co_t =(PI/4.)*(d_de_t_i**2. - d_of_t_e**2.) ;


************************************
* GEOMETRIA VOLTOP
```

```
****************************************
* Hypothesis to take into account:
* The voltop should contain early 5 l of helium
* during the cold condition (without thermal power)
* 2.5 l inside the cushion line
* 2.5 l inside the pressure line
* inside the voltop (5 l)=> 0.89 m height
* the level of water inside the voltop during
* the cold condition is 20 cm
*
*z_voltop = z_de - z_u_open ;
z_voltop = 0.89+0.2  ;
s_voltop = (PI/4.)*(d_if_t_i**2.) ;

* DIMENSION OF THE SOURCE/SINK WATER
D_DN6 = 6.E-3                          ;
S_DN6 = PI*D_DN6*D_DN6/4.              ;

****************************************
* GEOMETRY OF HOLES BETWEEN THE VOLTBOT
* AND DEBRIS (BOTTOM)
* FOUR UPPER OPENINGS WITH A HEIGHT OF
* 9 MM AND A WIDTH OF 29 MM
****************************************
h_hole_b = 9.0E-3 ;
w_hole_b = 29.0E-3 ;

s_hole_b = (h_hole_b)*(w_hole_b) ;
p_hole_b = 2.0*(h_hole_b + w_hole_b) ;
d_hole_b = (4.0*s_hole_b)/p_hole_b ;

****************************************
* GEOMETRY DEBRIS CATHER
****************************************
h_dc = 43.E-3+h_hole_b ;
d_dc = d_hc ;
p_dc = PI*(d_dc) ;
s_dc = (PI/4)*(d_dc)**2 ;



****************************************
* GEOMETRY VOLBOT
****************************************
z_vb_1 = 139.E-3 ;
d_vb_1 = d_if_b_i ;
*p_vb_1 = PI*(d_if_b_i) ;
s_vb_1 = (PI/4)*(d_vb_1)**2 ;

z_vb_2 = 46.E-3+h_hole_b ;
d_vb_2 = d_if_b_i ;
*p_vb_2 = PI*(d_if_b_i + d_hc_e) ;
s_vb_2 = (PI/4)*(d_vb_2**2-d_hc_e**2) ;

z_volbot = z_vb_1 + z_vb_2 ;

* HOT CHANNEL

HOT_CH = AXIAL j_b_hc DSTREAM j_t_hc USTREAM ;

ph1 = XAXIS (0.0) ;
ph2 = XAXIS (z_he_1 - z_volbot ) ;
ph3 = XAXIS (z_he_1 - z_volbot + 1.E-3) ;
ph4 = XAXIS (z_he_2 - z_volbot - 1.E-3) ;
ph5 = XAXIS (z_he_2 - z_volbot) ;
PH6 = XAXIS (z_he_3 - z_volbot -1.E-3) ;
PH7 = XAXIS (z_he_3 - z_volbot ) ;
PH8 = XAXIS (z_he_4_b - z_volbot) ;
PH9 = XAXIS (z_he_4_b - z_volbot + 1.E-3) ;
PH10 = XAXIS (z_he_4_t - z_volbot - 1.E-3) ;
PH11 = XAXIS (z_he_4_t - z_volbot ) ;
PH12 = XAXIS (z_hea_b - z_volbot ) ;
PH13 = XAXIS (z_ha_b - z_volbot ) ;
PH14 = XAXIS  (z_po_b - z_volbot) ;
PH15 = XAXIS (z_fuel_b - z_volbot) ;
PH16 = XAXIS (z_fuel_t - z_volbot) ;
ph17 = XAXIS  (z_po_t - z_volbot) ;
ph18 = XAXIS  (z_hea_t - z_volbot) ;
ph19 = XAXIS (z_he_5_b - z_volbot ) ;
ph20 = XAXIS  (z_he_5_b - z_volbot + 1.E-3 ) ;
ph21 = XAXIS  (z_ha_t - z_volbot ) ;
ph22 = XAXIS (z_he_5_t - z_volbot -1.E-3 ) ;
ph23 = XAXIS  (z_he_5_t - z_volbot ) ;
ph24 = XAXIS (z_If_b - z_volbot) ;
ph25 = XAXIS (z_if_t - z_volbot) ;
ph26 = XAXIS (z_lvdt_b - z_volbot) ;
ph27 = XAXIS (z_lvdt_b - z_volbot + 1.E-3) ;
ph28 = XAXIS (z_lvdt_t - z_volbot - 1.E-3) ;
ph29 = XAXIS (z_lvdt_t - z_volbot ) ;
ph30 = XAXIS (z_u_open - z_volbot) ;


m_hot   = ph1
          SEGMENT -25  ph2 COS 1.0  RATIO 1.0584
          SEGMENT 1  ph3 COS 1.0
          SEGMENT 6  ph4 COS 1.0
          SEGMENT 1  ph5 COS 1.0
          SEGMENT 4  ph6 COS 1.0
          SEGMENT 1  ph7 COS 1.0
          SEGMENT 8  ph8 COS 1.0
          SEGMENT 1  ph9 COS 1.0
          SEGMENT 5  ph10 COS 1.0
          SEGMENT 1  ph11 COS 1.0
          SEGMENT 2  ph12 COS 1.0
          SEGMENT 2  ph13 COS 1.0
          SEGMENT 3  ph14 COS 1.0
          SEGMENT 5  ph15 COS 1.0
          SEGMENT 24  ph16 COS 1.0
          SEGMENT 5  ph17 COS 1.0
          SEGMENT 3  ph18 COS 1.0
          SEGMENT 2  ph19 COS 1.0
          SEGMENT 1  ph20 COS 1.0
          SEGMENT 1  ph21 COS 1.0
          SEGMENT 5  ph22 COS 1.0
          SEGMENT 1  ph23 COS 1.0
          SEGMENT 5  ph24 COS 1.0
          SEGMENT 5  ph25 COS 1.0
          SEGMENT 6  ph26 COS 1.0
          SEGMENT 1 ph27 COS 1.0
          SEGMENT 4  ph28 COS 1.0
          SEGMENT 1 ph29 COS 1.0
          SEGMENT -25  ph30 COS 1.0  RATIO 0.978 ;

MESH hot_ch m_hot                                  ;
HYDR hot_ch ANNULAR                                ;

GEOM hot_ch
(ph1 AND ph4) SECT s_hc  PERI p_hc  SIZE  d_hc
(ph5 AND ph26) SECT s_hc_1  PERI p_hc_1  SIZE  d_hc
(ph27 AND ph28) SECT s_hc_2  PERI p_hc_2  SIZE  d_hc
(ph29 AND ph30) SECT s_hc_3  PERI p_hc_3  SIZE  d_hc  ;


* COLD CHANNEL

COLD_CH = AXIAL j_b_cc DSTREAM j_t_cc USTREAM          ;

pc1 = XAXIS (0.0) ;
pc2 = XAXIS (z_he_1 - z_volbot ) ;
pc3 = XAXIS (z_he_1 - z_volbot + 1.E-3) ;
pc4 = XAXIS (z_he_2 - z_volbot - 1.E-3) ;
pc5 = XAXIS (z_he_2 - z_volbot) ;
Pc6 = XAXIS (z_he_3 - z_volbot -1.E-3) ;
Pc7 = XAXIS (z_he_3 - z_volbot ) ;
Pc8 = XAXIS (z_he_4_b - z_volbot) ;
Pc9 = XAXIS (z_he_4_b - z_volbot + 1.E-3) ;
Pc10 = XAXIS (z_he_4_t - z_volbot - 1.E-3) ;
Pc11 = XAXIS (z_he_4_t - z_volbot ) ;
Pc12 = XAXIS (z_hea_b - z_volbot ) ;
Pc13 = XAXIS (z_ha_b - z_volbot ) ;
Pc14 = XAXIS  (z_po_b - z_volbot) ;
```

```
Pc15 = XAXIS (z_fuel_b - z_volbot) ;
Pc16 = XAXIS (z_fuel_t - z_volbot) ;
pc17 = XAXIS  (z_po_t - z_volbot) ;
pc18 = XAXIS  (z_hea_t - z_volbot) ;
pc19 = XAXIS (z_he_5_b - z_volbot ) ;
pc20 = XAXIS  (z_he_5_b - z_volbot + 1.E-3 ) ;
pc21 = XAXIS  (z_ha_t - z_volbot ) ;
pc22 = XAXIS (z_he_5_t - z_volbot -1.E-3 ) ;
pc23 = XAXIS  (z_he_5_t - z_volbot ) ;
pc24 = XAXIS (z_If_b - z_volbot) ;
pc25 = XAXIS (z_if_t - z_volbot) ;
pc26 = XAXIS (z_lvdt_b - z_volbot) ;
pc27 = XAXIS (z_lvdt_b - z_volbot + 1.E-3) ;
pc28 = XAXIS (z_lvdt_t - z_volbot - 1.E-3) ;
pc29 = XAXIS (z_lvdt_t - z_volbot ) ;
pc30 = XAXIS (z_u_open - z_volbot) ;



m_cold   = pc1
         SEGMENT -25  pc2 COS 1.0  RATIO 1.0584
         SEGMENT 1  pc3 COS 1.0
         SEGMENT 6  pc4 COS 1.0
         SEGMENT 1  pc5 COS 1.0
         SEGMENT 4  pc6 COS 1.0
         SEGMENT 1  pc7 COS 1.0
         SEGMENT 8  pc8 COS 1.0
         SEGMENT 1  pc9 COS 1.0
         SEGMENT 5  pc10 COS 1.0
         SEGMENT 1  pc11 COS 1.0
         SEGMENT 2  pc12 COS 1.0
         SEGMENT 2  pc13 COS 1.0
         SEGMENT 3  pc14 COS 1.0
         SEGMENT 5  pc15 COS 1.0
         SEGMENT 24  pc16 COS 1.0
         SEGMENT 5  pc17 COS 1.0
         SEGMENT 3  pc18 COS 1.0
         SEGMENT 2  pc19 COS 1.0
         SEGMENT 1  pc20 COS 1.0
         SEGMENT 1  pc21 COS 1.0
         SEGMENT 5  pc22 COS 1.0
         SEGMENT 1  pc23 COS 1.0
         SEGMENT 5  pc24 COS 1.0
         SEGMENT 5  pc25 COS 1.0
         SEGMENT 6  pc26 COS 1.0
         SEGMENT 1 pc27 COS 1.0
         SEGMENT 4  pc28 COS 1.0
         SEGMENT 1 pc29 COS 1.0
         SEGMENT -25  pc30 COS 1.0 RATIO 0.978 ;

MESH cold_ch m_cold                  ;
HYDR cold_ch ANNULAR                 ;

GEOM cold_ch
(pc1 AND pc2) SECT s_cc_1 PERI p_cc_1 SIZE  d_cc_b
(pc3 AND pc4) SECT s_cc_2  PERI p_cc_2 SIZE  d_cc_b
(pc5 AND pc6) SECT s_cc_3  PERI p_cc_3 SIZE  d_cc_b
(pc7 AND pc8) SECT s_cc_b_1 PERI p_cc_b SIZE  d_cc_b
(pc9 AND pc10) SECT s_cc_4 PERI p_cc_4 SIZE  d_cc_b
(pc11 AND pc19) SECT s_cc_b_1 PERI p_cc_b SIZE  d_cc_b
(pc20 AND pc22) SECT s_cc_5 PERI p_cc_5 SIZE  d_cc_b
(pc23 AND pc24) SECT s_cc_b_1 PERI p_cc_b SIZE d_cc_b
(pc25 AND pc30) SECT s_cc_t_1 PERI p_cc_t SIZE d_cc_t;


* COOLING CHANNEL

COOL_CH = AXIAL  j_b_co DSTREAM j_t_co USTREAM  ;

pcc0 = XAXIS (0.0)  ;
pcc1 = XAXIS (z_volbot) ;
pcc2 = XAXIS (z_he_1) ;
pcc3 = XAXIS (z_he_1 + 1.E-3) ;
pcc4 = XAXIS (z_he_2 - 1.E-3) ;
pcc5 = XAXIS (z_he_2 ) ;
Pcc6 = XAXIS (z_he_3 -1.E-3) ;
Pcc7 = XAXIS (z_he_3 ) ;
Pcc8 = XAXIS (z_he_4_b) ;
Pcc9 = XAXIS (z_he_4_b + 1.E-3) ;
Pcc10 = XAXIS (z_he_4_t - 1.E-3) ;
Pcc11 = XAXIS (z_he_4_t ) ;
Pcc12 = XAXIS (z_hea_b) ;
Pcc13 = XAXIS (z_ha_b ) ;
Pcc14 = XAXIS  (z_po_b) ;
Pcc15 = XAXIS (z_fuel_b) ;
Pcc16 = XAXIS (z_fuel_t) ;
pcc17 = XAXIS  (z_po_t ) ;
pcc18 = XAXIS  (z_hea_t ) ;
pcc19 = XAXIS (z_he_5_b  ) ;
pcc20 = XAXIS  (z_he_5_b + 1.E-3 ) ;
pcc21 = XAXIS  (z_ha_t ) ;
pcc22 = XAXIS (z_he_5_t  -1.E-3 ) ;
pcc23 = XAXIS  (z_he_5_t ) ;
pcc24 = XAXIS (z_If_b ) ;
pcc25 = XAXIS (z_if_t ) ;
pcc26 = XAXIS (z_lvdt_b) ;
pcc27 = XAXIS (z_lvdt_b + 1.E-3) ;
pcc28 = XAXIS (z_lvdt_t - 1.E-3) ;
pcc29 = XAXIS (z_lvdt_t ) ;
pcc30 = XAXIS (z_u_open) ;
pcc31 = XAXIS (z_de);

m_cool   = pcc0
         SEGMENT -25  pcc1 COS 1.0   RATIO 0.84
         SEGMENT -25  pcc2 COS 1.0  RATIO 1.0584
         SEGMENT 1  pcc3 COS 1.0
         SEGMENT 6  pcc4 COS 1.0
         SEGMENT 1  pcc5 COS 1.0
         SEGMENT 4  pcc6 COS 1.0
         SEGMENT 1  pcc7 COS 1.0
         SEGMENT 8  pcc8 COS 1.0
         SEGMENT 1  pcc9 COS 1.0
         SEGMENT 5  pcc10 COS 1.0
         SEGMENT 1  pcc11 COS 1.0
         SEGMENT 2  pcc12 COS 1.0
         SEGMENT 2  pcc13 COS 1.0
         SEGMENT 3  pcc14 COS 1.0
         SEGMENT 5  pcc15 COS 1.0
         SEGMENT 24  pcc16 COS 1.0
         SEGMENT 5  pcc17 COS 1.0
         SEGMENT 3  pcc18 COS 1.0
         SEGMENT 2  pcc19 COS 1.0
         SEGMENT 1  pcc20 COS 1.0
         SEGMENT 1  pcc21 COS 1.0
         SEGMENT 5  pcc22 COS 1.0
         SEGMENT 1  pcc23 COS 1.0
         SEGMENT 5  pcc24 COS 1.0
         SEGMENT 5  pcc25 COS 1.0
         SEGMENT 6  pcc26 COS 1.0
         SEGMENT 1 pcc27 COS 1.0
         SEGMENT 4 pcc28 COS 1.0
         SEGMENT 1 pcc29 COS 1.0
         SEGMENT -25  pcc30 COS 1.0 RATIO 0.978
         SEGMENT -11  pcc31 COS 1.0 RATIO 1.153 ;

*
MESH cool_ch m_cool            ;
HYDR cool_ch ANNULAR           ;

GEOM cool_ch
(pcc0 AND pcc24) SECT s_co_b PERI p_co_b SIZE d_co_b
(pcc25 AND pcc31) SECT s_co_t PERI p_co_t SIZE d_co_t;


VOLTOP = VOLUME j_t_cc DSTREAM j_t_hc DSTREAM
               j_t_vt  USTREAM       ;
*
GEOM voltop
       0.0       s_voltop
   z_voltop  s_voltop
```

```
j_t_cc BOTTOM LENGTH 0.
  SECT s_cc_t_1  PERI p_cc_t  SIZE  d_cc_t VERTICAL
j_t_hc BOTTOM LENGTH 0.
  SECT s_hc_3  PERI p_hc_3  SIZE  d_hc  VERTICAL
j_t_vt TOP LENGTH 0.0
  SECT (d_if_t_i*PI)/4. PERI (d_if_t_i*PI) SIZE
  d_if_t_i VERTICAL;



DEB_CAT = VOLUME j_b_hc USTREAM j_t_dc_2 DSTREAM ;
*
GEOM DEB_CAT
       0.0   s_dc
   h_dc  s_dc

j_b_hc TOP LENGTH 0.0
  SECT s_hc  PERI p_hc  SIZE  d_hc  VERTICAL

j_t_dc_2 ELEV h_dc LENGTH 3.E-3 WEIGHT 4
  SECT s_hole_b  PERI p_hole_b  SIZE  d_hole_b
  HORIZONT ;


VOLBOT = VOLUME j_b_cc USTREAM j_t_dc_2 USTREAM
         j_b_vb DSTREAM                                ;
*
GEOM volbot
       0.0             s_vb_1
       (z_vb_1-1.E-3)  s_vb_1
   z_vb_1          s_vb_2
       z_volbot        s_vb_2

j_b_cc TOP LENGTH 0.
    SECT s_cc_1  PERI p_cc_1  SIZE  d_cc_b VERTICAL
j_t_dc_2 ELEV z_volbot  LENGTH 0. WEIGHT 4
    SECT s_hole_b  PERI p_hole_b
    SIZE  d_hole_b  HORIZONT
j_b_vb BOTTOM LENGTH 0.0
    SECT (d_if_t_i*PI)/4 PERI (d_if_t_i*PI)
    SIZE d_if_t_i VERTICAL ;

* DEFINITION OF THE SINK/SOURCE OF WATER
SINWEI = SOURCE VOLUME VOLBOT EXTERNAL
         ELEV z_volbot  SECT (s_dn6)*2.0
         LENGTH 0.0 ;

*************************************
* BOUNDARY CONDITIONS of the device
*************************************

* BOUNDARY CONDITION TOP .
* PRESSURE FIXED

bc_out = BCONDIT  j_b_vb USTREAM;
                  MODEL bc_out BC4C
                  P (REALLIST 3.0E+5   3.0E+5 )
                  ABSTIME (REALLIST 0. 10000.  );

*BOUNDARY CONDITION BOTTOM.
bc_inlet = BCONDIT j_t_vt DSTREAM ;
           MODEL bc_inlet BC3B
TL      (REALLIST  50.   50.   50.    50.    50.    50.    )
TG      (REALLIST  100.  100.  250.   250.   250.   250.   )
ALFA    (REALLIST  1.e-5 1.e-5 0.9999 0.9999 0.9999 0.9999 )
X1      (REALLIST  1.e-5 1.e-5 0.9999 0.9999 0.9999 0.9999 )
X2      (REALLIST  1.E-5 1.E-5 1.E-5  1.E-5  1.E-5  1.E-5  )
VL      (REALLIST  0.1   0.1   0.5    0.5    1.E-5  1.E-5  )
VV      (REALLIST  0.1   0.1   1.0    1.0    1.E-5  1.E-5  )
ABSTIME (REALLIST  0.    1000. 1001.  1010.  1011.  1000000.);

*************************************
* BOUNDARY CONDITIONS cooling channel
*************************************

T_in_coo = 35.0                 ;
Q_in_coo = 2.5                  ;
P_ou_coo = 2.0E5                ;
v_coo_in = Q_in_coo/s_co_t/995.  ;

bc_coo_i = BCONDIT j_t_co DSTREAM          ;
           MODEL bc_coo_i BC3E
TL      ( REALLIST  T_in_coo  T_in_coo )
TG      ( REALLIST  -1.       -1.      )
ALFA    ( REALLIST  1.D-5     1.D-5    )
X1      ( REALLIST  1.D-5     1.D-5    )
QL      ( REALLIST  Q_in_coo  Q_in_coo )
QG      ( REALLIST  1.d-5     1.e-5    )
ABSTIME ( REALLIST  0.0D0     tendf    )   ;

bc_coo_o = BCONDIT j_b_co USTREAM  ;
           MODEL bc_coo_o BC4A
P (REALLIST P_ou_coo P_ou_coo)
ABSTIME (REALLIST 0. tendf  )      ;

*************************************
* DEFINITION OF INTERNAL POWER
*************************************

* GAMMA HEATING POWER
lawg= LAW 'time'  'power'
         0.     0.
    tendf 0. ;

* POWER ELECTRICAL HEATER
law_th= LAW 'time'  'power'
            0.      0.
     tendf  0. ;

* DISTRIBUTION FUEL POWER ALONG
* THE FUEL SAMPLE
LAW_PAST = LAW 'RADIUS' 'POWER'
               0.D0          1.D0
               (D_FUEL/2.0)  1.D0 ;

LAW_CRA = LAW 'time'   'power'
          0.      0.
      tendf      0. ;

* distance from the core (relative distance)
*  to obtain 40 W/cm
distan = 14.08                          ;
LHGR = 375.2 * exp (-0.159*distan)      ;
* volume fuel
VOL_FUEL = PI*D_FUEL**2. /4. *H_FUEL    ;
* Linear power
POW_LIN = LHGR*H_FUEL*100.              ;

*************************************
*  Power inside the fuel
*************************************
POW_VOL = LHGR*H_FUEL*100. /VOL_FUEL
*************************************

*************************************
*  POWER INSIDE THE THERMAL HEATER
*************************************
*   volume of the internal heater
V_HEAT1 = PI*DE_HEAT1**2.0*H_HEAT1/4.0  ;
Pow_heat = 1.5E3 / V_HEAT1              ;


* Gamma avarage power in the different
* media at distance 0 cm (W/g)
* The values are averaged along 70 cm of
* height
* pag 27/111 CDR Version 1.4.2016

* the media are in order :
*    cladding
```

```
*    hot channel
*    heater
*    cold channel
*    inner flask
*    helium gap
*    outer flask
*    cooling channel
*    neutron screen
*    device holder
****************************************

g_clad0 = 2.6                          ;
g_hch0  = 5.0                          ;
g_hea0  = 2.7                          ;
g_cch0  = 4.9                          ;
g_inPF0 = 2.9                          ;
g_he0   = 5.1                          ;
g_ouPF0 = 3.2                          ;
g_coch0 = 5.2                          ;
g_hf0   = 6.6                          ;
g_devh0 = 2.9                          ;

****************************************
* the reference for the law vs position is
* set on the SS external flask
* gamma power at the right location (W/g)
****************************************
g_ouPF = g_inPF0/g_inPF0*5.1711*exp (-0.087*distan) ;
g_clad = g_clad0/g_inPF0*5.1711*exp (-0.087*distan) ;
g_hch  = g_hch0/g_inPF0*5.1711*exp (-0.087*distan)   ;
g_hea  = g_hea0/g_inPF0*5.1711*exp (-0.087*distan)   ;
g_cch  = g_cch0/g_inPF0*5.1711*exp (-0.087*distan)   ;
g_inPF = g_inPF0/g_inPF0*5.1711*exp (-0.087*distan) ;
g_he   = g_he0/g_inPF0*5.1711*exp (-0.087*distan)     ;
g_coch = g_coch0/g_inPF0*5.1711*exp (-0.087*distan) ;
g_hf   = g_hf0/g_inPF0*5.1711*exp (-0.087*distan)     ;
g_devh = g_devh0/g_inPF0*5.1711*exp (-0.087*distan) ;

****************************************
* heat transfer coefficient to the pool
****************************************
htc_ext = 500.          ;
htc_ext1 = 100000.      ;

*Peaking factor for 70 cm of length gamma structures
PF =1.273 ;

* density of materials [kg/m^3], zircalloy,
* water, stainless steel, helium, hafnium
r_zir  = 6603.0 ;
r_wat  = 980.0 ;
r_sst  = 7860.0 ;
r_hel  = 0.65 ;
r_haf  = 13277.0 ;
r_inc  = 7287.0 ;

r_steam = 2.6680 ;

* Gamma power [W/m^3] in the water,
* hot-cold-cooling channels
P_HCP = (PF*r_steam*g_hch*1000.) ;
P_CC  = (PF*r_steam*g_cch*1000.) ;
P_CO  = (PF*r_wat*g_coch*1000.)  ;
P_DH  = (PF*r_zir*g_devh*1000.)  ;
P_HE  = (r_inc*g_hea*1000.)      ;
P_IN  = (r_sst*g_inPF*1000.)     ;
P_EL  = (r_hel*g_he*1000.)       ;
P_OU  = (r_sst*g_ouPF*1000.)     ;
P_HA  = (PF*r_haf*g_hf*1000.)    ;

* volumetric power [W/m^3]; average values
* in every wall we have to mutiply this
* values with the PF for 70 cm and the
* axial distribution normalized

PCLA_VOL = r_zir*g_clad*1000.0   ;
PHF_VOL  = r_haf*1000.0*g_hf     ;

* PERIMETER FOR GAMMA INSIDE THE WATER HOT_CH
PE_HC = s_hc/1.D-3               ;
PE_HC1 = s_hc_1 /1.D-3  ;
PE_HC2 = s_hc_2/1.D-3          ;
PE_HC3 = s_hc_3/1.D-3  ;

*PERIMETER FOR GAMMA INSIDE THE WATER COLD_CH
PE_CC_B = s_cc_b_1/1.D-3        ;
PE_CC_1 = s_cc_1/1.D-3        ;
PE_CC_2 = s_cc_2/1.D-3    ;
PE_CC_3 = s_cc_3/1.D-3    ;
PE_CC_4 = s_cc_4/1.D-3    ;
PE_CC_5 = s_cc_5/1.D-3    ;
PE_CC_T = s_cc_t_1/1.D-3    ;

*PERIMETER FOR GAMMA INSIDE THE WATER COOL_CH
PE_CO_B = s_co_b/1.D-3        ;
PE_CO_T = s_co_t/1.D-3    ;


*************************************
* PRESSURE DROPS HOT CHANNEL
* Handbook of Hydraulic Resistance Idelchik
*************************************
* Sudden contraction
* handbook of hydraulic resistence p. 216-217
SCHC_1 = (s_hc_1/ s_hc) ;
SCDP1_HC = (0.5*(1.-SCHC_1)**(3./4.)) ;
*
SCHC_2 = (s_hc_2/ s_hc_1) ;
SCDP2_HC = (0.5*(1.-SCHC_2)**(3./4.)) ;
*
* Sudden expansion
* handbook of hydraulic resistence p. 208
SEHC_1 = (s_hc_2/ s_hc_3) ;
SEDP1_HC = (0.5*(1.-SEHC_1)**(2.));
*
SINGULAR HOT_CH POINT PH5 POSITIVE SCDP1_HC
         NEGATIVE  SCDP1_HC    ;

SINGULAR HOT_CH POINT PH20 POSITIVE SCDP2_HC
         NEGATIVE SCDP2_HC   ;

SINGULAR HOT_CH POINT PH23 POSITIVE SEDP1_HC
         NEGATIVE SEDP1_HC    ;

*************************************
*PRESSURE DROPS COLD CHANNEL
*************************************
*Sudden contraction
* FROM HEATER CONNECTOR 1 TO HEATER CONNECTOR 2
SCCC_1 = (s_cc_2/s_cc_1) ;
SCDP1_CC = (0.5*(1.-SCCC_1)**(3./4.)) ;

* FROM HEATER TO HEATER CONNECTOR 4
SCCC_2 = (s_cc_4/s_cc_b_1) ;
SCDP2_CC = (0.5*(1.-SCCC_2)**(3./4.)) ;

* FROM HEATER TO HEATER CONNECTOR 5
SCCC_3 = (s_cc_5/s_cc_b_1) ;
SCDP3_CC = (0.5*(1.-SCCC_3)**(3./4.)) ;

*Sudden expansion
*FROM HEATER CONNECTOR 2 TO HEATER CONNECTOR 3
SECC_1 = (s_cc_2/ s_cc_3) ;
SEDP1_CC = (0.5*(1.-SECC_1)**(2.));

*FROM HEATER CONNECTOR 3 TO HEATER
SECC_2 = (s_cc_3/ s_cc_b_1) ;
SEDP2_CC = (0.5*(1.-SECC_2)**(2.));

*FROM HEATER CONNECTOR 4 TO HEATER
```

```
SECC_3 = (s_cc_4/ s_cc_b_1) ;
SEDP3_CC = (0.5*(1.-SECC_3)**(2.));

*FROM HEATER CONNECTOR 5 TO HEATER
SECC_4 = (s_cc_5/ s_cc_b_1) ;
SEDP4_CC = (0.5*(1.-SECC_4)**(2.));

SINGULAR COLD_CH POINT PC3 POSITIVE SCDP1_CC
         NEGATIVE SCDP1_CC    ;

SINGULAR COLD_CH POINT PC9 POSITIVE SCDP2_CC
         NEGATIVE SCDP2_CC    ;

SINGULAR COLD_CH POINT PC20 POSITIVE SCDP3_CC
         NEGATIVE SCDP3_CC    ;

SINGULAR COLD_CH POINT PC5 POSITIVE SEDP1_CC
         NEGATIVE SEDP1_CC   ;

SINGULAR COLD_CH POINT PC7 POSITIVE SEDP2_CC
         NEGATIVE SEDP2_CC   ;

SINGULAR COLD_CH POINT PC11 POSITIVE SEDP3_CC
         NEGATIVE SEDP3_CC   ;

SINGULAR COLD_CH POINT PC23 POSITIVE SEDP4_CC
         NEGATIVE SEDP4_CC   ;


* DIVERGENT PART; diagram 5-23, pag 316 IIdelchik
EPSI_CON = 0.46 ;
SINGULAR COLD_CH POINT PC24 POSITIVE EPSI_CON
         NEGATIVE EPSI_CON    ;

PGAM_CO = REALLIST
0.45639*P_CO 0.47728*P_CO 0.49842*P_CO 0.51975*P_CO
0.54125*P_CO 0.57916*P_CO 0.63352*P_CO 0.68748*P_CO
0.74024*P_CO 0.79094*P_CO 0.83864*P_CO 0.88235*P_CO
0.92100*P_CO 0.95344*P_CO 0.97846*P_CO 0.99479*P_CO
1.00107*P_CO 1.00107*P_CO 0.99479*P_CO 0.97846*P_CO
0.95343*P_CO 0.92099*P_CO 0.88234*P_CO 0.83862*P_CO
0.79090*P_CO 0.74019*P_CO 0.68742*P_CO 0.63345*P_CO
0.57907*P_CO 0.54116*P_CO 0.51965*P_CO 0.49831*P_CO
0.47717*P_CO 0.45627*P_CO ;


P_DH_W =REALLIST
0.00000*P_DH 0.00000*P_DH 0.00000*P_DH 0.45639*P_DH
0.47728*P_DH 0.49842*P_DH 0.51975*P_DH 0.54125*P_DH
0.57916*P_DH 0.63352*P_DH 0.68748*P_DH 0.74024*P_DH
0.79094*P_DH 0.83864*P_DH 0.88235*P_DH 0.92100*P_DH
0.95344*P_DH 0.97846*P_DH 0.99479*P_DH 1.00107*P_DH
1.00107*P_DH 0.99479*P_DH 0.97846*P_DH 0.95343*P_DH
0.92099*P_DH 0.88234*P_DH 0.83862*P_DH 0.79090*P_DH
0.74019*P_DH 0.68742*P_DH 0.63345*P_DH 0.57907*P_DH
0.54116*P_DH 0.51965*P_DH 0.49831*P_DH 0.47717*P_DH
0.45627*P_DH 0.00000*P_DH 0.00000*P_DH 0.00000*P_DH
0.00000*P_DH 0.00000*P_DH 0.00000*P_DH 0.00000*P_DH ;


P_HA_W =REALLIST
0.00000*P_HA 0.00000*P_HA 0.00000*P_HA 0.45639*P_HA
0.47728*P_HA 0.49842*P_HA 0.51975*P_HA 0.54125*P_HA
0.57916*P_HA 0.63352*P_HA 0.68748*P_HA 0.74024*P_HA
0.79094*P_HA 0.83864*P_HA 0.88235*P_HA 0.92100*P_HA
0.95344*P_HA 0.97846*P_HA 0.99479*P_HA 1.00107*P_HA
1.00107*P_HA 0.99479*P_HA 0.97846*P_HA 0.95343*P_HA
0.92099*P_HA 0.88234*P_HA 0.83862*P_HA 0.79090*P_HA
0.74019*P_HA 0.68742*P_HA 0.63345*P_HA 0.57907*P_HA
0.54116*P_HA 0.51965*P_HA 0.49831*P_HA 0.47717*P_HA
0.45627*P_HA 0.00000*P_HA 0.00000*P_HA 0.00000*P_HA
0.00000*P_HA 0.00000*P_HA 0.00000*P_HA 0.00000*P_HA ;


* DEFINITION FUEL SAMPLE VARIABLES

TAB1CRAD = 0.2999331E-02      ;
*
TAB1VEVI = 0.3076102E-06      ;

TAB1VPLS = 0.2108495E-05      ;
*
TAB1VPLI = 0.0000000E+00      ;
*
TAB1VCR  = 0.8046442E-06      ;
*
TAB1VPOR = 0.2523035E-07      ;
*
TAB1TPLG = 0.0000000E+00      ;
*
TAB1VOLF = 0.9862677E+00      ;
*
TAB1PORS = 0.4294068E-01      ;


* 5 micron oxide (internal-external)
CRAYON = FUEL HOT_CH INTERNAL
         SEGMENT PH15 PH16
         ISO 8 DIAM 0.0 D_FUEL
         UO2 IRRAFUEL
         WZUO 1.0
         LAW LAW_PAST
         GAP 1.E-6
     OXIDE EOI 5.E-6 EOE 5.E-6
         CLADDING ZRCEA
         RM 4.4505E-3 ;
*
*
CHARCRAY = FUELCHAR HOT_CH
           GAP DELTFUEL 1.E-10
           GAPP 10.E5
           CRAD TAB1CRAD
           FUELP INTERNAL
           POWNEUT POW_LIN
           POWRESI 1.E-10
           LAWNEUT LAW_CRA
           LAWRESI LAW_CRA
           GASVOL VOIDV TAB1VEVI
           EXPANV TAB1VPLS
           BPLUGV TAB1VPLI
           CRACKV TAB1VCR
           POROSV TAB1VPOR
           TPLUGV TAB1TPLG
           VOLFRAC TAB1VOLF
           PORos TAB1PORS
           XNEUT 0.9994 ;
*           OXTYPE STANDARD;
           INTEGRATE CRAYON NUMBER 1 CHARCRAY ;
           PNRSHAPE CHARCRAY SIGNAL 1
  1.
0.535068 0.612231 0.685999 0.755233
0.818905 0.876096 0.925996 0.967905
1.001233 1.025497 1.040326 1.045457
1.040737 1.026121 1.001677 0.967578
0.924109 0.871665 0.810747 0.741969
0.666052 0.583829 0.496240 0.404335 ;
*

* GAMMA POWER INSIDE THE STEAM
* NOT CONSIDERED (VERY SMALL)

*gam_hc = WALL hot_ch INTERNAL PLANE
*         SEGMENT ph14 ph17
*         YYYYYY04 ISO 1 THICK 0.0D0 1.D-3
*         HPERIM CONST PE_HC1
*         SOURCE MEDIUM 1
*       LAW lawg
*         VOLPOWER PGAM_HC ;
**************************************
```

```
*gam_cc = WALL cold_ch INTERNAL PLANE
*         SEGMENT pc14 pc17
*         YYYYYY04 ISO 1 THICK 0.0D0 1.D-3
*         HPERIM CONST  PE_CC_B
*
*         (PC5 AND PC6)  PE_CC_3
*         (PC7 AND PC8)  PE_CC_B
*         (PC9 AND PC10)  PE_CC_4
*         (PC11 AND PC14)  PE_CC_B
*         (PC15 AND PC16)  PE_CC_5
*         (PC17 AND PC19)  PE_CC_B
*          PC19   PE_CC_B
*          C21   PE_CC_T
*          SOURCE MEDIUM 1
*        LAW lawg
*          VOLPOWER PGAM_CC ;
*
************************************

gam_co= WALL cool_ch INTERNAL PLANE
               SEGMENT pcc14 pcc17
               YYYYYY04 ISO 1 THICK 0.0D0 1.D-3
               HPERIM CONST PE_CO_B

*
*              PCC19 PE_CC_B
*              PCC21 PE_CC_T
*             (PCC20 AND PCC21)  PE_CC_T
               SOURCE MEDIUM 1
               LAW lawg
               VOLPOWER PGAM_CO ;
*

************************************
* Shroud lower region - Pure SS
************************************

shr_B= EXCHANGER  hot_ch cold_ch IMPLICIT
       PRIMARY CYLINDER
       SEGMENT ph1 ph2 DIRECT pc1 pc2
       INOX316 ISO 5 DIAM  d_hc d_he_1_e
       HPERIM  CONST  (PI*d_hc)

       SEGMENT ph2 ph3 DIRECT pc2 pc3
       INOX316 ISO 5 DINI  d_hc d_he_1_e
                     DEND  d_hc d_he_2_e
                     HPERIM CONST (PI*d_hc)

       SEGMENT ph3 ph4 DIRECT pc3 pc4
       INOX316 ISO 5 DIAM  d_hc d_he_2_e
       HPERIM  CONST  (PI*d_hc)

       SEGMENT ph4 ph5 DIRECT pc4 pc5
       INOX316 ISO 5 DINI  d_hc d_he_2_e
                     DEND  d_hc d_he_3_e
       HPERIM  CONST  (PI*d_hc)

       SEGMENT ph5 ph6 DIRECT pc5 pc6
       INOX316 ISO 5 DIAM  d_hc d_he_3_e
       HPERIM  CONST  (PI*d_hc)

       SEGMENT ph6 ph7 DIRECT pc6 pc7
       INOX316 ISO 5 DINI  d_hc d_he_3_e
               DEND  d_hc d_hc_e
               HPERIM CONST  (PI*d_hc)

       SEGMENT ph7 ph8 DIRECT pc7 pc8
       INOX316 ISO 5 DIAM  d_hc d_hc_e
       HPERIM  CONST  (PI*d_hc)

       SEGMENT ph8 ph9 DIRECT pc8 pc9
       INOX316 ISO 5 DINI  d_hc d_hc_e
                     DEND  d_hc d_he_4_e
       HPERIM  CONST  (PI*d_hc)

       SEGMENT ph9 ph10 DIRECT pc9 pc10
       INOX316 ISO 5 DIAM  d_hc d_he_4_e
       HPERIM  CONST  (PI*d_hc)

       SEGMENT ph10 ph11 DIRECT pc10 pc11
       INOX316 ISO 5 DINI  d_hc  d_he_4_e
                     DEND  d_hc d_hc_e
       HPERIM CONST  (PI*d_hc) ;

************************************
* Shroud - Heater part
************************************
heater= EXCHANGER  hot_ch cold_ch IMPLICIT
        PRIMARY
        CYLINDER
        SEGMENT  ph11 ph12 DIRECT pc11 pc12
        INOX316  ISO 5 DIAM d_hc d_hc_e
        HPERIM   CONST  (PI*d_hc)

        SEGMENT  ph12 ph18 DIRECT pc12 pc18
        INCON718 ISO 5 DIAM  d_hc d_hc_e
        HPERIM   CONST  (PI*d_hc)

        SEGMENT  ph18 ph19 DIRECT pc18 pc19
        INOX316 ISO 5 DIAM  d_hc d_hc_e
        HPERIM CONST  (PI*d_hc)

        SEGMENT  ph19 ph20 DIRECT pc19 pc20
        INOX316 ISO 5 DINI  d_hc  d_hc_e
                      DEND  d_hc  d_he_5_e
        HPERIM CONST  (PI*d_hc)

        SEGMENT  ph20 ph21 DIRECT pc20 pc21
        INOX316 ISO 5 DIAM d_hc d_he_5_e
        HPERIM CONST  (PI*d_hc)  ;

shr_U = EXCHANGER  hot_ch cold_ch IMPLICIT
        PRIMARY
        CYLINDER
        SEGMENT  ph21 ph22 DIRECT pc21 pc22
        INOX316 ISO 5 DIAM d_hc d_he_5_e
        HPERIM CONST  (PI*d_hc)

        SEGMENT  ph22 ph23 DIRECT pc22 pc23
        INOX316 ISO 5 DINI  d_hc  d_he_5_e
                      DEND  d_hc d_hc_e
        HPERIM CONST  (PI*d_hc)

        SEGMENT  ph23 ph30 DIRECT pc23 pc30
        INOX316  ISO 5 DIAM  d_hc d_hc_e
        HPERIM  CONST  (PI*d_hc) ;


Fla_B = EXCHANGER cool_ch cold_ch IMPLICIT
        PRIMARY CYLINDER
        SEGMENT  pcc1 pcc11 REVERSE pc1 pc11
        INOX316  ISO  10 DIAM  d_if_b_i d_if_b_e
        XXXXXXX6 ISO  4  DIAM  d_if_b_e d_of_b_i
        INOX316  ISO  10 DIAM  d_of_b_i d_of_b_e
    HPERIM   CONST (pi*d_if_b_i)    ;


Fla_M = EXCHANGER cool_ch cold_ch IMPLICIT
        PRIMARY
        CYLINDER
        SEGMENT  pcc11 pcc21 REVERSE pc11 pc21
        INOX316  ISO  10 DIAM d_if_b_i d_if_b_e
        XXXXXXX6 ISO  4  DIAM  d_if_b_e d_of_b_i
        INOX316  ISO  10 DIAM  d_of_b_i d_of_b_e
        HPERIM CONST (pi*d_if_b_i) ;

Fla_U = EXCHANGER cool_ch cold_ch IMPLICIT
        PRIMARY
    CYLINDER
        SEGMENT pcc21 pcc24 REVERSE pc21 pc24
```

```
        INOX316  ISO  10 DIAM d_if_b_i d_if_b_e
        XXXXXXX6 ISO  4  DIAM  d_if_b_e d_of_b_i
        INOX316  ISO  10 DIAM  d_of_b_i d_of_b_e
        HPERIM CONST (pi*d_if_b_i)

        SEGMENT pcc24 pcc25 REVERSE pc24 pc25
        INOX316  ISO  10 DINI d_if_b_i d_if_b_e
                         DEND d_if_t_i d_if_t_e
        XXXXXXX6 ISO  4  DINI d_if_b_e d_of_b_i
                         DEND d_if_t_e  d_of_t_i
        INOX316  ISO 10  DINI d_of_b_i d_of_b_e
                         DEND d_of_t_i d_of_t_e
        HPERIM POINT     pc24 d_if_b_i
                         pc25 d_if_t_i

       SEGMENT pcc25 pcc30 REVERSE pc25 pc30
       INOX316  ISO  10 DIAM  d_if_t_i d_if_t_e
       XXXXXXX6      ISO  4  DIAM  d_if_t_e d_of_t_i
       INOX316  ISO  10 DIAM  d_of_t_i d_of_t_e
   HPERIM CONST (pi*d_if_t_i)    ;

ExtWaB = WALL cool_ch EXTERNAL
         SEGMENT pcc0 pcc11
         ZIRCALOY  ISO  10 DIAM   d_de_b_i d_de_b_e
     HPERIM CONST (pi*d_de_b_i)
     LOSS HEXT htc_ext
         TEXT 35.0      ;

ExtWaM1 = WALL cool_ch EXTERNAL
          SEGMENT pcc11 pcc13
          ZIRCALOY  ISO  20 DIAM d_ha_e  d_de_b_e
          HPERIM CONST (pi*d_de_b_e)
          LOSS HEXT htc_ext
          TEXT 35.0

          SEGMENT pcc13 pcc21
          XXXXXXX3  ISO  10 DIAM  d_ha_i d_ha_e
          ZIRCALOY  ISO  10 DIAM d_ha_e  d_de_b_e

      HPERIM CONST (pi*d_de_b_e)
          LOSS HEXT htc_ext
          TEXT 35.0

          SOURCE MEDIUM 1 LAW lawg
          VOLPOWER P_HA_W
      SOURCE MEDIUM 2 LAW lawg
          VOLPOWER P_DH_W
      LOSS HEXT htc_ext TEXT 35.0     ;


ExtWaU =  WALL cool_ch EXTERNAL
          SEGMENT pcc21 pcc24
          ZIRCALOY  ISO  10 DIAM d_de_b_i d_de_b_e
      HPERIM CONST (pi*d_de_b_e)

          SEGMENT pcc24 pcc25
          ZIRCALOY  ISO  10  DINI d_de_b_i d_de_b_e
                             DEND d_de_t_i d_de_t_e
          HPERIM POINT pcc24 d_de_b_e
                       pcc25 d_de_t_e

          SEGMENT pcc25 pcc31
          ZIRCALOY  ISO  10 DIAM   d_de_t_i d_de_t_e
      HPERIM CONST (pi*d_de_t_i)
      LOSS HEXT htc_ext
          TEXT 35.0      ;


**************************************
* Flask top of the device
**************************************

flaskTop = WALL cool_ch INTERNAL
           SEGMENT  pcc30 pcc31
           INOX316  ISO  10 DIAM  d_if_t_i d_if_t_e
           XXXXXXX6 ISO  4  DIAM  d_if_t_e d_of_t_i
           INOX316  ISO  10 DIAM  d_of_t_i d_of_t_e
           HPERIM  CONST (pi*d_of_t_e)
       LOSS HEXT 1.E4
           TEXT 140.      ;

**************************************
*  suppression of the lost heat to the
*  cooling channel from the upper plenum
**************************************

**************************************
* Flask bottom of the device
**************************************
flaskBot = WALL cool_ch INTERNAL
           SEGMENT  pcc0 pcc1
           INOX316  ISO  10 DIAM  d_if_b_i d_if_b_e
           XXXXXXX6      ISO  4  DIAM  d_if_b_e d_of_b_i
           INOX316  ISO  10 DIAM  d_of_b_i d_of_b_e
       HPERIM CONST (pi*d_of_b_e)
       LOSS HEXT 1.E4
           TEXT 140.      ;

**************************************
*  suppression of the lost heat to the
*  cooling channel from the lower plenum
**************************************

* thermal resistance bottom device
* to produce steam

THERMA = WALL hot_ch INTERNAL
         SEGMENT  ph1 ph2
         INOX316 ISO  8 DIAM  0.0   DE_HEAT1
     HPERIM CONST (pi*DE_HEAT1 )
     SOURCE MEDIUM 1
     LAW law_th
         VOLPOWER Pow_heat     ;

**************************************
* REACTOR
**************************************

displor = CIRCUIT  volbot
                   deb_cat
                   cold_ch
                   hot_ch
           voltop
               bc_inlet
                   bc_out
                   list_gaz ;

coolinch = CIRCUIT cool_ch
               bc_coo_i
                   bc_coo_o
                   list_gaz ;

*
CIRCTOT = REACTOR displor coolinch ;
*

END DATA ;


**************************************
*           EXEC BLOCK
**************************************

DOUBLE  TIME DTO DT POW_FUEL ;
DOUBLE  lost_bot  t_bot lost_top  t_top
        PRESSU H_REG VOL_LIQ ;
DOUBLE  LEV1 LEVELR  PRESS1 XPRESS  MASS
        MAS_REF MASS1 MASS_CIRC MDIFF;
INTEGER NSTEPS ipower IPOWER1 IPOWER4
        IPOWER5 IPOWER6 IPOWER7 TSATU ;
```

```
INTEGER VALVE1 VALVE2 ;
RESTORE;
REACTOR CIRCTOT;


****************************************
*            STEADY STATE
****************************************
*
****************************************
* INITIALIZATION
****************************************
*
PERMINIT displor
         voltop
         cold_ch
         hot_ch
         deb_cat
         volbot
         bc_inlet
         bc_out                  ;

PERMINIT coolinch
         cool_ch
     bc_coo_i
         bc_coo_o                ;


****************************************
* INITIAL CONDITIONS
****************************************
*
REALC  j_t_vt
       P    3.0E+5
   HLSAT
   TV   100.
   ALFA 1.e-5
        X1   1.e-5
        X2   1.e-5
        VL   0.01
        VV   0.01
   ;

REALC  j_t_co
       P    2.0E+5
   TL    33.
        HVSAT
   ALFA  1.0E-5
        X1    1.0E-5
        X2    1.0E-5
        VL    v_coo_in
        VV    v_coo_in    ;

ECHPOWER heater 0.       ;
ECHPOWER shr_U 0.        ;
ECHPOWER shr_B 0.        ;
ECHPOWER Fla_B 0.        ;
ECHPOWER Fla_M 0.        ;
ECHPOWER Fla_U 0.        ;

TIME     = 0.D0 ;
DT0      = 1.0D-4 ;
NSTEPS   = 3.0D+6 ;
ipower   = 1 ;
IPOWER1  = 0 ;
IPOWER4  = 0 ;
IPOWER5  = 0 ;
IPOWER6  = 0 ;
IPOWER7  = 0 ;

H_REG   = (0.125+0.05) ;
VOL_LIQ = (1/4)*PI*(H_REG)*(d_hc)**2  ;
MAS_REF = (VOL_LIQ)*r_wat ;

****************************************
GOPERM
****************************************

OPEN SINWEI  ;
*
SAVE 111 append ;

PERIOD displor SECOND  500.D0 ;
RESULT CIRCTOT SECOND  250.D0 ;

****************************************
****************************************
*           TRANSIENT          *
****************************************
****************************************

OPTION rocp 100.;
OPTION DTMIN 1.E-10 ;
OPTION MAXREP 50 ;
* Time step for transient
DT = DT0  ;
*
*PNRSHAPX CHARCRAY SIGNAL 1.                                                    ;
*
REPEAT BLOCK1 NSTEPS ;
  TIME = TIME + DT ;
  TRANSIENT CIRCTOT TIME DT ;
  DT = NEWDT ;
  IF ( DT > 1. ) THEN ;
  DT = 1. ;
  ENDIF ;
****************************************

TIME = NEWTIME ;
  IF ( TIME > 2000. ) THEN ;
  QUIT BLOCK1 ;
  ENDIF ;
END BLOCK1 ;

OPTION rocp 1.     ;
****************************************
* Stop of forced flow;  the system is
* closed
****************************************
BCMOD bc_inlet BLIND ;
BCMOD bc_out BLIND ;
****************************************

REPEAT BLOCK2 NSTEPS ;
  TIME = TIME + DT ;
  TRANSIENT CIRCTOT TIME DT ;
  DT = NEWDT ;
  IF ( DT > 10. ) THEN ;
  DT = 10. ;
  ENDIF ;


TIME = TIME + DT ;
 TRANSIENT CIRCTOT TIME DT ;
 DT = NEWDT ;

TSATU = VALUE SATTEMP VOLTOP SUP ;
MESSAGE ' !!!!!!!  SATTEMP IS ' TSATU ;


*REFERENT MASS INSIDE THE DISPO 1.2 KG
MAS_REF = 1.2 ;

****************************************
* Some water is injected inside the device,
* the regulation is done with the source SINWEI
****************************************

IF  ((IPOWER4 EQ 0)  AND ( TIME > 5000. )) THEN ;
    MASS_CIR = VALUE  LIQMASS DISPLOR ;
```

```
    MESSAGE ' !!!MASS REF IS' MAS_REF ;
    MESSAGE ' !!!MASS CIRCUIT IS' MASS_CIR ;
    IF (MASS_CIR < 1.2)  ;
        WRITE 0.2 LIQFLOW  SINWEI ;
        WRITE 0. UNDERSAT SINWEI ;
    ELSE ;
        WRITE 0.0 LIQFLOW  SINWEI ;
        MESSAGE ' !!!!!!!  STOP VOLTOP MASS REGULATION' TIME ;
        IPOWER4 = 1 ;
        ENDIF ;
ENDIF ;
```

```
TIME = NEWTIME ;
  IF ( TIME > tendf ) THEN ;
  QUIT BLOCK2 ;
  ENDIF ;

END BLOCK2 ;
CLOSE SINWEI  ;
*
SAVE 211 append ;
*
END EXEC;
```

B.2 Restart input for the Dry phase

```
****************************************
****************************************
*
*  LORELEI - TEST SECTION
*
****************************************
***  DRY PHASE  P_(EH)=1 kW
***  AT 12000 s the electrical heater
***  is activated
***  AT 16000 s the device starts to move
***  toward the core at 6 cm/s
****************************************

****************************************
* VARIABLES
****************************************

DOUBLE TIME DT0 DT PI
       lost_bot  t_bot lost_top
       t_top PRESSU g_coch0
       LEV1 LEVELR QSOURCE QSINKE XDIFF
       XDIFFR PRESS1 XPRESS
       g_hea0 g_inPF0 g_he0 g_ouPF0
       HTC_EXT HTC_EXT1 g_1 g_2 C1 dist
       P_HE P_IN P_EL P_OU g_hea g_inPF
       g_he g_ouPF PF distan0 PCR PC
       r_sst r_hel r_inc LHGR POW_LIN
       PRESS2 T_RUP  TEMP_RUP THICCLA
       POWE1  POWE2  POWE3  POWE4
       POWE5  POWE6  POWE7  POWE8
       POWE9  POWE10 POWE11 POWE12
       POWE13 POWE14 POWE15 POWE16
       POWE17 POWE18 POWE19 POWE20
       POWE21 POWE22 POWE23 POWE24
       POWI1  POWI2  POWI3  POWI4
       POWI5  POWI6  POWI7  POWI8
       POWI9  POWI10 POWI11 POWI12
       POWI13 POWI14 POWI15 POWI16
       POWI17 POWI18 POWI19 POWI20
       POWI21 POWI22 POWI23 POWI24
       POTOTE POTOTI OXIPOW
       TGAICONS  TGAINMES  distanew ;
```

```
INTEGER NSTEPS ipower IPOWER1 IPOWER4 IPOWER5
        IPOWER6 IPOWER7 IPOWER8
        RUPT NUPT L1 ;                                                  *


RESTORE 211  ;
REACTOR CIRCTOT ;

OPTION rocp 100.;
OPTION DTMIN 1.E-10 ;
OPTION MAXREP 50 ;
DT = DT0  ;

NSTEPS  = 3000000 ;
ipower = 1 ;
IPOWER1 = 0 ;
IPOWER4 = 0 ;
IPOWER5 = 0 ;
IPOWER6 = 0 ;
IPOWER7 = 0 ;
IPOWER8 = 0 ;
L1 = 0 ;

* to obtain 35 W/cm

distan0 = 15.            ;
WRITE distan0 XUSER 101  ;

LHGR = 375.2 * exp (-0.159*distan0)  ;

POW_LIN = LHGR*60.0 ;

g_hea0  = 2.9       ;
g_inPF0 = 3.1       ;
g_he0   = 5.1       ;
g_ouPF0 = 3.3       ;
g_coch0 = 5.0       ;


* METHOD TO REGULATE THE WALL POWER
* INITIAL DISTANCE (STEADY STATE)
```

```
dist = 14.08                                          ;
g_1 = g_coch0/g_inPF0*5.1711*exp (-0.087*dist)        ;

*********************************************
* the reference for the law vs position is
* set on the SS external flask
* gamma power at the right location (W/g)
*********************************************

g_ouPF = g_inPF0/g_inPF0*5.1711*exp (-0.087*distan0) ;
g_hea = g_hea0/g_inPF0*5.1711*exp (-0.087*distan0)   ;
g_inPF = g_inPF0/g_inPF0*5.1711*exp (-0.087*distan0) ;
g_he = g_he0/g_inPF0*5.1711*exp (-0.087*distan0)     ;

* density of materials [kg/m^3], zircalloy, water,
* stainless stell, helium, hafnium
r_sst = 7860.0 ;
r_hel = 0.6500 ;
r_inc = 7287.0 ;

PI = 3.141592654D0 ;
d_clad_e = 9.5E-3 ;

* Gamma power [W/m^3] in the water,
* hot-cold-cooling channels

P_HE = (r_inc*g_hea*1000) ;
P_IN = (r_sst*g_inPF*1000) ;
P_EL = (r_hel*g_he*1000) ;
P_OU = (r_sst*g_ouPF*1000) ;

*************************************
* DEFINITION OF THE INTERNAL POWERS
*************************************

*************************************
* fuel power wall
*************************************

PNRSHAPX CHARCRAY SIGNAL 1.
POWER CHARCRAY POWNEUT  POW_LIN
      ABSOLUTE REALLIST
      0.0   22000.0
      POWER REALLIST
      0.00  0.000  ;

POWER ExtWaM1  gam_co
      ABSOLUTE REALLIST
      0.0  22000.0
      POWER REALLIST
      0.0  0.0  ;

*************************************
* ACTIVATION OF THE ELECTRICAL POWER (EH)
*************************************
POWER THERMA
ABSOLUTE REALLIST
0.0   12000.  12001.0  22000.0
POWER REALLIST
0.0   0.0      0.66     0.66  ;

OPTION rocp 1.     ;

PERIOD displor SECOND  250.D0 ;
RESULT CIRCTOT SECOND  250.D0 ;

GOFUEL CIRCTOT            ;
OXRATE CHARCRAY STANDARD  ;

REPEAT BLOCK4 NSTEPS ;
  TIME = TIME + DT ;
  TRANSIENT CIRCTOT TIME DT ;
  DT = NEWDT ;
  IF ( DT > 1. ) THEN ;
  DT = 1. ;
  ENDIF ;

*************************************
* BLOCK of Temperature regulation at
* 1200 ÂřC in the middle of the fuel sample
*************************************

IF (TIME GT 16000. ) THEN ;
   PERIOD displor SECOND  50.D0 ;
   RESULT CIRCTOT SECOND  50.D0 ;

TGAICONS = 1200.D0     ;
TGAINMES = VALUE WALLWETT CHARCRAY 12  ;

IF (TGAINMES > (TGAICONS+50.) ) THEN   ;
   distanew = distan0 + 6.E-1*DT       ;
ENDIF                                  ;
IF (TGAINMES < (TGAICONS-50.) ) THEN   ;
   distanew = distan0 - 6.E-1*DT       ;
ENDIF                                  ;
                  ;
IF (distanew GT 35.0D0) THEN    ;
   distanew = 35.0D0    ;
ENDIF        ;
IF (distanew LT 10.0D0) THEN    ;
   distanew = 10.0D0            ;
ENDIF        ;

LHGR = 375.2 * exp (-0.159*distanew)   ;
POW_LIN = 375.2 * exp (-0.159*distanew)*60.0     ;
PNRSHAPX CHARCRAY SIGNAL 1.                      ;
POWER CHARCRAY POWNEUT POW_LIN
      RELATIVE REALLIST 0.D0  5.D5
      POWER    REALLIST   1.0 1.0          ;

g_ouPF = g_inPF0/g_inPF0*5.1711*exp (-0.087*distanew) ;
g_hea = g_hea0/g_inPF0*5.1711*exp (-0.087*distanew)   ;
```

```
g_inPF = g_inPF0/g_inPF0*5.1711*exp (-0.087*distanew) ;
g_he = g_he0/g_inPF0*5.1711*exp (-0.087*distanew)     ;
g_2 = g_coch0/g_inPF0*5.1711*exp (-0.087*distanew)    ;
C1 = g_2/g_1 ;

POWER
ExtWaM1  gam_co
ABSOLUTE REALLIST
0.0      22000.0
POWER REALLIST
C1       C1        ;

P_HE = (r_inc*g_hea*1000)       ;
P_IN = (r_sst*g_inPF*1000)      ;
P_EL = (r_hel*g_he*1000)        ;
P_OU = (r_sst*g_ouPF*1000)      ;

   EXCPOWER HEATER
   INCON718
   RELATIVE REALLIST    0.0  22000.0
   POWER  REALLIST      1.0  1.0
PROFILE  REALLIST
0.00000   0.00000   0.00000   0.00000   0.00000
0.00000   0.00000   0.45639   0.47728   0.49842
0.51975   0.54125   0.57373   0.61722   0.66060
0.70347   0.74541   0.78598   0.82470   0.86106
0.89453   0.92454   0.95051   0.97181   0.98780
0.99779   1.00109   1.00109   0.99779   0.98779
0.97181   0.95050   0.92453   0.89451   0.86104
0.82467   0.78595   0.74537   0.70342   0.66054
0.61715   0.57364   0.54116   0.51965   0.49831
0.47717   0.45627   0.00000   0.00000   0.00000
0.00000   0.00000   0.00000   0.00000   0.00000
0.00000   0.00000   0.00000
VOLPOWER P_HE ;


   EXCPOWER FLA_M
   INOX316  XXXXXXX6  INOX316
   RELATIVE REALLIST    0.0  22000.0
   POWER  REALLIST      1.0  1.0
PROFILE  REALLIST
0.00000   0.00000   0.00000   0.00000   0.00000
0.00000   0.00000   0.45639   0.47728   0.49842
0.51975   0.54125   0.57373   0.61722   0.66060
0.70347   0.74541   0.78598   0.82470   0.86106
0.89453   0.92454   0.95051   0.97181   0.98780
0.99779   1.00109   1.00109   0.99779   0.98779
0.97181   0.95050   0.92453   0.89451   0.86104
0.82467   0.78595   0.74537   0.70342   0.66054
0.61715   0.57364   0.54116   0.51965   0.49831
0.47717   0.45627   0.00000   0.00000   0.00000
0.00000   0.00000   0.00000   0.00000   0.00000
0.00000   0.00000   0.00000
VOLPOWER  P_IN P_EL P_OU ;

distan0 = distanew                    ;
MESSAGE 'distance vs core =' distanew  ;
MESSAGE 'power of fuel (W/cm) =' LHGR              ;
MESSAGE 'TEMPERATURE cladding (middle)=' TGAINMES   ;
WRITE distanew XUSER 101 ;
ENDIF ;

************************************
* Activation of the subroutine UTIL to
* take into account the radiative
* heat transfer
************************************
UTIL1 ;

************************************
* End of temperature regulation
************************************

PRESS2 = VALUE PRESSURE VOLTOP SUP ;
MESSAGE 'PRESSURE VOLTOP' PRESS2 ;
MESSAGE 'IPOWER8 IS' IPOWER8 ;

************************************
* Calculation of the Power due to
* the cladding oxidation
************************************

* Power generated by cladding oxidation
* on internal side (W/cm)

POWE1  = VALUE POWEROXE CHARCRAY 1  ;
POWE2  = VALUE POWEROXE CHARCRAY 2  ;
POWE3  = VALUE POWEROXE CHARCRAY 3  ;
POWE4  = VALUE POWEROXE CHARCRAY 4  ;
POWE5  = VALUE POWEROXE CHARCRAY 5  ;
POWE6  = VALUE POWEROXE CHARCRAY 6  ;
POWE7  = VALUE POWEROXE CHARCRAY 7  ;
POWE8  = VALUE POWEROXE CHARCRAY 8  ;
POWE9  = VALUE POWEROXE CHARCRAY 9  ;
POWE10 = VALUE POWEROXE CHARCRAY 10 ;
POWE11 = VALUE POWEROXE CHARCRAY 11 ;
POWE12 = VALUE POWEROXE CHARCRAY 12 ;
POWE13 = VALUE POWEROXE CHARCRAY 13 ;
POWE14 = VALUE POWEROXE CHARCRAY 14 ;
POWE15 = VALUE POWEROXE CHARCRAY 15 ;
POWE16 = VALUE POWEROXE CHARCRAY 16 ;
POWE17 = VALUE POWEROXE CHARCRAY 17 ;
POWE18 = VALUE POWEROXE CHARCRAY 18 ;
POWE19 = VALUE POWEROXE CHARCRAY 19 ;
POWE20 = VALUE POWEROXE CHARCRAY 20 ;
POWE21 = VALUE POWEROXE CHARCRAY 21 ;
POWE22 = VALUE POWEROXE CHARCRAY 22 ;
POWE23 = VALUE POWEROXE CHARCRAY 23 ;
POWE24 = VALUE POWEROXE CHARCRAY 24 ;

* Power generated by cladding oxidation
```

```
* on internal side (W/cm)
POWI1  = VALUE POWEROXI CHARCRAY 1  ;
POWI2  = VALUE POWEROXI CHARCRAY 2  ;
POWI3  = VALUE POWEROXI CHARCRAY 3  ;
POWI4  = VALUE POWEROXI CHARCRAY 4  ;
POWI5  = VALUE POWEROXI CHARCRAY 5  ;
POWI6  = VALUE POWEROXI CHARCRAY 6  ;
POWI7  = VALUE POWEROXI CHARCRAY 7  ;
POWI8  = VALUE POWEROXI CHARCRAY 8  ;
POWI9  = VALUE POWEROXI CHARCRAY 9  ;
POWI10 = VALUE POWEROXI CHARCRAY 10 ;
POWI11 = VALUE POWEROXI CHARCRAY 11 ;
POWI12 = VALUE POWEROXI CHARCRAY 12 ;
POWI13 = VALUE POWEROXI CHARCRAY 13 ;
POWI14 = VALUE POWEROXI CHARCRAY 14 ;
POWI15 = VALUE POWEROXI CHARCRAY 15 ;
POWI16 = VALUE POWEROXI CHARCRAY 16 ;
POWI17 = VALUE POWEROXI CHARCRAY 17 ;
POWI18 = VALUE POWEROXI CHARCRAY 18 ;
POWI19 = VALUE POWEROXI CHARCRAY 19 ;
POWI20 = VALUE POWEROXI CHARCRAY 20 ;
POWI21 = VALUE POWEROXI CHARCRAY 21 ;
POWI22 = VALUE POWEROXI CHARCRAY 22 ;
POWI23 = VALUE POWEROXI CHARCRAY 23 ;
POWI24 = VALUE POWEROXI CHARCRAY 24 ;

**************************************
* power generated by cladding oxidation
* on external face (W)
POTOTE = 2.5*(POWE1+POWE2+POWE3+POWE4+POWE5+
             POWE6+POWE7+POWE8+POWE9+POWE10+
             POWE11+POWE12+POWE13+POWE14+POWE15+
             POWE16+POWE17+POWE18+POWE19+
             POWE20+POWE21+POWE22+POWE23+POWE24) ;

* power generated by cladding oxidation
* on internal face (W)
POTOTI = 2.5*(POWI1+POWI2+POWI3+POWI4+POWI5+
             POWI6+POWI7+POWI8+POWI9+POWI10+
             POWI11+POWI12+POWI13+POWI14+POWI15+
             POWI16+POWI17+POWI18+POWI19+
             POWI20+POWI21+POWI22+POWI23+POWI24) ;


* CALCULATION OF THE OXIDATION POWER
*TOTAL power generated by cladding oxidation (W)

OXIPOW = POTOTE + POTOTI ;

MESSAGE 'POWER OXIDATION 1' OXIPOW ;
WRITE OXIPOW XUSER 215 ;
WRITE POTOTE XUSER 200 ;
WRITE POTOTI XUSER 201 ;


* flag to indicate if rupture has occurred
RUPT = VALUE INDRUP CHARCRAY ;

* node where the rupture has occurred
NUPT = VALUE NODRUP CHARCRAY ;

* time when the rupture occurs.
* temperature of external cladding when the
* rupture occurs.

IF ((RUPT EQ 1) AND (IPOWER7 EQ 0));
T_RUP = TIME  ;
TEMP_RUP = VALUE WALLTEMP CHARCRAY NUPT ;
IPOWER7 = 1 ;
ENDIF ;

WRITE T_RUP XUSER 300 ;
WRITE TEMP_RUP XUSER 305 ;


WRITE TOTOXY XUSER 306 ;
WRITE THICCLA XUSER 307 ;
WRITE OXYRAT XUSER 308 ;


MESSAGE 'FLAG OF THE RUPTURE' RUPT ;
MESSAGE 'NODE OF RUPTURE' NUPT ;
MESSAGE 'TIME OF RUPTURE'  T_RUP ;
MESSAGE 'TEMPERATURE OF RUPTURE'  TEMP_RUP ;


TIME = NEWTIME ;
IF ( TIME > 17500. ) THEN ;
*   IF ( TIME > T_2) THEN ;
 QUIT BLOCK4 ;
ENDIF ;


lost_bot = VALUE TOTLOSS FlaskBot     ;
*lost_top = VALUE TOTLOSS FlaskTop    ;
*WRITE lost_bot INJECVOL ca_volb      ;
*WRITE lost_top INJECVOL ca_volt      ;
*t_bot = VALUE LIQTEMP volbot INF     ;
*t_top = VALUE LIQTEMP voltop INF     ;
*WRITE t_bot TEXT Flaskbot -1         ;
*WRITE t_top TEXT Flasktop -1         ;

END BLOCK4 ;

SAVE 311 append ;
*
END EXEC;
```

Nomenclature

Symbols

A	Area
Bi	Biot number
Cp	Specific heat at constant pressure
D	Diameter
D_h	Hydraulic diameter
E	Entrainment rate
Gr	Grashof number
h	Enthalpy
k	Thermal conductivity
Nu	Nusselt number
P	Power, Pressure
Pe	Peclet number
Pr	Prandtl number
q''	Heat flux per unit area
q'''	Heat flux per unit volume
R	Radius
R_s	Stratification rate
Ra	Rayleigh number
Re	Reynolds number
St	Stelton number
u	Velocity
V	Volume

R	Perfect gas constant

Greek symbols

α	Void fraction
$\dot{\epsilon}$	Creep strain
ϵ	Radiation heat transfer coefficient
Γ	Mass flux
Λ	Fuel heat-up rate
μ	Dynamic viscosity
Ω	Resistance
ρ	Density
σ	Surface tension
σ_{es}	Elastic stress
σ_{sb}	Stefan-Boltzmann constant
ϖ	Maximum cladding elongation
ζ	Thickness

List acronyms

BWR	Boiling Water Reactor
CATHARE	Code for Analysis of THermalhydraulics during an Accident of Reactor and safety Evaluation
CEA	Commissariat á l'énergie atomique et aux énergies alternatives
CHF	Critical Heat Flux
DBA	Design Basis Accident
DD	Displacement Device
ECCS	Emergency Core Cooling System
EDF	Électricité de France
IAEC	Israel Atomic Energy Agency
IAEC	Israel Atomic Energy Association
IRSN	Institut de Radioprotection et de Sûreté Nucléaire
JHR	Jules Horowitz Reactor
LHGR	Linear Heat Generation Rate

LOCA	Loss of Coolant Accident
LWR	Light Water Reactor
MOX	Mixed Oxide Fuel
NFZ	Neutron Flux Zone
ONB	Onset of Nucleate Boiling
PSD	Preventive Shut Down
PWR	Pressurized Water Reactor
RCS	Reactor Coolant System
STST	Stainless steel
TLF	Thermosiphon Liquid Flow
VVER	Vodo-Vodyanoi Enegetichesky Reactor

Subscript

α	Associated to the alpha phase in the zirconium medium
β	Associated to the beta phase in the zirconium medium
b	Associated to the fuel cladding burst
CHF	Associated to the critical heat flux
$clad$	Associated to the fuel cladding
$cold$	Associated to the cold channel
$cond$	Associated to the conduction
con	Associated to the convection
$cool$	Associated to the cooling channel
DD	Associated to the displacement device
EH	Associated to the electrical heater
e	Associated to the external side
$fail$	Associated to the fuel cladding failure
FST	Associated to the flow separation tube
$fuel$	Associated to the fuel sample
gap	Associated to the fuel gap
g	Associated to the gas phase
hot	Associated to the hot channel

hp	Associated to the hot point
IPF	Associated to the inner pressure flask
i	Associated to the internal side
l	Associated to the liquid phase
mfs	Associated to the minimum film boiling
mix	Associated to the liquid-gas mixture
m	Associated to the mean value
nb	Associated to the nucleated boiling
OPF	Associated to the outer pressure flask
oxy	Associated to the oxidation
rad	Associated to the radiation
sat	Associated to the saturation condition
sys	Associated to the entire system
v	Associated to the vapor phase
w	Associated to the wall

List of Figures

List of Tables